Title
Functional and Mechanistic Characterization of Bacterial Nitric Oxide Signaling Pathways

Author
Rao, Minxi

Publication Date
2016

Peer reviewed|Thesis/dissertation

Functional and Mechanistic Characterization of Bacterial Nitric Oxide Signaling Pathways

By

Minxi Rao

A dissertation submitted in partial satisfaction of the

requirements for the degree of

Doctor of Philosophy

in

Chemistry

in the

Graduate Division

of the

University of California, Berkeley

Committee in charge:

Professor Michael A. Marletta, Chair
Professor Jamie H.D. Cate
Professor Michelle C.Y. Chang
Professor Michiko E. Taga

Fall 2016

Abstract

Functional and Mechanistic Characterization of Bacterial Nitric Oxide Signaling Pathways

By

Minxi Rao

Doctor of Philosophy in Chemistry

University of California, Berkeley

Professor Michael A. Marletta, Chair

Nitric oxide (NO) is a well-established signaling molecule and cytotoxic agent in mammals. NO is synthesized by nitric oxide synthase (NOS) by macrophages at high concentrations as a key part of the host immune response, and at low concentrations in endothelial and neuronal cells as a signaling agent. In endothelial cells, the primary NO receptor is soluble guanylate cyclase (sGC), which contains a heme-nitric oxide/oxygen binding domain (H-NOX). Selective binding of NO to the H-NOX domain is responsible for activation of sGC. Thus, the mammalian NO signaling system involves NO synthesis by NOS, and NO sensing by the H-NOX domain of sGC.

NOS and H-NOX proteins have also been identified in a number of bacterial species, including pathogens. Putative roles for bacterial NOS proteins include protection against oxidative stress and antibiotics, while bacterial H-NOX proteins have been shown to govern processes such as biofilm formation and bioluminescence via interactions with signaling proteins such as diguanylate cyclases (DGC) or histidine kinases (HK). Here, various aspects of NO signaling from three different organisms are characterized: the marine alphaproteobacterium *Silicibacter* sp. TrichCH4B; the soil-dwelling gammaproteobacterium *Shewanella oneidensis*; and the marine cyanobacterium *Synechococcus* sp. PCC 7335. This work and other recent studies seek to understand not only the diverse roles for NO in bacteria, but also the molecular mechanisms of bacterial NO signaling.

Silicibacter sp. TrichCH4B is the first bacterial organism discovered to contain both an NOS and H-NOX, thus capable of both NO synthesis and sensing, analogous to mammalian systems. The H-NOX protein from *Silicibacter* is found in an operon adjacent to an HK, forming part of a two-component phospho-relay signaling network. The response regulator of the network was identified to be a diguanylate cyclase (DGC), which is inactivated upon phosphorylation and establishes the link between NO and intracellular cyclic-di-GMP levels, and consequently biofilm formation. It was also determined that *Silicibacter* NOS activity is stimulated by a signaling protein from an algal symbiont, *Trichodesmium erythraeum*, which is a major marine nitrogen fixer. Thus, in the presence of *Trichodesmium*, the increase in NOS activity results in *Silicibacter* biofilm

formation and poising the two species for nutrient exchange, revealing a novel role for NO in interspecies communication and symbiosis.

Given the diverse processes governed by NO/H-NOX signaling, it is crucial to understand the molecular mechanism by which H-NOX regulates HK autophosphorylation activity, the most common outcome of a NO-bound H-NOX. Here, the interaction and signal transduction between the H-NOX-HK signaling pair from *Shewanella oneidensis* are characterized. Binding kinetics measurements and analytical gel filtration revealed that NO-bound H-NOX has a tighter affinity for the HK compared with H-NOX in the unliganded state, correlating binding affinity with kinase inhibition. Kinase activity assays with a panel of binding-deficient H-NOX mutants further reveal that while formation of the H-NOX-HK protein complex is required to stabilize the HK, H-NOX conformational changes upon NO binding are necessary for HK inhibition.

Characterization of H-NOX proteins has led to an increased understanding of bacterial NO sensing. However, NO production in bacteria is less well-understood, and here the NOS protein from *Synechococcus* sp. PCC 7335 is characterized. Mammalian NOS proteins are comprised of a P450-like heme/oxidase domain responsible for catalysis, and a reductase domain responsible for electron transfer. While most bacterial NOS proteins discovered to date contain only the heme/oxidase domain, *Synechococcus* NOS contains both the oxidase and reductase domains, and additionally contains a predicted globin domain resembling bacterial flavohemoglobins. Spectroscopic and biochemical characterization of the globin indicated a possible role in redox communication in this novel class of bacterial NOS enzymes.

TABLE OF CONTENTS

LIST OF ABBREVIATIONS

2Fe-2S	iron-sulfur cluster
AGF	analytical gel filtration
ATP	adenosine-5'-triphosphate
ATPγS	adenosine-5'-O-(3-thio) triphosphate
BeF_x	beryllium fluoride
BLAST	Basic Local Alignment Search Tool
BLI	Bio-Layer Interferometry
CA	histidine kinase catalytic and ATP-binding domain
CaM	calmodulin
cDNA	complementary DNA
cGMP	cyclic guanosine monophosphate
CO	carbon monoxide
$CoCl_2 \cdot 6H_2O$	cobalt(II) chloride hexahydrate
Cs	*Caldanaerobacter subterraneus*
CV	column volume
c-di-GMP	3',5'-cyclic diguanosine monophosphate
C-Term	C-terminal
DEA	diethanolamine
DEA-NONOate	Diethylammonium (Z)-1-(N,N-diethylamino)diazen-1-ium-1,2-diolate
DETA-NONOate	(Z)-1-[N-(2-aminoethyl)-N-(2-ammonioethyl)amino]diazen-1-ium-1,2-diolate
DGC	diguanylate cyclase
DHp	histidine kinase dimerization and histidine phosphorylation domain
DMSO	dimethyl sulfoxide
DNA	2'-deoxyribonucleic acid
DTT	dithiothreitol
EAL	c-di-GMP phosphodiesterase domain containing an EAL motif
EDTA	ethylenediaminetetraacetic acid
FAD	flavin adenine dinucleotide
$FeCl_3 \cdot 6H_2O$	iron(III) chloride hexahydrate
FMN	flavin mononucleotide
GGDEF	c-di-GMP diguanylate cyclase domain containing a GGDEF motif
GST	glutathione-*S*-transferase
GTP	guanosine-5'-triphosphate
H-NOX	*H*eme-*N*itric oxide/*Ox*ygen binding domain
H_4B	6*R*-tetrahydrobiopterin
H_4F	tetrahydrofolate

HaCE	H-NOX-associated- cyclic-di-GMP-processing enzyme
HD-GYP	c-di-GMP phosphodiesterase domain containing an HD-GYP motif
HDX-MS	hydrogen-deuterium exchange mass spectrometry
HEPES	4-(2-hydroxyethyl)piperazine-1-ethanesulfonic acid
His_6	hexahistidine affinity tag
HK	histidine kinase
HPLC	high performance liquid chromatography
HPT	histidine-containing phosphotransfer domain
HRP	horseradish peroxidase
IPTG	isopropyl β-D-1-thiogalactopyranoside
LB	Luria-Bertani medium
LC-MS	liquid chromatography mass spectrometry
L-Arg	L-arginine
L-Cit	L-citrulline
MBP	maltose binding protein
MCP	methyl-accepting chemotaxis protein
$MgCl_2$	magnesium chloride
$MnCl_2 \cdot 4H_2O$	manganese chloride tetrahydrate
MWCO	molecular weight cutoff
N_2	nitrogen
$Na_2MoO_4 \cdot 2H_2O$	sodium molybdate dihydrate
NaCl	sodium chloride
$NaH_2PO_4 \cdot H_2O$	sodium phosphate monobasic monohydrate
NAD	nicotinamide adenine dinucleotide
NADPH	nicotinamide adenine dinucleotide phosphate
NaOH	sodium hydroxide
NHA	*N*-hydroxy-arginine
Ni-NTA	nickel nitrilotriacetic acid
NO	nitric oxide
NOA	Nitric Oxide Analyzer
NOS	nitric oxide synthase
NOS_{glb}	nitric oxide synthase globin domain
NOS_{ox}	nitric oxide synthase heme/oxygenase domain
NOS_{red}	nitric oxide synthase reductase domain
Ns	*Nostoc* sp. PCC 7120
N-Term	N-terminal
O_2	oxygen
OD	optical density
ODQ	1H-[1,2,4]oxadiazolo[4,3-a]quinoxalin-1-one
PAS	Per/ARNT/SIM domain
PBST	phosphate buffered saline, 0.5% Tween 20

PCR	polymerase chain reaction
PDB	Protein Data Bank
PDE	phosphodiesterase
pGpG	5’-phosphoguanylyl-(3’-5’)-guanosine
PNBM	*para*-nitrobenzyl mesylate
RT-qPCR	real-time quantitative PCR
rpoD	RNA polymerase sigma factor
RNA	ribonucleic acid
RR	response regulator
RT	room temperature
Sc	*Sorangium cellulosum*
SDS-PAGE	sodium dodecyl sulfate polyacrylamide gel electrophoresis
sGC	soluble guanylate cyclase
Sili	*Silicibacter* sp. TrichCH4B
Sl	*Spirosoma linguale*
SMART	Simple Modular Architecture Research Tool
So	*Shewanella oneidensis*
Sw	*Shewanella woodyi*
SOW	synthetic ocean water
SWC	Seawater Complete media
Syn	*Synechococcus* sp. PCC 7335
TCEP	tris(2-carboxylethyl)phosphine
TCS	two-component signaling
TEA	triethanolamine
TEV	tobacco etch virus
TFA	trifluoroacetic acid
Tris	tris(hydroxymethyl)aminomethane
TSM	*Trichodesmium* spent media
UV	ultraviolet
Vc	*Vibrio cholerae*
vis	visible
WT	wild-type
$ZnSO_4 \cdot 7H_2O$	zinc sulfate heptahydrate

LIST OF FIGURES AND SCHEMES

LIST OF TABLES

ACKNOWLEDGEMENTS

My graduate school experience would not have been the same without the amazing mentors, colleagues, friends, and family who have provided their insight, guidance, and moral support along the way. I am thankful to all of them, for everything that they have given me.

First and foremost, I would like to thank my advisor Michael Marletta. I first met Michael during my interview weekend at Berkeley, and I remember being excited by his research projects, and more importantly inspired by the way that he talked about them. I felt so fortunate when he welcomed me into his lab, and since then, he has been the best mentor that any student could have ever wished for. He encouraged independence and gave me the freedom to develop my own research projects, and at the same time provided guidance and insight from his vast wealth of knowledge and expertise. He also promotes a collaborative and stimulating work environment and expects everyone in the lab to be helpful and kind towards one another. Thanks to Michael's mentorship, I have learned what it means to be a "good scientist" – not only someone who works hard and is capable of critical thinking, but is also helpful to others, open-minded to new ideas, and resilient in the face of challenges. Michael has taught me to be creative when my mind is stuck and to be persistent when I feel defeated, and he has demonstrated how to handle even the toughest of situations with grace and optimism. I am greatly indebted to him and hope that I will keep the lessons that I have learned with me in my career and my life.

I would also like to thank Jack Dixon, who has generously welcomed me into his lab as a "foster" student when the Marletta lab moved back to Berkeley as I was finishing up my studies. Jack treated me just the same as other members of his lab, providing helpful feedback and advice for my projects. Jack is an incredible scientist and mentor, and I am so grateful that I was able to spend time in his lab, where I was able to expand my knowledge into the area of secreted protein kinases and even make some small contributions to the lab by sharing my knowledge of bacterial signaling networks.

I would also like to express my gratitude towards the many other professors who have helped me along the way. In particular, I am grateful to the members of my thesis committee: Michelle Chang, Jamie Cate, and Michi Taga, who have supported and encouraged me throughout graduate school. I am especially thankful to Michelle, who mentored me in her lab while I was an undergraduate student in the Amgen Scholars summer research program. I had no prior experience in molecular biology or biochemistry, and Michelle patiently taught me all the basics of molecular cloning, protein expression and purification, and performing enzyme assays. The summer that I spent in Michelle's lab led me to pursue biochemistry, so I say without exaggeration that I would not be here without her. In addition, I would like to thank my undergraduate advisors, Eric Toone and Fred Dietrich at Duke University, and my first mentor in the Toone lab, Dave Carlson. I knew

nothing about laboratory research when I first stepped into the Toone lab as a freshman 10 years ago, and Dave patiently taught me not only the basic laboratory skills, but also the principles behind the experiments. It is thanks to Dave's enthusiasm and encouragement that I decided to pursue graduate school.

I would like to thank the members of the Marletta lab, who have provided a wonderfully friendly and helpful lab environment. I am grateful to Brian Smith, my rotation mentor, for taking the time to train me and patiently answering all of my questions, and for all the help that he provided in my project. He was also an invaluable resource when I was writing my first paper and helped me to become a better writer. I am also thankful for Mark Herzik, with whom I had a wonderful collaboration and shared many intellectually stimulating as well as fun-filled conversations. During my time in San Diego away from the Marletta lab, Mark served as my local connection to the lab, always willing to chat over coffee or beer to make sure that I never felt overwhelmed or isolated. Other senior graduate students in the lab, Michael Winter and Lars Plate, gave me a warm welcome and have provided much-needed encouragement and insight on research, graduate school, and life. Many thanks to my officemates at TSRI, Eric Underbakke and Basak Surmeli, who could always cheer me up and make me laugh, even on the days when nothing seemed to be going well. I will always remember our time in Office 534 with a big smile. And last but definitely not least, I am very grateful for my "lab twin", Charles Hespen. We joined the lab at the same time, and throughout the years, we have shared countless discussions and chats about science, career, life, and everything in between. My graduate school experience would not have been the same without your friendship.

In addition to those whom I have already mentioned, I would also like to thank all the members of the Marletta lab, past and present – Marco Agostoni, Katy Barglow, Will Beeson, Loes Bevers, Andrew Birnberg, Sarah Bissonnette, Megan Brophy, Joel Bruegger, Tyler Detomasi, Yirui Guo, John Hangasky, Tracey Hinder, Ben Horst, Christopher Lemon, Frederike Muskens, Elizabeth Ndontsa, Alexander Nierth, Chris Phillips, Christine Phillips-Piro, Elise Span, Peter 't Hart, Jakob Trendel, Van Vu, Emily Weinert, and Sarah Wynia-Smith – for their support and guidance. I am truly blessed to have worked with such a wonderful group of colleagues and friends. I am also thankful to all the members of the Dixon lab – Sourav Banerjee, Natalie Chen, Jixin Cui, Kim Nguyen, Adam Pollak, Greg Taylor, Sandy Wiley, and Carolyn Worby – who welcomed me into their lab and made me feel right at "home". Thank you all for making my graduate school experience such a positive one.

Lastly, I am infinitely grateful to my friends and family, especially my mother, for all their love and support. Coming from a culture that traditionally places less emphasis on girls' education, I am so grateful that my family deviated from the norm and encouraged me to dream big.

CHAPTER 1:

INTRODUCTION

Nitric Oxide Biology

Nitric oxide (NO) is a highly reactive and toxic gas that serves as a signaling agent in nature. In mammals, NO at low (i.e. nanomolar) concentrations serves as a signaling agent, and higher (i.e. micromolar) concentrations as a cytotoxin, serving as part of the host defense mechanism against pathogens (1). The diverse roles of NO in mammalian biology have been studied extensively, as disruptions in NO signaling are linked to hypertension, erectile dysfunction, stroke, heart disease, and neurodegeneration (2–6).

NO Synthesis: Nitric Oxide Synthase

Mammalian Nitric Oxide Synthases

NO synthesis is carried out by the enzyme nitric oxide synthase (NOS) in two catalytically distinct steps, converting L-arginine (L-Arg) to L-citrulline (L-Cit) and NO via the intermediate *N*-hydroxy-L-arginine (NHA) via a 5-electron oxidation, utilizing NADPH and O_2. Mammalian NOS enzymes have a complex domain organization, consisting of an N-terminal P450-like heme/oxidase domain, which is responsible for catalysis, and a C-terminal reductase domain, which is responsible for electron transfer. The reductase domain can be further divided into FAD/NADPH-binding and FMN-binding subdomains. In the eNOS and nNOS isoforms, a calmodulin (CaM)-binding interface spans across the two major domains, regulating cross-talk and electron transfer. The oxidase domain binds the L-Arg substrate, heme, and the redox-active cofactor 6*R*-tetrahydrobiopterin (H_4B). The reductase domain binds the cofactors FMN, FAD, and NADPH. During catalysis, electrons are transferred from NADPH to FAD and FMN, then from FMN to the P450-type heme (**Figure 1.1**).

Three NOS isoforms exist in mammals: inducible NOS (iNOS) is found in macrophages, and its activity is transcriptionally controlled to produce cytotoxic concentrations of NO at the site of infection or inflammation (7). The other two isoforms, endothelial NOS (eNOS) and neuronal NOS (nNOS), are constitutively expressed, and the NO generated by these isoforms regulate a variety of signaling processes, including vasodilation, platelet aggregation, myocardial functions, and neurotransmission (8, 9). The activity of these constitutive NOS isoforms is governed by intracellular Ca^{2+} concentrations. In the vascular system, eNOS is activated by influx of Ca^{2+} into

endothelial cells, which binds to CaM. The CaM:Ca^{2+} complex subsequently binds and activates eNOS, producing a low, nanomolar concentration of NO. NO then diffuses into an adjacent smooth muscle cell for activation of soluble guanylate cyclase.

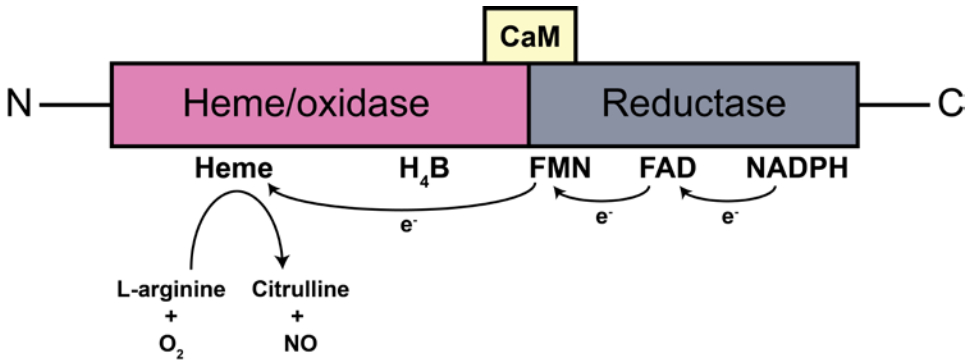

Figure 1.1. Domain architecture of mammalian NOS. Mammalian NOS is comprised of two primary domains: an N-terminal heme/oxidase domain that binds heme and the H_4B cofactor, and a C-terminal reductase domain that binds NADPH and the flavin cofactors FMN and FAD. In the eNOS and nNOS isoforms, a CaM-binding motif spans the interface between the two domains. During catalysis, electrons are transferred from NADPH to FMN and FAD, and finally to the heme for conversion of L-arginine and O_2 to L-citrulline and NO.

Bacterial Nitric Oxide Synthases

In recent years, bacterial NOS proteins have also been discovered via BLAST searches using the heme/oxidase domain of mammalian NOS as a query sequence. Initially discovered in the radiation-resistant organism *Deinococcus radiodurans* and *Bacillus subtilis*, these bacterial NOS proteins comprise of a standalone heme/oxidase domain (10, 11) (**Figure 1.2**). X-ray crystallography of the NOS from *B. subtilis* revealed that it has a similar overall fold to the mammalian NOS oxidase domain, but lacks the N-terminal hook and zinc-binding region present in the structure of iNOS (11, 12). Subsequently, NOS proteins were characterized from *Staphylococcus aureus*, *Bacillus anthracis*, *Streptomyces turgidiscabies*, and *Geobacillus stearothermophilis*, all of which are standalone P450-type oxidase proteins. Thus, in order to catalyze the conversion of L-Arg and O_2 to L-Cit and NO, a separate reductase domain is required (13–16).

The first characterization of a so-called "full-length" bacterial NOS – that is, with oxidase and reductase domains fused in a single polypeptide – was from the gram-negative organism *Sorangium cellulosum*. However, the domain organization of *S. cellulosum* a NOS (scNOS) differs vastly from that of mammalian NOS. In scNOS, the reductase domain is located at the N-terminus, and it contains a 2Fe-2S cluster in addition to FAD-binding and NAD-binding motifs (**Figure 1.2**). scNOS was shown to be catalytically active in the presence of substrates and cofactors, yet its function within the organism is still unknown (17).

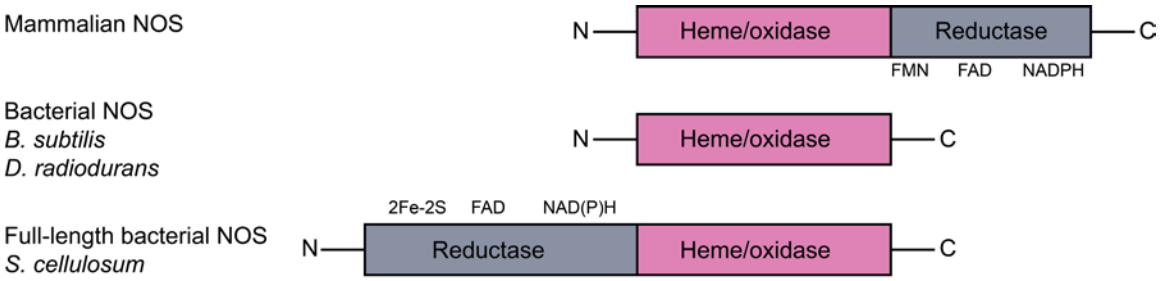

Figure 1.2. Domain organization of mammalian vs. bacterial NOS proteins. "Stand-alone" bacterial NOS proteins, such as ones isolated from *B. subtilis* and *D. radiodurans*, only contain the heme/oxidase domain responsible for catalysis. "Full-length" bacterial NOS proteins have been identified recently in a number of organisms, many of which remain uncharacterized.

The function of bacterial NOS proteins and bacterially-derived NO has been explored. In *S. turgidiscabies*, NOS is found on the same pathogenicity island that causes potato scab disease, including genes for the biosynthesis of thaxtomins, a class of plant toxins. Thaxtomins contain a nitrated tryptophanyl moiety (18). NO derived from *S. turgidiscabies* NOS is most likely responsible for the nitration as disruption of the *nos* gene abrogated thaxtomin production, which was re-established upon *nos* complementation (15). In *D. radiodurans*, deletion of the *nos* gene compromised its ability to recover from exposure to UV radiation, suggesting a role for NOS in the organism's stress response (19). In *B. subtilis*, *B. anthracis*, and *S. aureus*, NO also appears to mediate oxidative stress response and thiol protection, possibly via transcriptional regulation (20, 21). Unfortunately, the mechanistic details of how NOS-derived NO activates the antioxidant response in these organisms are still unclear. Currently, new roles for bacterial NOS and NO are being explored.

NO Sensing: Soluble Guanylate Cyclase and H-NOX Proteins

The primary NO receptor in mammals is soluble guanylate cyclase (sGC), which converts GTP to the second messenger cyclic GMP (cGMP) upon the binding of NO to its heme cofactor. sGC is a heterodimeric protein comprised of two subunits, α1 and β1, with Per/Arnt/Sim (PAS), coiled-coil, and cyclase domains that are homologous to both subunits (**Figure 1.3**). The N-terminal 194 residues of the β1 subunit were determined to be sufficient for heme binding, and this sequence was found to contain a conserved His residue, required for coordination to the iron in the porphyrin (22–24).

Hemoproteins in the ferrous (Fe^{II}) state are capable of coordinating several diatomic gas ligands, such as O_2, NO, and CO; however, most of them are unable to distinguish between these gases (25–27). In contrast, sGC has remarkably exquisite ligand selectivity for NO over O_2,

showing no measurable affinity for O_2 (28). This discrimination against O_2 is crucial for sGC as a selective NO sensor, since O_2 is present at 1000-fold excess over NO in aerobic environments.

Homologs of the sGC heme-binding domain were identified in many different organisms through bioinformatics searches (29–31). In prokaryotes, the heme domain was found in obligate anaerobes as fusions to methyl-accepting chemotaxis proteins, and they show affinity for both NO and O_2. sGC heme domain homologs that are selective for NO are found in facultative anaerobes, as stand-alone protein in the same operon as histidine kinases or diguanylate cyclases (**Figure 1.3**). Thus, because of the capability for both NO- and O_2-binding, the sGC heme domain and prokaryotic homologs were termed the heme-nitric oxide/oxygen binding proteins (H-NOX).

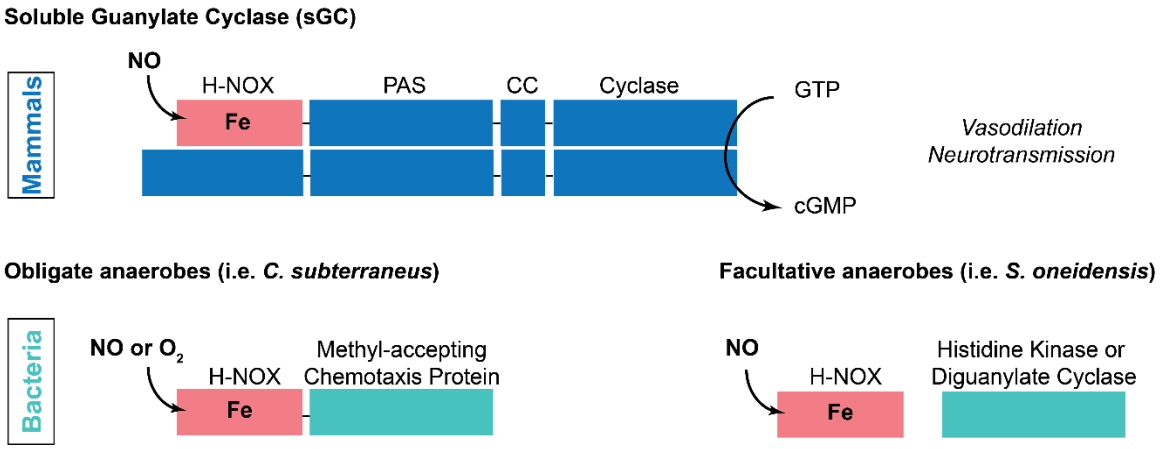

Figure 1.3. Domain architecture of soluble guanylate cyclase (sGC) and bacterial H-NOX signaling pairs. The sGC heterodimer contains an H-NOX domain at the N-terminus of the β1 subunit. H-NOX proteins from obligate anaerobes are found as N-terminal fusions to membrane chemoreceptors, while H-NOX proteins from facultative anaerobes are in operons adjacent to histidine kinases or diguanylate cyclases.

The first crystal structure of an H-NOX family member was from *Caldanaerobacter subterraneus* subsp. *tengcongensis* (*Cs* H-NOX, formerly *Tt* H-NOX), which showed a distinct overall fold from other heme-based gas sensors. H-NOX domains consist of N-terminal and C-terminal subdomains that flank the proximal and distal faces of the heme, respectively. The heme cofactor is bound at the interface between the two subdomains, via ligation to a conserved histidine residue on α-helix F. Additionally, the heme propionate groups form salt bridges to an absolutely conserved YxSxR motif, further stabilizing heme binding (29). Subsequent structures of H-NOX proteins from *Nostoc* sp. PCC 7120 (*Ns* H-NOX) and *Shewanella oneidensis* (*So* H-NOX) reveal a conserved overall fold for the H-NOX protein family (32, 33) (**Figure 1.4A**).

Ligand Selectivity in H-NOX Domains

Structural and biochemical characterization of prokaryotic H-NOX domains have elucidated the mechanism for ligand discrimination, particularly of NO over O_2 in aerobic environments. The crystal structure of *Cs* H-NOX, an O_2-binding H-NOX from an obligate anaerobe, reveals a hydrogen-bonding network in the heme distal pocket consisting of the residues W9, N74, and Y140 that stabilize O_2 binding (29) (**Figure 1.4C**). Sequence alignments show that the tyrosine, as well as other H-bonding network residues, are conserved in the O_2-binding class of H-NOX proteins, while the NO-selective H-NOX domains have hydrophobic residues in the distal pocket, including sGC. Mutations that disrupted the H-bonding network in *Cs* H-NOX, in particular Y140, resulted in decreased O_2-binding affinity (34).

On the other hand, introduction of a Tyr into the distal heme pocket of the NO-selective H-NOX from *Legionella pneumophila* (F142Y) resulted in the formation of an O_2 complex, confirming that the distal pocket Tyr is a key determinant for O_2 binding (34). Crystal structures of the non-O_2-binding *Ns* H-NOX and *So* H-NOX provided additional support for this hypothesis, as both of these structures lack H-bonding residues in the distal heme pocket (32, 33, 35, 36). The structures reveal that the distal pockets of non-O_2-binding H-NOX proteins are predominantly non-polar, in stark contrast to the polar distal pockets of O_2-binding H-NOX proteins, which may be additional factors that contribute to the selectivity of NO over O_2 (**Figure 1.4D**). However, it is important to note that mutation of full-length sGC to include a distal pocket Tyr did not result in O_2 binding, but addition of the Tyr in an sGC truncation (β1-385) resulted in a weak O_2 complex (37), and incorporation of a minimal H-bonding network into full-length sGC (I145Y/I149Q) resulted in a transient O_2 complex (38). This suggests that there are additional factors responsible for ligand discrimination in sGC.

Additional factors that contribute to ligand selectivity in H-NOX proteins include heme distortion, heme pocket conformational changes, changes in protein dynamics, and a tunnel network for ligand entry and exit (36, 39–41). Structures of several H-NOX proteins reveal that the heme cofactor is severely distorted from planarity due to the presence of a proline (P115 in *Cs* H-NOX) in the proximal heme pocket (29, 33, 39). The *Cs* H-NOX P115A mutant, which has a relaxed, planar heme, showed tighter O_2 binding, demonstrating that heme geometry influences ligand affinity and redox potential (**Figure 1.4B**) (39). The importance of the heme pocket conformation and correct positioning of the H-bonding network has also been demonstrated. Introduction of phenylalanine residues in the heme pocket of *Cs* H-NOX cause the H-bonding Tyr to shift away from the heme, significantly weakening O_2 binding (40, 41). Finally, in NO-selective H-NOX proteins, a tunnel network extending from the protein surface to the heme was identified to modulate ligand flux near the heme (33, 36). The increased ligand flow in NO-selective H-NOX proteins could also play a role in modulating ligand affinity.

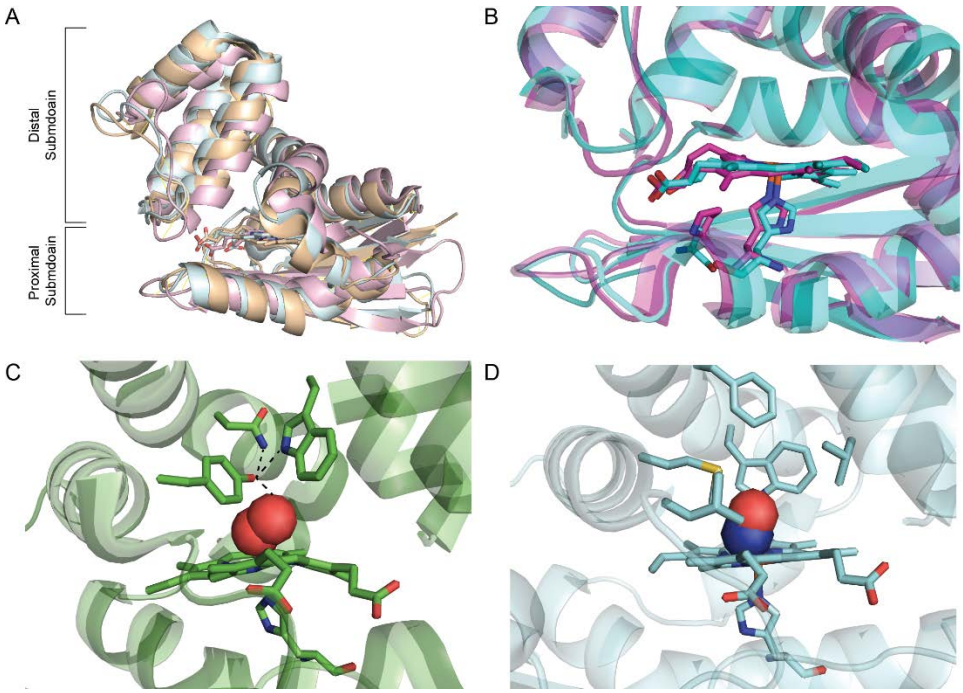

Figure 1.4. Structural features of bacterial H-NOX domains. (**A**) Overlay of H-NOX crystal structures from *Shewanella oneidensis* (wheat; PDB ID 4U9B), *Caldanaerobacter subterraneus* (pink; PDB ID 1U55), and *Nostoc sp*. PCC 7120 (light blue; PDB ID 2O0C) (29, 32, 33). H-NOX domains share a distinct overall fold, with distal and proximal subdomains and heme at the interface between the two subdomains. (**B**) Comparison of the heme distortion in wild-type (magenta; PDB ID 1U55) and P115A mutant (teal; PDB ID 3EEE) *Cs* H-NOX. The P115A mutant shows a significantly flattened heme (29, 39). (**C**) Zoomed-in view of the heme pocket of the O_2-binding *Cs* H-NOX, which contains the H-bonding network consisting of Y140, W9, and N74 (29). (**D**) Zoomed-in view of the heme pocket of the NO-selective *Ns* H-NOX, which contains hydrophobic residues (32).

H-NOX Signaling Partners

Bacterial H-NOX domains have diverse signaling partners. As mentioned above, H-NOX domains in bacteria are found either as free-standing proteins, or as domains of membrane-bound methyl-accepting chemotaxis proteins (MCPs) (**Figure 1.3**). Interestingly, nearly all of the H-NOX-MCP fusions are found in obligate anaerobes, most commonly from the class Clostridia, and their H-NOX domain contains the distal pocket Tyr that serves as a major determinant for O_2 binding (34). MCPs govern the bacterial chemotaxis response towards chemical attractants and away from repellants via controlling flagellar rotation (42). *Cs* H-NOX has been demonstrated to respond specifically to O_2 (43), and thus H-NOX-MCPs are believed to serve as O_2 sensors that can direct obligate anaerobes away from toxic O_2 sources.

The function of free-standing, NO-selective H-NOX proteins was explored by examining the operons for functionally-related and co-transcribed genes. The majority of the operons contain histidine kinase (HK) genes directly adjacent to the H-NOX gene (44). HKs are part of the bacterial two-component signaling system and are often membrane-bound proteins with periplasmic or extracellular sensor domains, which trigger a change in HK autophosphorylation activity in response to a chemical stimulus (45). However, the HKs found adjacent to H-NOX proteins do not have sensor domains, nor are they predicted to be membrane-incorporated, suggesting that H-NOX proteins can serve as the sensor. Interactions between the H-NOX and HK, and NO-dependent control of HK autophosphorylation, have indeed been observed (44).

In two-component signaling, HKs transfer a phosphoryl group to a response regulator (RR), which typically contains an effector domain. The phosphorylation state of the RR alters the effector domain function and consequently the overall output of the signaling system (45, 46). Cognate RRs of H-NOX-associated HKs have been identified with diverse effector domains, including EAL phosphodiesterases, HD-GYP phosphohydrolases, and transcriptional regulators (**Figure 1.5, *bottom***). In these studies, bioinformatics and phosphotransfer profiling methods were employed to identify the cognate RR of the H-NOX-associated HK, as a majority of these HKs are orphans and lack an RR gene in the same operon (47, 48).

Lastly, free-standing H-NOX proteins are also commonly found in the same operons adjacent to GGDEF diguanylate cyclases and EAL phosphodiesterases, which regulate the synthesis and/or degradation of the bacterial second messenger, cyclic diguanosine monophosphate (cyclic-di-GMP) (**Figure 1.5, *top***). Cyclic-di-GMP controls bacterial motility and aggregation, switching from a motile to a sedentary lifestyle with concomitant biofilm formation (49). H-NOX proteins have been shown to interact with these GGDEF-EAL proteins, and NO-dependent control of activity has been demonstrated (50, 51). The details of H-NOX interaction and regulation of their partners will be addressed below.

H-NOX Activation Mechanism

In order to serve as an effective gas sensor, H-NOX proteins must undergo a structural change upon appropriate ligand binding in order to effectively communicate with downstream effectors. Structural characterization of H-NOX proteins in different ligation states have provided insight into the activation mechanism and conformational changes triggered by gas binding.

The crystal structure of *Cs* H-NOX revealed severe heme distortion from planarity (**Figure 1.4B**) (29). Similar distortion is observed in the structures of *So* H-NOX and *Ns* H-NOX (32, 33), although to lesser extents. As discussed above, the heme pocket proline (P115 in *Cs* H-NOX) presses against one of the heme pyrroles while a conserved hydrophobic residue (I5 in *Cs* H-NOX) on the N-terminal αA helix pushes against the neighboring pyrrole surface from the distal side, creating a distinct kink in the heme. The amount of heme distortion correlates with the relative

positioning of the distal and proximal subdomains, and removal of the heme distortion by the *Cs* H-NOX P115A mutant resulted in a different orientation of the distal subdomain compared with wild-type protein. I5 moves correspondingly with the distortion created by P115, indicating that the heme and protein conformations are linked and that ligand binding to the heme could result in substantial structural changes in H-NOX proteins (39).

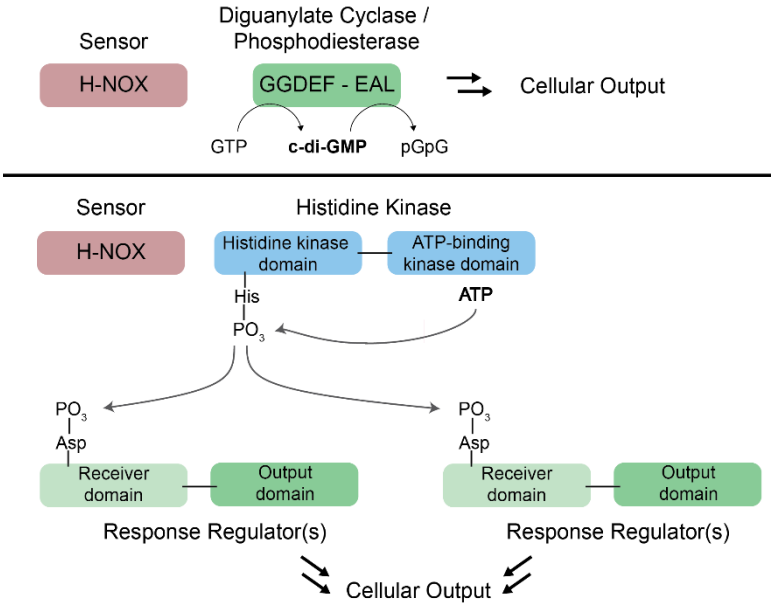

Figure 1.5. H-NOX signaling partners. ***Top***: H-NOX proteins are found adjacent to GGDEF and/or EAL-containing cyclic-di-GMP processing enzymes. In *L. pneumophila* and *S. woodyi*, NO-bound H-NOX decreases DGC and/or increases PDE activity, resulting in decreased cyclic-di-GMP levels and biofilm dispersal. ***Bottom***: H-NOX proteins are found adjacent to HKs, which are part of bacterial two-component signaling networks. In *S. oneidensis* and *V. cholerae*, the HK phosphorylates multiple cognate RR partners, including PDEs, which ultimately increase biofilm formation.

Extensive characterization of H-NOX proteins have determined that NO initially binds at the open coordination site of 5-coordinate ferrous (Fe^{II}) heme, forming a transient 6-coordinate complex. In most H-NOX domains including sGC, NO association severely weakens the iron-histidine bond (so-called trans effect), leading to dissociation of the histidine to yield a 5-coordinate Fe^{II}-NO complex. Crystal structures of NO-selective H-NOX proteins in the Fe^{II} and Fe^{II}-NO states, as well as O_2-binding H-NOX proteins in the Fe^{II}, Fe^{II}-NO, and Fe^{II}-O_2 states have provided insight into the conformational changes upon ligand binding.

The first crystal structures of NO-bound H-NOX were from *Nostoc* sp. (*Ns* H-NOX), and the structures revealed a 6-coordinate NO complex without significant changes in protein conformation compared with the unliganded state (32). This observation is in agreement with

previous biochemical data indicating that the key activation event is the cleavage of the iron-histidine bond (52). Further studies comprised of structural mimics that substitute the heme-ligating histidine with a glycine, and retaining heme binding using imidazole (35, 53). Comparison of these mutants with the wild-type Fe^{II} structure revealed that artificial "cleavage" of the iron-histidine bond causes a rotational displacement of the N-terminal subdomain, in particular relative to the signaling αF helix containing the heme-coordinating His.

Subsequent crystal structures of the NO-selective *So* H-NOX in the Fe^{II} and Fe^{II}-NO ligation states confirmed that scission of the iron-histidine bond results in major structural changes in the protein. The heme-ligating His, H103, is displaced by ~8.5 Å, and consequently the residues surrounding H103 on the αF signaling helix undergo a ~45° rotation along the length of the helix. In addition, the N-terminal H-NOX distal subdomain undergoes a ~4° rotation about the heme, resulting in a ~2.5 Å displacement (**Figure 1.6A**). The distal subdomain pivot point is located within the αD helix, on which a conserved glycine residue (G70 in *So* H-NOX) is located. Together with another conserved glycine, G144 (in *So* H-NOX), these residues form the "glycine hinge" that maintains the αD-αG helical interface and allows for displacement of the distal subdomain about the αD helix upon NO binding (33).

Structural comparison of the O_2-binding *Cs* H-NOX in Fe^{II}, Fe^{II}-O_2, Fe^{II}-NO, and Fe^{II}-CO ligation states reveals further insight into H-NOX activation upon ligand binding. Alignment of the Fe^{II}-O_2 and Fe^{II} structures at the proximal subdomain reveals a large conformational shift of the distal subdomain by ~4.5 Å (43). The heme-ligating His (H102 in *Cs* H-NOX) is rotated ~90° along the Fe-N coordination axis. The heme is also substantially flattened in the Fe^{II} structure, resembling the flattened porphyrin from the *Cs* H-NOX P115A mutant (**Figure 1.6B**). Finally, Fe^{II}-unliganded *Cs* H-NOX displays a ~8° rotation along the glycine hinge, compared with the Fe^{II}-O_2 form (43). These differences resemble the global conformational changes observed between Fe^{II} and Fe^{II}-NO *So* H-NOX (33). In an interesting contrast to *So* H-NOX, the distal subdomain rotation and heme flattening occur in *Cs* H-NOX with the Fe-His bond remaining intact.

Orthogonal signaling assays *Cs* H-NOX and the histidine kinase from *V. cholerae* (*Vc* HK) indicated that the Fe^{II} form was inhibitory towards kinase activity, similar to Fe^{II}-NO *Vc* H-NOX. Correspondingly, *Vc* HK incubated with Fe^{II}-O_2 *Cs* H-NOX displayed similar activity levels as kinase alone. Structural comparisons revealed that Fe^{II} *Cs* H-NOX and Fe^{II}-NO *Vc* H-NOX adopt an "open" conformation with a planar, relaxed heme and compacted distal subdomain, whereas Fe^{II}-O_2 *Cs* H-NOX and Fe^{II} *Vc* H-NOX are in a "closed" conformation with the distinctive distorted heme (**Figure 1.6C**) (43). Taken together, this suggests that *Cs* H-NOX is specific to O_2, and that the conformational changes in H-NOX proteins upon ligand binding or dissociation are key in signal transduction.

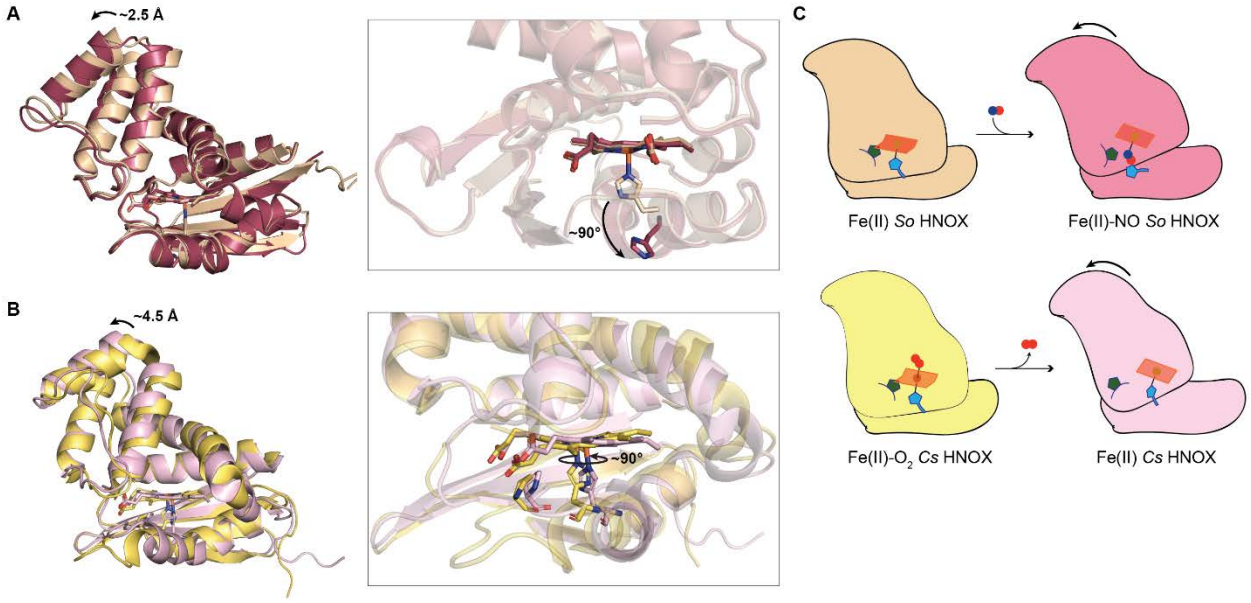

Figure 1.6. H-NOX activation mechanism. (**A**) Overlay of Fe^{II} (wheat) and Fe^{II}-NO (ruby) *So* H-NOX reveals a distal subdomain displacement of ~2.5 Å. Close-up of the heme pocket reveals that H103 swings ~90° away from the heme upon NO binding (33). (**B**) Overlay of Fe^{II} (pink) and Fe^{II}-O_2 (yellow) *Cs* H-NOX reveals a distal subdomain displacement of ~4.5 Å. Close-up of the heme pocket reveals that H102 rotates ~90° along the Fe-N coordination axis, and P115 shifts away from the pocket (43). (**C**) Activation scheme of *So* H-NOX compared with *Cs* H-NOX. [Fe^{II}]-*So* H-NOX and [Fe^{II}-O_2]-*Cs* H-NOX adopt similar "closed" conformations with a distorted heme. Binding of NO to *So* H-NOX and dissociation of O_2 from *Cs* H-NOX cause displacement of the distal subdomain, result in an "open" conformation with a planar, relaxed heme.

Nitric Oxide in Bacteria

NO governs diverse communal behavior in bacteria via H-NOX signaling. As discussed above, many H-NOX proteins are found in operons adjacent to diguanylate cyclase (DGC) and phosphodiesterase (PDE) genes, and many of the cognate RRs for H-NOX-associated HKs contain effector domains that process cyclic-di-GMP. Cyclic-di-GMP is a bacterial second messenger molecule that controls diverse functions, including virulence, cell cycle progression, and motility and cellular aggregation (49). Cyclic-di-GMP is produced from two molecules of GTP by GGDEF DGCs, and can be hydrolyzed to 5'-phosphoguanylyl-(3'-5')-guanosine (pGpG) by either EAL or HD-GYP PDEs (49, 54, 55).

In the opportunistic pathogen *Legionella pneumophila*, an H-NOX protein is encoded adjacent to an active DGC protein. Deletion of the *hnoX1* gene in the organism produced elevated biofilm levels, while mild overexpression of the H-NOX-associated DGC increases biofilm formation, confirming a role for cyclic-di-GMP. Finally, *in vitro* characterization of the DGC

showed that the NO-bound state of the H-NOX led to decreased cyclic-di-GMP synthesis (51). Similarly, the marine organism *Shewanella woodyi* also encodes an H-NOX-associated-cyclic-di-GMP-processing enzyme (HaCE) that contains active DGC and PDE domains. *Sw* HaCE was shown have predominant DGC activity when the H-NOX is in the unliganded state, while PDE activity was higher when the H-NOX was in the NO-bound state. Finally, *in vivo* experiments showed that in the presence of NO, *S. woodyi* had lower cyclic-di-GMP concentrations and decreased biofilm, and deletion of the *hnoX* gene alleviated the decrease in biofilm formation (50). These studies in *L. pneumophila* and *S. woodyi* present a model for NO/H-NOX-dependent biofilm dispersal via inhibition of DGC activity or increasing PDE activity, leading to lower cyclic-di-GMP concentrations and biofilm dispersal. The implications for NO-induced biofilm dispersal in these organisms, however, has yet to be explored.

In contrast to the H-NOX-associated DGC/PDE proteins, H-NOX regulation of HKs in a multicomponent signaling network leads to increased biofilm formation, as shown in *Shewanella oneidensis*. NO-bound state of *So* H-NOX was shown *in vitro* to inhibit HK autophosphorylation activity (56), and three cognate RRs for *So* HK were identified: a degenerate HD-GYP protein, an active EAL PDE, and a transcription regulator. Phosphorylation of the RRs led to increased PDE activity and lower cyclic-di-GMP levels. Thus, NO-bound H-NOX inhibition of HK removes RR phosphorylation, decreasing PDE activity and ultimately increases cyclic-di-GMP and biofilm levels (48). An analogous H-NOX/HK signaling network was identified in the pathogen *Vibrio cholerae* (48), which has also been shown to increase biofilm formation in the presence of NO (C. Hespen unpublished data). In these organisms, biofilm formation may serve as a defense mechanism in response to the toxic NO molecule. In addition, biofilm formation has been identified as a key step in *V. cholerae* infection and colonization, and cells in the biofilm state were shown to be more infectious than planktonic cells (57, 58). Thus, NO-dependent biofilm formation may play a key role in *V. cholerae* virulence.

In addition to regulation of cyclic-di-GMP levels and biofilm formation/dispersal, NO/H-NOX signaling has been implicated in quorum sensing in another *Vibrio* species, *Vibrio harveyi*, which is an opportunistic pathogen of marine organisms. The NO/H-NOX/HK signaling system in *V. harveyi* has been attributed to regulation of light production via the quorum sensing pathway LuxU/LuxO/LuxR (59). In addition, NO has also been shown to influence biofilm formation by *V. harveyi*, suggesting that NO/H-NOX signaling can play simultaneous roles in many bacterial processes (60).

Finally, NO/H-NOX signaling in the bioluminescent marine organism *Vibrio fischeri* has been proposed to mediate symbiosis with the Hawaiian bobtail squid *Euprymna scolopes*. *V. fischeri* colonizes the light organ of the squid, and the bioluminescence from the bacteria protects the squid from predators by providing counter-illumination to prevent the squid from casting a shadow at night (61). The NO/H-NOX/HK signaling pathway in *V. fischeri* was demonstrated to repress iron uptake and utilization genes (62). Surprisingly, deletion of *hnoX* in *V. fischeri*

demonstrated a colonization advantage in the squid, attributed to more efficient iron utilization in the low iron environment of the light organ (62). However, the limitation of iron uptake by NO/H-NOX was ultimately determined to be a survival strategy for *V. fischeri*, as an excess of iron can generate harmful free radicals with host-generated H_2O_2 during the early colonization process (62). *V. fischeri* encounters host-generated NO before entering the light organ ducts (63), which inactivates iron uptake genes through H-NOX signaling and effectively primes the organism for reactive oxygen species (ROS) exposure. As a result, the NO/H-NOX signaling pathway is at least partly responsible for the survival and colonization advantage of *V. fischeri* over other nearby bacteria, suggesting a key role for NO in symbiosis (62).

Thesis Research

The focus of this dissertation encompasses bacterial NO signaling, examining both NO synthesis by bacterial NOS, and NO sensing by H-NOX/HK two-component systems. While H-NOX/HK signaling has revealed important roles for NO in various bacterial processes, the sources of NO have typically been from the host organism with which the bacteria interacts (*e.g. V. cholerae* and *V. fischeri*), or nitrate reduction occurring in the bacteria's surrounding environment such as soil (*e.g. S. oneidensis*). Contrastingly, active NOS proteins have been characterized in various bacteria, but the NO receptors in these organisms have yet to be identified.

Chapter 2 discusses the NO signaling pathway in the marine alphaproteobacteria *Silicibacter* sp. strain TrichCH4B, which contains both an active NOS protein (SiliNOS) and the H-NOX sensor (SiliH-NOX) with an associated HK (SiliHK). SiliHK is a hybrid HK containing a receiver domain, requiring an additional Hpt protein for phosphotransfer to an RR. The cognate signaling partners for SiliHK were identified by a combination of bioinformatics and phosphotransfer profiling, and the RR was characterized to be GGDEF diguanylate cyclase (SiliDGC). NO/H-NOX signaling activates SiliDGC activity and increases cyclic-di-GMP concentrations, resulting in increased biofilm formation. Unlike other organisms discussed above which senses NO from external sources, SiliNOS generates the NO in *Silicibacter*. SiliNOS activity is stimulated by an algal symbiont, *Trichodesmium erythraeum*. NO-induced biofilms in *Silicibacter* in the proximity of *T. erythraeum* poises the two species for nutrient exchange.

Chapter 3 is focused on the inhibition of HK by NO-bound H-NOX. NO activation of H-NOX proteins has been studied structurally and mechanistically, however, the mechanism of signal transduction between H-NOX and its associated HK is less well-understood. The H-NOX and HK pair from *S. oneidensis* was used as a model to study their interaction and gain further insight into HK inhibition. *So* H-NOX and *So* HK were demonstrated to form a complex, with increased affinity upon NO binding to *So* H-NOX. The binding interface between the two proteins was determined using hydrogen-deuterium exchange mass spectrometry, site-directed mutagenesis, and pull-down assays. The effect of proper H-NOX-HK complex formation on kinase activity was also investigated.

Chapter 4 discusses a novel class of bacterial NOS enzymes, initially discovered in the cyanobacteria *Synechococcus* sp. PCC 7335. SynNOS is a so-called "full-length" bacterial NOS, containing both the heme/oxidase and reductase domains, resembling mammalian NOS. It also contains a unique globin domain at the N-terminus with homology to bacterial flavohemoglobins. The SynNOS globin domain was characterized biochemically, and the role of this novel globin was explored.

References

1. Alderton, W. K., Cooper, C. E., and Knowles, R. G. (2001) Nitric oxide synthases: structure, function and inhibition. *Biochem. J.* **357**, 593–615
2. Bredt, D. S. (1999) Endogenous nitric oxide synthesis: biological functions and pathophysiology. *Free Radic. Res.* **31**, 577–596
3. Condorelli, R. A., Calogero, A. E., Vicari, E., Favilla, V., Morgia, G., Cimino, S., and La Vignera, S. (2013) Vascular regenerative therapies for the treatment of erectile dysfunction: Current approaches. *Andrology*. **1**, 533–540
4. Serafim, R. a M., Primi, M. C., Trossini, G. H. G., and Ferreira, E. I. (2012) Nitric oxide: state of the art in drug design. *Curr. Med. Chem.* **19**, 386–405
5. Srivastava, K., Bath, P. M. W., and Bayraktutan, U. (2012) Current therapeutic strategies to mitigate the eNOS dysfunction in ischaemic stroke. *Cell. Mol. Neurobiol.* **32**, 319–336
6. Friebe, A., Mergia, E., Dangel, O., Lange, A., and Koesling, D. (2007) Fatal gastrointestinal obstruction and hypertension in mice lacking nitric oxide-sensitive guanylyl cyclase. *Proc. Natl. Acad. Sci. U. S. A.* **104**, 7699–704
7. Macmicking, J., Xie, Q., and Nathan, C. (1997) Nitric Oxide and Macrophage Function. *Annu. Rev. Immunol.* **15**, 323–350
8. Dinerman, J. L., Lowenstein, C. J., and Snyder, S. H. (1993) Molecular Mechanisms of Nitric Oxide Regulation - Potential Relevance to Cardiovascular Disease. *Circ. Res.* **73**, 217–222
9. Bredt, D. S., and Snyder, S. H. (1992) Nitric oxide, a novel neuronal messenger. *Neuron*. **8**, 3–11
10. Adak, S., Bilwes, A. M., Panda, K., Hosfield, D., Aulak, K. S., McDonald, J. F., Tainer, J. A., Getzoff, E. D., Crane, B. R., and Stuehr, D. J. (2002) Cloning, expression, and characterization of a nitric oxide synthase protein from Deinococcus radiodurans. *Proc. Natl. Acad. Sci. U. S. A.* **99**, 107–112
11. Pant, K., Bilwes, A. M., Adak, S., Stuehr, D. J., and Crane, B. R. (2002) Structure of a nitric oxide synthase heme protein from Bacillus subtilis. *Biochemistry*. **41**, 11071–11079
12. Crane, B. R., Sudhamsu, J., and Patel, B. A. (2010) Bacterial nitric oxide synthases. *Annu. Rev. Biochem.* **79**, 445–470
13. Bird, L. E., Ren, J., Zhang, J., Foxwell, N., Hawkins, A. R., Charles, I. G., and Stammers, D. K. (2002) Crystal structure of SANOS, a bacterial nitric oxide synthase oxygenase

protein from Staphylococcus aureus. *Structure*. **10**, 1687–1696
14. Midha, S., Mishra, R., Aziz, M. A., Sharma, M., Mishra, A., Khandelwal, P., and Bhatnagar, R. (2005) Cloning, expression, and characterization of recombinant nitric oxide synthase-like protein from Bacillus anthracis. *Biochem. Biophys. Res. Commun.* **336**, 346–356
15. Johnson, E. G., Sparks, J. P., Dzikovski, B., Crane, B. R., Gibson, D. M., and Loria, R. (2008) Plant-pathogenic Streptomyces species produce nitric oxide synthase-derived nitric oxide in response to host signals. *Chem. Biol.* **15**, 43–50
16. Sudhamsu, J., and Crane, B. R. (2006) Structure and reactivity of a thermostable prokaryotic nitric-oxide synthase that forms a long-lived oxy-heme complex. *J. Biol. Chem.* **281**, 9623–9632
17. Agapie, T., Suseno, S., Woodward, J. J., Stoll, S., Britt, R. D., and Marletta, M. A. (2009) NO formation by a catalytically self-sufficient bacterial nitric oxide synthase from Sorangium cellulosum. *Proc. Natl. Acad. Sci. U. S. A.* **106**, 16221–16226
18. Healy, F. G., Wach, M., Krasnoff, S. B., Gibson, D. M., and Loria, R. (2000) The txtAB genes of the plant pathogen Streptomyces acidiscabies encode a peptide synthetase required for phytotoxin thaxtomin A production and pathogenicity. *Mol. Microbiol.* **38**, 794–804
19. Patel, B. A., Moreau, M., Widom, J., Chen, H., Yin, L., Hua, Y., and Crane, B. R. (2009) Endogenous nitric oxide regulates the recovery of the radiation-resistant bacterium Deinococcus radiodurans from exposure to UV light. *Proc. Natl. Acad. Sci.* **106**, 18183–18188
20. Gusarov, I., and Nudler, E. (2005) NO-mediated cytoprotection: instant adaptation to oxidative stress in bacteria. *Proc. Natl. Acad. Sci. U. S. A.* **102**, 13855–13860
21. Hochgräfe, F., Wolf, C., Fuchs, S., Liebeke, M., Lalk, M., Engelmann, S., and Hecker, M. (2008) Nitric oxide stress induces different responses but mediates comparable protein thiol protection in Bacillus subtilis and Staphylococcus aureus. *J. Bacteriol.* **190**, 4997–5008
22. Karow, D. S., Pan, D., Davis, J. H., Behrends, S., Mathies, R. A., and Marletta, M. A. (2005) Characterization of functional heme domains from soluble guanylate cyclase. *Biochemistry*. **44**, 16266–16274
23. Zhao, Y., Schelvis, J. P. M., Babcock, G. T., and Marletta, M. A. (1998) Identification of histidine 105 in the α1 subunit of soluble guanylate cyclase as the heme proximal ligand. *Biochemistry*. **37**, 4502–4509
24. Foerster, J., Harteneck, C., Malkewitz, J., Schultz, G., and Koesling, D. (1996) A functional heme-binding site of soluble guanylyl cyclase and pI subunits requires intact N-termini of aII. **386**, 380–386
25. Gilles-Gonzalez, M. a, Gonzalez, G., Perutz, M. F., Kiger, L., Marden, M. C., and Poyart, C. (1994) Heme-based sensors, exemplified by the kinase FixL, are a new class of heme protein with distinctive ligand binding and autoxidation. *Biochemistry*. **33**, 8067–73
26. Gilles-Gonzalez, M. A., and Gonzalez, G. (2005) Heme-based sensors: Defining characteristics, recent developments, and regulatory hypotheses. *J. Inorg. Biochem.* **99**, 1–22
27. Farhana, A., Saini, V., Kumar, A., Lancaster, J. R., and Steyn, A. J. C. (2012)

Environmental Heme-Based Sensor Proteins: Implications for Understanding Bacterial Pathogenesis. *Antioxid. Redox Signal.* **17**, 1232–1245
28. Derbyshire, E. R., and Marletta, M. A. (2009) Biochemistry of Soluble Guanylate Cyclase. in *cGMP: Generators, Effectors and Therapeutic Implications* (Schmidt, H. H. H. W., Hofmann, F., and Stasch, J.-P. eds), pp. 17–31, Springer Berlin Heidelberg, Berlin, Heidelberg, 10.1007/978-3-540-68964-5_2
29. Pellicena, P., Karow, D. S., Boon, E. M., Marletta, M. A., and Kuriyan, J. (2004) Crystal structure of an oxygen-binding heme domain related to soluble guanylate cyclases. *Proc. Natl. Acad. Sci. U. S. A.* **101**, 12854–12859
30. Karow, D. S., Pan, D., Tran, R., Pellicena, P., Presley, A., Mathies, R. A., and Marletta, M. A. (2004) Spectroscopic characterization of the soluble guanylate cyclase-like heme domains from Vibrio cholerae and Thermoanaerobacter tengcongensis. *Biochemistry*. **43**, 10203–10211
31. Boon, E. M., Davis, J. H., Tran, R., Karow, D. S., Huang, S. H., Pan, D., Miazgowicz, M. M., Mathies, R. a, and Marletta, M. a (2006) Nitric oxide binding to prokaryotic homologs of the soluble guanylate cyclase beta1 H-NOX domain. *J. Biol. Chem.* **281**, 21892–902
32. Ma, X., Sayed, N., Beuve, A., and van den Akker, F. (2007) NO and CO differentially activate soluble guanylyl cyclase via a heme pivot-bend mechanism. *EMBO J.* **26**, 578–588
33. Herzik, M. A., Jonnalagadda, R., Kuriyan, J., and Marletta, M. A. (2014) Structural insights into the role of iron-histidine bond cleavage in nitric oxide-induced activation of H-NOX gas sensor proteins. *Proc. Natl. Acad. Sci. U. S. A.* **111**, E4156-4164
34. Boon, E. M. E., Huang, S. H., and Marletta, M. A. M. M. A. (2005) A molecular basis for NO selectivity in soluble guanylate cyclase. *Nat. Chem. Biol.* **1**, 53–59
35. Erbil, W. K., Price, M. S., Wemmer, D. E., and Marletta, M. A. (2009) A structural basis for H-NOX signaling in Shewanella oneidensis by trapping a histidine kinase inhibitory conformation. *Proc. Natl. Acad. Sci. U. S. A.* **106**, 19753–19760
36. Winter, M. B., Herzik, M. A., Kuriyan, J., and Marletta, M. A. (2011) Tunnels modulate ligand flux in a heme nitric oxide/oxygen binding (H-NOX) domain. *Proc. Natl. Acad. Sci. U. S. A.* **108**, E881-889
37. Martin, E., Berka, V., Bogatenkova, E., Murad, F., and Tsai, A. L. (2006) Ligand selectivity of soluble guanylyl cyclase: Effect of the hydrogen-bonding tyrosine in the distal heme pocket on binding of oxygen, nitric oxide, and carbon monoxide. *J. Biol. Chem.* **281**, 27836–27845
38. Derbyshire, E. R., Deng, S., and Marletta, M. A. (2010) Incorporation of tyrosine and glutamine residues into the soluble guanylate cyclase heme distal pocket alters NO and O2 binding. *J. Biol. Chem.* **285**, 17471–17478
39. Olea Jr., C., Boon, E. M., Pellicena, P., Kuriyan, J., and Marletta, M. A. (2008) Probing the function of heme distortion in the H-NOX family. *ACS Chem. Biol.* **3**, 703–710
40. Weinert, E. E., Phillips-Piro, C. M., Tran, R., Mathies, R. a, and Marletta, M. a (2011) Controlling Conformational Flexibility of an O(2)-Binding H-NOX Domain. *Biochemistry*. **50**, 6832–6840
41. Weinert, E. E., Plate, L., Whited, C. A., Olea, C., and Marletta, M. A. (2010) Determinants of ligand affinity and heme reactivity in H-NOX domains. *Angew. Chemie* -

Int. Ed. **49**, 720–723
42. Hazelbauer, G. L., Falke, J. J., and Parkinson, J. S. (2008) Bacterial chemoreceptors: high-performance signaling in networked arrays. *Trends Biochem. Sci.* **33**, 9–19
43. Hespen, C. W., Bruegger, J. J., Phillips-Piro, C. M., and Marletta, M. A. (2016) Structural and Functional Evidence Indicates Selective Oxygen Signaling in Caldanaerobacter subterraneus H-NOX. *ACS Chem. Biol.* **11**, 2337–2346
44. Plate, L., and Marletta, M. A. (2013) Nitric oxide-sensing H-NOX proteins govern bacterial communal behavior. *Trends Biochem. Sci.* **38**, 566–575
45. Stock, A. M., Robinson, V. L., and Goudreau, P. N. (2000) Two-component signal transduction. *Annu. Rev. Biochem.* **69**, 183–215
46. Galperin, M. Y., Nikolskaya, A. N., and Koonin, E. V. (2001) Novel domains of the prokaryotic two-component signal transduction systems. *FEMS Microbiol. Lett.* **203**, 11–21
47. Arora, D. P., and Boon, E. M. (2012) Nitric oxide regulated two-component signaling in Pseudoalteromonas atlantica. *Biochem. Biophys. Res. Commun.* **421**, 521–526
48. Plate, L., and Marletta, M. A. (2012) Nitric Oxide Modulates Bacterial Biofilm Formation through a Multicomponent Cyclic-di-GMP Signaling Network. *Mol. Cell*. **46**, 449–460
49. Hengge, R. (2009) Principles of c-di-GMP signalling in bacteria. *Nat. Rev. Microbiol.* **7**, 263–273
50. Liu, N., Xu, Y., Hossain, S., Huang, N., Coursolle, D., Gralnick, J. A., and Boon, E. M. (2012) Nitric oxide regulation of cyclic di-GMP synthesis and hydrolysis in Shewanella woodyi. *Biochemistry*. **51**, 2087–2099
51. Carlson, H. K., Vance, R. E., and Marletta, M. A. (2010) H-NOX regulation of c-di-GMP metabolism and biofilm formation in Legionella pneumophila. *Mol. Microbiol.* **77**, 930–942
52. Dierks, E. A., Hu, S., Vogel, K. M., Yu, A. E., Spiro, T. G., and Burstyn, J. N. (1997) Demonstration of the Role of Scission of the Proximal Histidine-Iron Bond in the Activation of Soluble Guanylyl Cyclase through Metalloporphyrin Substitution Studies. *J. Am. Chem. Soc.* **119**, 7316–7323
53. Olea, C., Herzik, M. A., Kuriyan, J., and Marletta, M. A. (2010) Structural insights into the molecular mechanism of H-NOX activation. *Protein Sci.* **19**, 881–887
54. Schmidt, A. J., Ryjenkov, D. A., and Gomelsky, M. (2005) The ubiquitous protein domain EAL is a cyclic diguanylate-specific phosphodiesterase: Enzymatically active and inactive EAL domains. *J. Bacteriol.* **187**, 4774–4781
55. Camilli, A., and Bassler, B. L. (2006) Bacterial small-molecule signaling pathways. *Science*. **311**, 1113–6
56. Price, M. S., Chao, L. Y., and Marletta, M. A. (2007) Shewanella oneidensis MR-1 H-NOX regulation of a histidine kinase by nitric oxide. *Biochemistry*. **46**, 13677–13683
57. Zhu, J., and Mekalanos, J. J. (2003) Quorum sensing-dependent biofilms enhance colonization in Vibrio cholerae. *Dev. Cell*. **5**, 647–656
58. Faruque, S. M., Biswas, K., Udden, S. M. N., Ahmad, Q. S., Sack, D. A., Nair, G. B., and Mekalanos, J. J. (2006) Transmissibility of cholera: In vivo-formed biofilms and their relationship to infectivity and persistence in the environment. *Proc. Natl. Acad. Sci.* **103**, 6350–6355

59. Henares, B. M., Higgins, K. E., and Boon, E. M. (2012) Discovery of a nitric oxide responsive quorum sensing circuit in vibrio harveyi. *ACS Chem. Biol.* **7**, 1331–1336
60. Henares, B., Xu, Y., and Boon, E. (2013) A Nitric Oxide-Responsive Quorum Sensing Circuit in Vibrio harveyi Regulates Flagella Production and Biofilm Formation. *Int. J. Mol. Sci.* **14**, 16473–16484
61. Visick, K. L., and Ruby, E. G. (2006) Vibrio fischeri and its host: it takes two to tango. *Curr. Opin. Microbiol.* **9**, 632–638
62. Wang, Y., Dufour, Y. S., Carlson, H. K., Donohue, T. J., Marletta, M. A., and Ruby, E. G. (2010) H-NOX-mediated nitric oxide sensing modulates symbiotic colonization by Vibrio fischeri. *Proc. Natl. Acad. Sci. U. S. A.* **107**, 8375–8380
63. Davidson, S. K., Koropatnick, T. A., Kossmehl, R., Sycuro, L., and McFall-Ngai, M. J. (2004) NO means “yes” in the squid-vibrio symbiosis: Nitric oxide (NO) during the initial stages of a beneficial association. *Cell. Microbiol.* **6**, 1139–1151

CHAPTER 2:

NITRIC OXIDE MEDIATES BIOFILM FORMATION AND SYMBIOSIS IN *SILICIBACTER* SP. STRAIN TRICHCH4B*

Summary

In this chapter, the nitric oxide signaling pathway of the alphaproteobacteria *Silicibacter* sp. TrichCH4B was characterized. *Silicibacter* sp. TrichCH4B is the first bacteria reported to harbor both the NOS and H-NOX proteins, making it uniquely capable of both synthesizing and sensing NO, analogous to mammalian NO signaling. In *Silicibacter*, NO regulates an H-NOX-associated two-component signaling pathway and ultimately increases intracellular levels of the bacterial second messenger cyclic-di-GMP, which promotes biofilm formation. Additionally, NO synthesis is activated in *Silicibacter* by its algal symbiont, *Trichodesmium erythraeum*, revealing a novel role for NO in bacterial communication and symbiosis.

Introduction

Nitric oxide (NO) serves dual biological roles as both a signaling molecule and a cytotoxin (1–3). NO is synthesized by nitric oxide synthase (NOS), which has been extensively characterized in mammals. As a gaseous signaling molecule, NO can diffuse freely across cellular membranes to neighboring cells. For instance, in mammalian signaling, nanomolar concentrations of NO are generated by NOS in endothelial cells. This NO diffuses to neighboring smooth muscle cells, where NO activates soluble guanylate cyclase (sGC), leading to formation of the second messenger cyclic guanosine monophosphate (cGMP), which increases vasodilation (4, 5). sGC senses NO via a heme cofactor that selectively binds NO, but not O_2. The sGC heme domain is a member of the *h*eme-*n*itric oxide/*ox*ygen binding (H-NOX) protein family, which is also present in many bacteria, including a number of pathogens (6–8).

Besides its role in signaling, NO is also an important component in the host response to infection, acting as a cytotoxic antimicrobial agent when generated at localized micromolar concentrations (9, 10). H-NOX proteins are one of several bacterial NO sensors that mediate response to the gas, through conserved signaling mechanisms that regulate histidine kinases (HK) or diguanylate cyclases (DGC) contained within the same operon (8). H-NOX proteins in *Legionella pneumophila* and *Shewanella woodyi* inhibit biofilm formation by regulating the activity of a diguanylate cyclase/phosphodiesterase fusion protein that decreases levels of the bacterial second messenger cyclic diguanosine monophosphate (c-di-GMP) (11, 12). In

* The work described in this chapter was performed in collaboration with Dr. Brian C. Smith in Professor Michael A. Marletta's laboratory (UC Berkeley). B.C.S. aided in protein construct design and cloning. This work led to the following publication: Rao M, Smith BCS, & Marletta MA (2014) Nitric Oxide Mediates Biofilm Formation and Symbiosis in *Silicibacter* sp. Strain TrichCH4B. *mBio* 6: e00206-15.

Shewanella oneidensis, the H-NOX protein functions as a sensor protein for a HK, forming part of a bacterial two-component signaling pathway (13, 14). *S. oneidensis* contains a particularly complex NO-controlled multi-component regulatory network, in which the HK activity is inhibited by the NO-bound H-NOX, and the HK has three cognate response regulators (RR). Two of these RRs regulate biofilm formation by controlling c-di-GMP concentrations while the third RR acts as a transcriptional regulator that controls the signaling network in a positive feedback loop (14, 15). A similar signaling network is found in *Vibrio cholerae*, suggesting a broader role for H-NOX proteins as part of the bacterial defense mechanism to form biofilm as protection against NO toxicity (14). In *V. cholerae*, the NO sensed by the H-NOX is likely produced by mammalian NOS (mNOS) activity from the host, but for the rest of these bacteria the physiologically relevant source of NO for bacterial H-NOX signaling is unclear.

NOS catalyzes the conversion of arginine into NO and citrulline, consuming O_2 and NADPH as cosubstrates (9, 16, 17). mNOS contains an oxygenase domain responsible for catalysis, and a reductase domain involved in electron transfer. mNOS forms a complex with Ca^{2+}-calmodulin (CaM) that promotes electron transfer between the oxygenase and reductase domains. Electrons are transferred from NADPH via flavin adenine dinucleotide (FAD) and flavin mononucleotide (FMN) bound within the reductase domain, to the P450-type heme in the oxygenase domain. Through sequence searching of genome databanks, bacterial open reading frames coding for proteins with high sequence similarity to the oxygenase domain of mNOS have been discovered. These isolated bacterial oxygenase domains were initially characterized from *Deiniococcus radiodurans* and *Bacillus subtilis* (18, 19), and subsequently from pathogens such as *Bacillus anthracis* and *Staphylococcus aureus* (20, 21). In the presence of a separate flavin-containing reductase protein, these bacterial NOS homologs were shown to have NOS activity. This bacterially-derived NO has been proposed to protect against oxidative stress and antibiotics (18–20, 22). A full-length bacterial NOS containing a fused oxygenase and reductase domain in one polypeptide sequence was later discovered in *Sorangium cellulosum* (23). In contrast to mNOS, the reductase domain cofactors of *S. cellulosum* NOS (scNOS) are FAD and an iron-sulfur cluster (**Fig. 2.1**). The function of NO generated from scNOS remains unclear, and the physiological inputs that stimulate NOS activity in these bacteria are unknown. H-NOX proteins are well-characterized NO sensors; however, to date a bacterium known to encode both the NOS and H-NOX proteins for a full NO signaling pathway had not been characterized.

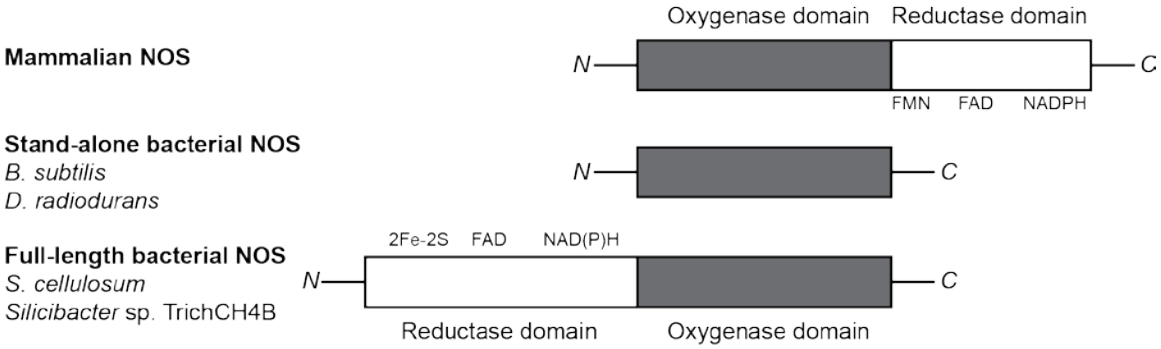

Figure 2.1. Comparison of mammalian and bacterial nitric oxide synthases domain architecture. The N- and C-termini and relative position of the identified NOS domains are indicated. The heme/oxygenase

domains are shown in gray, and the reductase domains are shown in white. Representative organisms with the stand-alone bacterial NOS oxygenase domain are indicated. *S. cellulosum* and *Silicibacter* sp. TrichCH4B are the only two known organisms to encode an NOS with an N-terminal reductase domain containing a 2Fe-2S cluster.

In this chapter, we report a novel NO signaling pathway in the alphaproteobacterium *Silicibacter* sp. TrichCH4B, which contains both a full-length NOS and an H-NOX NO sensor protein, resembling the mammalian NOS/sGC signaling system with NOS-derived NO binding to the H-NOX to activate downstream signaling. Additionally, the H-NOX of *Silicibacter* sp. TrichCH4B is encoded adjacent to a histidine kinase, suggesting involvement in a two-component signaling pathway. While bacterial NOS and H-NOX proteins have separately been shown to sense and defend against NO, in *Silicibacter* sp. TrichCH4B NO acts as a signaling molecule that controls biofilm formation through a two-component phospho-relay system. Furthermore, the NO signaling pathway in *Silicibacter* sp. TrichCH4B is activated through interaction with its algal symbiont *Trichodesmium erythraeum*, indicating that NO plays a previously unknown role in bacterial communication.

Experimental Procedures

SiliNOSox, SiliH-NOX, SiliHK, and SiliHpt Expression and Purification

Plasmids containing the desired genes were transformed into *E. coli* BL21(DE3) cells. Expression cultures were grown at 37°C, induced with 1 mM of IPTG at OD_{600} ~ 0.6, and grown at 18°C for 20-22 hours. Cells were pelleted and resuspended in lysis buffer (for SiliNOSox: 50 mM sodium phosphate pH 8.0, 150 mM NaCl, 10% v/v glycerol, 10 mM imidazole, 1 mM Pefabloc, 1 mM benzamidine; for all others: 50 mM diethanolamine (DEA) pH 8.0, 300 mM NaCl, 10% v/v glycerol, 10 mM imidazole, 1 mM Pefabloc, 1 mM benzamidine) and lysed by passage through a high-pressure homogenizer (Avestin). Cell debris was removed by centrifugation at 100,000×*g* for 30 min using an Optima XL-100K ultracentrifuge with a Ti-45 rotor (Beckman). The supernatant was loaded onto ~5 mL nickel resin (Ni-NTA Superflow from Qiagen) pre-equilibrated with wash buffer (for SiliNOSox: 50 mM sodium phosphate pH 8.0, 150 mM NaCl, 10% v/v glycerol, 10 mM imidazole; for all others: 50 mM DEA pH 8.0, 300 mM NaCl, 10% v/v glycerol, 10 mM imidazole). The resin was washed with 20 column volumes of wash buffer, and protein was eluted with 200 mM imidazole in wash buffer. Proteins were exchanged into storage buffer (wash buffer without imidazole) by dialysis, flash frozen in liquid nitrogen, and stored at -80°C.

GST-SiliHpt, SiliDGC, other RRs

For expression, plasmids containing the desired genes were transformed into *E. coli* BL21(DE3) pLysS cells (Life Technologies). Expression cultures were grown at 37°C, induced with 1 mM of IPTG at OD_{600} ~ 0.6, and grown at 20°C for 20-22 hr. Cell pellets were resuspended in lysis buffer (50 mM DEA pH 8.0, 300 mM NaCl, 10% v/v glycerol, 1 mM Pefabloc, 1 mM benzamidine). Supernatant was prepared in the same manner as described above and loaded onto ~5 mL glutathione resin (GE Healthcare) pre-equilibrated with wash buffer (50 mM DEA pH 8.0, 300 mM NaCl, 10% v/v glycerol). The resin was then washed with 10 column volumes of wash

buffer, and protein was eluted with 10 mM reduced glutathione in wash buffer. Proteins were exchanged into storage buffer (wash buffer without glutathione) by dialysis, flash frozen in liquid nitrogen, and stored at -80°C.

UV/Vis Spectroscopy

Spectra were collected on a Varian Cary 300 Bio UV/vis spectrophotometer. SiliNOSox was reduced to the ferrous (Fe^{2+}) state by addition of 1 mM $Na_2S_2O_4$ for 20 min at 25°C and desalted using a PD-10 column (GE Healthcare) equilibrated with deoxygenated buffer (50 mM sodium phosphate pH 8.0, 150 mM NaCl, 10% v/v glycerol). The protein was placed in a sealed anaerobic cuvette, and spectra were measured against a baseline of buffer from 200 to 700 nm. Fe^{2+}, Fe^{2+}-NO, and Fe^{2+}-CO SiliH-NOX were prepared as previously described (13), and spectra were collected in the same manner as SiliNOSox. Fe^{2+}-O_2 SiliH-NOX was not observed upon exposing the cuvette to oxygen, or upon addition of aerobic buffer to the protein sample.

SiliNOSox Single Turnover Assay

NO formation was measured using an NO Analyzer (NOA) (GE Analytical Instruments, Sievers model 270) as previously described (23). Briefly, reactions were carried out at room temperature in sealed Reacti-vials. A 40 µL final assay mix contained 500 µM *N*-hydroxy-arginine, 0 or 200 µM H_4B or H_4F, and 100 µM reduced SiliNOSox (Fe^{2+}) in 100 mM HEPES pH 7.4. Reduced SiliNOSox was prepared as described above. Reactions were initiated with 40 µL of aerobic buffer. NO formation was measured in 30 sec intervals by sampling 500 µL of Reacti-vial headspace using a gas-tight syringe (Hamilton) and injecting into the NOA reaction vessel. Each reaction was sampled 4 times.

SiliHK Autophosphorylation Assay

The kinase activity of SiliHK was assayed using ATPγS as previously described (24). Briefly, 5 µM of SiliHK was mixed with 5 mM $MgCl_2$ and 1 mM ATPγS in 50 mM DEA pH 8.0, 150 mM NaCl, 5% v/v glycerol in 20 µL reactions. Reactions were quenched with 2.5 µL of 500 mM EDTA, and 1.5 µL of 50 mM *para*-nitrobenzylmesylate (PNBM) was added to alkylate the thiophosphate and incubated for 1 hr at room temperature. Proteins were separated on 10-20% Tris-glycine SDS-PAGE gels (Life Technologies), and then transferred to nitrocellulose membranes (Whatman) and blocked with 5% w/v non-fat dry milk in phosphate buffered saline pH 8.0 with 0.5% v/v Tween 20 (PBST). Primary antibody specific for the alkylated thiophosphate ester (αPNBM) (Epitomics, monoclonal Ab 51-8) was added at 1:5000 dilution and incubated overnight at 4°C. The blot was then washed 3 times for 10 min each with PBST at room temperature. Secondary antibody, goat anti-rabbit HRP (Pierce) was then added at 1:1000 dilution and incubated at room temperature for 1 hr. The blot was then washed again 3 times for 10 min each with PBST at room temperature. The blot was developed using Luminata Classico Western HRP Substrate (Millipore) and imaged using a Chemidoc MP imager (BioRad).

SiliH-NOX/SiliHK Activity Assay

SiliHK (5 μM) was incubated with 30 μM Fe^{2+}, Fe^{2+}-NO, or Fe^{2+}-CO SiliH-NOX and 5 mM $MgCl_2$. The reaction buffer was the same as for the SiliHK autophosphorylation assays. Reactions were initiated with 1 mM ATPγS. The reaction was quenched at specified times, and data were collected as described above for the SiliHK autophosphorylation assays.

SiliHK/SiliHpt Phosphotransfer Assay

SiliHK (5 μM) was incubated with 10 μM SiliHpt and 5 mM $MgCl_2$. Reactions were initiated with 1 mM ATPγS. The reaction buffer was the same as for the SiliHK autophosphorylation assays. The reaction was quenched at specified times, and data were collected as described above for the SiliHK autophosphorylation assays.

Phosphotransfer Profiling of Orphan Response Regulators

Twelve orphan response regulators identified through the SMART database (25, 26) were tested for phosphotransfer from SiliHK/SiliHpt. SiliHK (15 μM) and GST-SiliHpt (5 μM) were pre-incubated with 1 mM ATP, 5 μCi [γ-^{32}P]ATP, and 5 mM $MgCl_2$ for 15 min, then desalted over a PD-10 column (GE Healthcare) to remove excess ATP. Each individual RR (10 μM) was then added to a separate reaction mix. At endpoints, reactions were quenched with 6× SDS loading dye, and the proteins were separated by SDS-PAGE. Gels were dried overnight on a slab gel dryer (Hoeffer Scientific Instruments), and dried gels were exposed overnight (16-20 hr) on a Kodak phosphorimaging plate. Data were collected on a Typhoon Phosphorimager at 100 μm resolution.

Diguanylate Cyclase Assay

Purified SiliDGC protein was incubated in 50 mM DEA pH 8.0, 150 mM NaCl, 5% v/v glycerol with 10 mM $MgCl_2$, and reactions were initiated by addition of 0.5 mM GTP. An internal HPLC standard, 0.5 mM tryptophan, was also included. Aliquots (10 μL) were quenched at different time points by addition of 25 μL trifluoroacetic acid (2% v/v in water). Quenched reaction volumes were adjusted to 100 μL, and the samples were filtered through a 0.2 μm spin filter and analyzed by HPLC on a Nova-Pak C18 4 μm (3.9 × 150 mm) column at a flow rate of 1 mL/min using the following gradient: 0-6 min: 100% 20 mM ammonium acetate; 6-7.5 min: 95% 20 mM ammonium acetate/5% v/v acetonitrile; 7.5-8.4 min: 85% 20 mM ammonium acetate/15% v/v acetonitrile; 8.4-9 min: 5% 20 mM ammonium acetate/95% v/v acetonitrile; 9.1-13.5 min: 100% 20 mM ammonium acetate. C-di-GMP concentration was calculated from peak integration and a standard curve of c-di-GMP. The c-di-GMP standard was synthesized enzymatically as previously described (14).

To examine the effects of phosphorylation on SiliDGC activity, phosphotransfer partners were included in the assay, SiliHK (15 μM) and SiliHpt (15 μM) were pre-phosphorylated with 0.5 mM ATP for 15 min. SiliDGC was then added to the reaction and incubated for 15 min before initiating reactions by the addition of 0.5 mM GTP. SiliDGC activity assays in the presence of beryllium fluoride were performed as previously described (14, 27). All experiments were performed in triplicate.

Crystal Violet Biofilm Assay

Biofilm assays with DETA-NONOate were performed in an anaerobic glove bag (Coy Laboratory Products) in 12-well polystyrene plates. *Silicibacter* sp. TrichCH4B was grown aerobically in Seawater Complete (SWC) media at 30°C overnight. Anaerobic SWC was inoculated with 100-fold diluted overnight cultures. Freshly prepared DETA-NONOate (Cayman Chemicals) in 10 mM NaOH was added at varying concentrations. Cells were grown statically at 25°C, and a 3 mL reference culture was grown for OD measurements and normalization. Biofilm formation was quantified after 20 hr and normalized to growth (OD_{600}). Crystal violet staining was performed in the same manner as previously described (14, 28). Measurement from individual wells were averaged and normalized to growth (OD_{600}).

Biofilm assays with concentrated *T. erythraeum* spent media (TSM) were performed aerobically to provide the necessary O_2 for NOS activity, in the same manner as above. Reported results are from the average of three 12-well experiments on separate days.

Trichodesmium erythraeum Growth and Spent Media Concentration

A non-axenic culture of *Trichodesmium erythraeum* IMS101 (obtained from D. Hutchins, University of Southern California) was grown at 25°C with a 12 hr light/dark cycle (70-100 $\mu E\ m^{-2}\ s^{-1}$) in a modified Aquil* medium (29). The modified medium is composed of: Synthetic Ocean Water (SOW) with 10 µM $NaH_2PO_4 \cdot H_2O$, 10 µM EDTA, 1 µM $FeCl_3 \cdot 6H_2O$, 79,7 nM $ZnSO_4 \cdot 7H_2O$, 121 nM $MnCl_2 \cdot 4H_2O$, 50.3 nM $CoCl_2 \cdot 6H_2O$, 100 nM $Na_2MoO_4 \cdot 2H_2O$, 297 nM thiamine, 2.25 nM biotin, and 0.37 nM cyanocobalamin. Cultures were diluted into fresh media (volume increased by 2-5 times each transfer) every 7 days. Spent media from 14-28 days of *T. erythraeum* culture growth was collected by filtration through a 0.2 µm filter, then concentrated 1000× by tangential flow filtration with a 5 kDa MWCO membrane (Millipore). Further concentration was performed using a Macrosep Advance centrifugal device (Pall) to obtain a final protein concentration of ~1 mg/mL.

Heat treatment of the concentrated spent media was performed by heating the solution for 5 min at 95°C. Protease treatment of the concentrated spent media was performed by adding Proteinase K (0.5 mg/mL final concentration) (Qiagen) according to the manufacturer's instructions.

Silicibacter sp. TrichCH4B NO Formation

Overnight cultures of *Silicibacter* sp. TrichCH4B was inoculated into 10 mL aerobic SWC media in sealed Hungate tubes. When examining the effects of *T. erythraeum* on NO formation by *Silicibacter* sp. TrichCH4B, TSM was added to the cultures in specified amounts. Cultures were grown with shaking for 20 hr at 30°C. 10 min before measuring NO, 1 mL of aerobic SWC media was delivered via syringe into the Hungate tubes to provide sufficient oxygen for the NOS reaction. Headspace (100 µL) was injected into an NO analyzer, and peaks were integrated using the NOAnalysis Software for relative quantification. All experiments were performed in triplicate.

Silicibacter sp. TrichCH4B RNA Preparation and Quantitative PCR

Cultures of *Silicibacter* sp. TrichCH4B (5 mL) were grown in the presence of varying amounts of TSM. Cells were harvested after 12 hr of growth. Total RNA was extracted using an RNeasy purification kit (Qiagen) according to the manufacturer's instructions. cDNA was synthesized from RNA with a SuperScript III Reverse Transcriptase kit according to the manufacturer's instructions (Life Technologies). Control reaction mixtures lacking reverse transcriptase were included to confirm the absence of contaminating genomic DNA. Quantitative PCR (qPCR) amplification of *siliNOS* was performed using SYBR Green (Life Technologies) with SiliNOS qPCR primers (Table 2.1) on a C1000 Thermal Cycler with a CFX96 Real-Time System (BioRad). A two-step amplification procedure was used: 95°C for 10 min, followed by 40 cycles of 95°C for 15 sec, then 55°C for 30 sec. Results were analyzed using the BioRad CFX Manager Software. Results were normalized relative to the level of expression of the housekeeping gene *rpoD* (30). The relative expression values represent the means ± standard deviations of triplicate samples from three independent experiments.

Table 2.1. Primers and plasmids used in this chapter.

Gene	Forward Primer	Reverse Primer	Vector
SiliNOSox	GGAATTCCATATGAGTCCTGA GCGGCTCCTTTGTG	ATAGTTTAGCGGCCGCCAATTTAG AAGGACCGGATATCATCTC	pET20b
SiliH-NOX	GGAATTCCATATGAAAGGTCT CATTTTCGTTGAGC	ATAGTTTAGCGGCCGCAGCCACCC AACGCACTG	pET20b
SiliHK	CATGCCATGGGTTCCAATGCT AATGGTAGC	ATAGTTTAGCGGCCGCTAGCGGTC CTTGGTCAGCAG	pET28b
SiliHpt	CACCATGATTGATTGGCCACG CGTACG	CCGCTCGAGTCAGGACATCGTTTT TACGTCAGCAAG	pDEST-15
SiliDGC	CACCGTGCAAGGCACGATCCT GGTCATA	CCGCTCGAGTCAGGCCGCCGCGCT TT	pDEST-15
SiliNOS qPCR	GAACTGCACCATCCAGACGAA	AACCGATCTCAGTACCCATGT	N/A

Results

SiliNOSox forms NO under single-turnover conditions

The NOS of *Silicibacter* sp. TrichCH4B (SiliNOS) was identified as a putative nitric oxide synthase through sequence homology to the mammalian NOS oxygenase domain, and to the full-length NOS in *Sorangium cellulosum* (scNOS) (23). SiliNOS has a similar domain architecture to scNOS, containing an N-terminal reductase domain with NAD(P)H and FAD-binding sites and a predicted 2Fe-2S cluster. Attempts to express full-length SiliNOS were unsuccessful, most likely due to improper folding of the 2Fe-2S cluster. Therefore, a SiliNOS oxygenase domain (SiliNOSox) construct, designed based on alignment with both the mammalian and *S. cellulosum* NOS proteins, was expressed and purified from *E. coli*.

The activity of SiliNOSox in the presence of oxygen, substrate, and other cofactors was investigated under single turnover conditions using *N*-hydroxy-arginine (NHA), the product of the first catalytic step of the NOS reaction, as a substrate. Following a similar protocol as previously described for scNOSox (oxygenase domain of scNOS) (23), the heme cofactor of SiliNOSox was reduced from the ferric to the ferrous state with a molar equivalent of dithionite, and the reduced SiliNOSox was incubated with NHA and cofactor tetrahydrobiopterin (H_4B) or tetrahydrofolate

(H_4F) under anaerobic conditions. Aerobic buffer was introduced to provide the O_2 required to initiate the reaction, and NO in the headspace was determined using a nitric oxide analyzer. NO was only detected in samples containing NHA, oxygen, and either H_4B or H_4F (**Fig. 2.2**), demonstrating that SiliNOSox is capable of synthesizing NO.

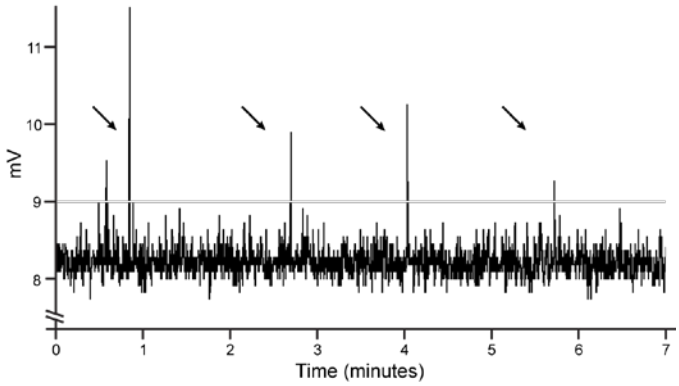

Figure 2.2. Single turnover NO formation by SiliNOSox. Representative NO Analyzer trace of a SiliNOSox single turnover experiment as described under Materials and Methods. A 40 μL assay contained ferrous SiliNOSox (100 μM) with 500 μM NHA and 200 μM H_4B in a sealed Reacti-vial, and the reaction was initiated by introducing aerobic buffer to provide the necessary oxygen for NOS activity. Reaction headspace was then injected into the NOA via a gastight syringe. Arrows indicate timing of injection of reaction headspace into the NOA.

SiliH-NOX binds nitric oxide but not oxygen

NO generated from SiliNOS could interact with the *Silicibacter* sp. TrichCH4B H-NOX protein (SiliH-NOX). SiliH-NOX was expressed and purified from *E. coli*. Purified SiliH-NOX contains a ferrous heme that forms stable NO and CO complexes, displaying spectra nearly identical to the H-NOX from *S. oneidensis* (SoH-NOX) (13) (**Fig. A.1**). Like SoH-NOX, SiliH-NOX has no measurable affinity to O_2, indicating that SiliH-NOX likely functions as a selective NO sensor.

NO-bound SiliH-NOX inhibits SiliHK histidine kinase activity

The gene encoding SiliH-NOX is located adjacent to a gene encoding a histidine kinase in the *Silicibacter* sp. TrichCH4B genome (SiliHK), suggesting that SiliH-NOX could function as a sensor for SiliHK. SiliHK is a hybrid histidine kinase, containing both a kinase and a receiver domain with an aspartic acid predicted to be the phosphoryl acceptor from the kinase domain (**Fig. A.2**). To test SiliHK autophosphorylation activity, SiliHK was incubated with ATPγS as a substrate. After quenching the ATPγS reaction with EDTA, the alkylating agent *para*-nitrobenzylmesylate (PNBM) was added, which alkylates thiophosphates and cysteines, and an antibody specific for the alkylated thiophosphate was then used to detect the resulting thiophosphate esters (24). SiliHK autophosphorylation activity was observed by immunoblotting (**Fig. 2.3A**).

Next, the effect of the SiliH-NOX ligation state on SiliHK autophosphorylation was investigated. Unliganded (Fe^{2+}) and ferrous-carbonyl (Fe^{2+}-CO) SiliH-NOX did not affect kinase

activity. However, the SiliH-NOX ferrous-nitrosyl (Fe^{2+}-NO) complex inhibited SiliHK autophosphorylation. At a five-fold excess of [Fe^{2+}-NO]-SiliH-NOX, SiliHK autophosphorylation was nearly completely inhibited (**Fig. 2.3B**), indicating that SiliHK is regulated by SiliH-NOX in an NO-dependent manner.

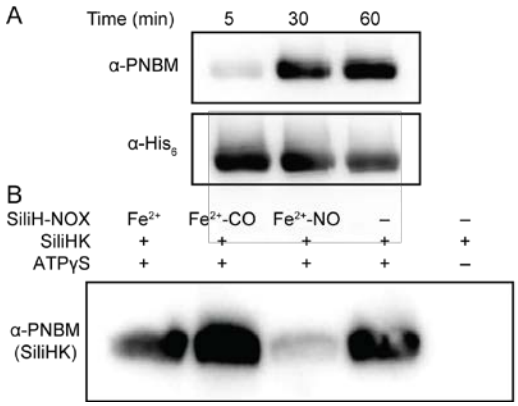

Figure 2.3. SiliHK autophosphorylation and regulation by SiliH-NOX. (**A**) Autophosphorylation of SiliHK. Kinase autophosphorylation assays were carried out with ATPγS, and aliquots were taken at 5, 30, and 60 min and analyzed by Western blot as described under Experimental Procedures. (**B**) Effect of SiliH-NOX on the kinase activity of SiliHK. Kinase assays containing 5 μM SiliHK were incubated for 30 min with 1 mM ATPγS in the presence 30 μM SiliH-NOX in the ligation states indicated. Samples were analyzed by Western blot as described under Experimental Procedures.

Phosphotransfer from SiliHK to SiliHpt and SiliDGC

SiliHK is a hybrid histidine kinase; therefore, a Histidine Phosphotransfer Protein (Hpt) is required to mediate phosphotransfer to its cognate response regulator (31). Using the SMART domain database (25, 26), searching the *Silicibacter* sp. TrichCH4B genome for stand-alone Hpt proteins resulted in only one gene, hereafter referred to as SiliHpt. Therefore, SiliHpt was cloned and then expressed and purified from *E. coli*.

Physiological cognate phosphotransfer partners are predicted to display fast phosphotransfer kinetics *in vitro* (32, 33). In phosphotransfer assays with both SiliHpt and SiliHK, SiliHpt phosphorylation was monitored by immunoblotting for PNBM adducts as previously described (24). SiliHpt phosphorylation was observed within 1 minute after assay initiation (**Fig. 2.4A**), consistent with the rapid transfer expected for an *in vivo* cognate pair (34).

Having determined that SiliHpt can serve as an intermediary between SiliHK and its cognate response regulator, we next searched for orphan response regulators within the *Silicibacter* sp. TrichCH4B genome using the SMART domain database. Orphan response regulators contain a receiver domain, but no histidine kinase in the same or nearby operons. Each of the 12 orphan response regulators discovered using this method was cloned, expressed and purified from *E. coli*, and then tested for phosphotransfer from SiliHK and SiliHpt (14, 35). SiliHK and SiliHpt were phosphorylated with [γ-^{32}P]ATP prior to addition of response regulator. Rapid (within 1 minute) loss of phosphorylation from both SiliHK and SiliHpt was observed for only one of the response regulators, SCH4B_1503 (**Fig. 2.4B**), whereas for the other response regulators, slow loss of

phosphorylation from SiliHK/SiliHpt occurred over 15 to 30 minutes (**Fig. A.3**). Likely due to the instability of phosphoaspartate esters (36), a phosphorylation signal for SCH4B_1503 was not observed. The SCH4B_1503 protein is annotated to contain a GGDEF domain found in diguanylate cyclases (37), and hereafter will be referred to as SiliDGC.

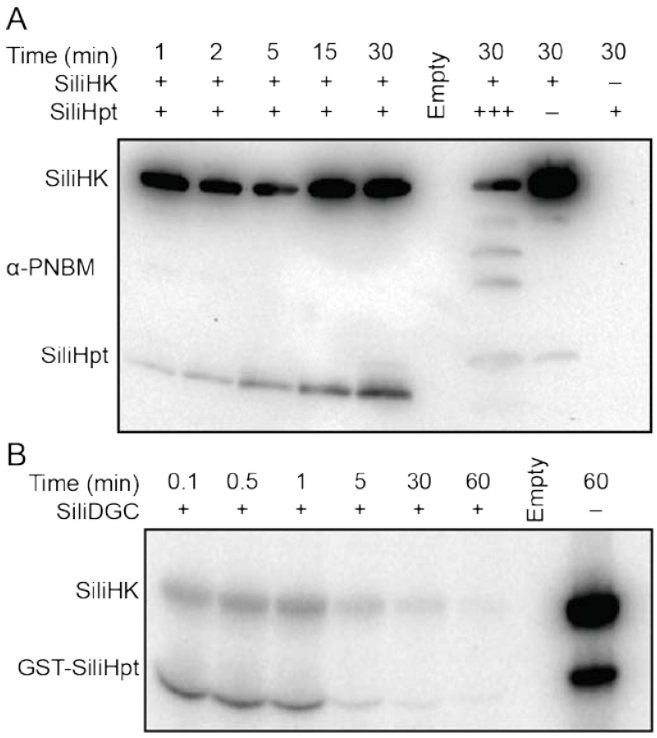

Figure 2.4. Phosphotransfer from SiliHK to its cognate partners. (**A**) Phosphotransfer between SiliHK and SiliHpt. SiliHK (5 μM) was mixed with SiliHpt (10 μM) in the presence of ATPγS (1 mM) for a 30 min time course as described under Experimental Procedures. SiliHPT phosphorylation was observed within 1 min. (**B**) Phosphotransfer from SiliHK/SiliHpt to SiliDGC. Loss of SiliHK/SiliHpt phosphorylation was used to monitor phosphotransfer to a cognate response regulator, SiliDGC. SiliHK and SiliHpt were mixed with 5 μCi [γ-32P]-ATP for 15 min, then desalted to remove excess ATP. SiliDGC (10 μM) was then added to the reaction mix for a 60 min time course as described under Experimental Procedures. SiliDGC was the only RR from a panel of twelve orphan RRs to cause rapid loss of SiliHK/SiliHpt phosphorylation (between 1 and 5 min).

Phosphorylation inhibits SiliDGC activity

Diguanylate cyclases catalyze the formation of c-di-GMP from two molecules of GTP. Sequence alignment with characterized diguanylate cyclases confirmed the presence of the conserved GGDEF active site residues in SiliDGC. To confirm that SiliDGC is a functional diguanylate cyclase, SiliDGC was recombinantly expressed and purified from *E. coli* and incubated with GTP. Formation of c-di-GMP was observed by HPLC, confirming that SiliDGC is an active diguanylate cyclase (**Fig. A.4**).

Phosphorylation of response regulator domains generally modulates the activity of the connected enzymatic or binding domains within the protein, and so we then investigated the effect

of response regulator phosphorylation on SiliDGC activity. When SiliDGC was incubated with SiliHK, SiliHpt, and ATP, the diguanylate cyclase activity decreased by ~40% (**Fig. 2.5A**). When any of the phosphotransfer components (*i.e.* SiliHpt or ATP) were omitted, the activity was similar to that of SiliDGC alone. Addition of the SiliHK D386A receiver domain mutant, which is incapable of phosphotransfer, in place of wild-type SiliHK also did not significantly inhibit SiliDGC activity (**Fig. 2.5A**). A similar trend was observed when SiliDGC was incubated with beryllium fluoride (BeF_x), a known phosphorylation mimic (27) that is not subject to hydrolysis and thus more stable compared to phosphorylation. Titration of increasing BeF_x concentrations resulted in decreasing levels of DGC activity, as SiliDGC activity decreased by ~80% in the presence of 0.5 mM BeF_x (**Fig. 2.5B**). Taken together, these results indicate that phosphorylation of SiliDGC by SiliHK/SiliHpt decreases SiliDGC activity and therefore should decrease cellular c-di-GMP levels.

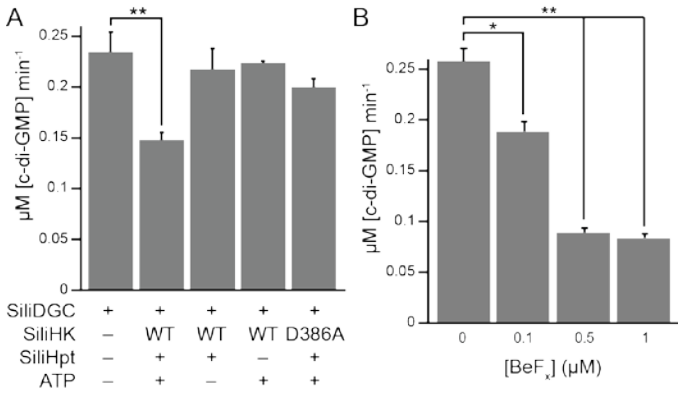

Figure 2.5. SiliDGC activity decreases in the presence of HK/HPT and ATP. (**A**) Phosphorylation of SiliDGC by SiliHK/SiliHpt inhibits SiliDGC activity. An assay containing 5 μM SiliDGC was incubated with some or all of the phosphotransfer components: SiliHK, SiliHpt, and ATP and c-di-GMP formation was monitored by HPLC as described under Materials and Methods. A receiver domain mutant of the histidine kinase, SiliHK D386A, which is incapable of phosphotransfer to SiliHPT was used as an additional control. Loss of SiliDGC activity was only observed with addition of all of the necessary phosphotransfer components: SiliHK, SiliHpt, and ATP. (**B**) SiliDGC is inhibited by a phosphorylation mimic. An assay containing 5 μM SiliDGC was incubated with the phosphorylation mimic, beryllium fluoride (BeF_x) for 15 min before the reaction was initiated, and c-di-GMP formation was monitored by HPLC as described under Materials and Methods. Loss of SiliDGC activity was observed with increasing BeF_x concentrations.
* indicates $p < 0.05$; ** indicates $p < 0.01$.

Silicibacter sp. TrichCH4B biofilm formation is induced by exogenous NO

Cyclic-di-GMP controls bacterial processes such as motility, cellular aggregation, and biofilm formation (38). In particular, NO-mediated control of c-di-GMP levels has been shown to regulate bacterial biofilm formation (11, 12, 14). We tested whether NO induces a similar effect in *Silicibacter* sp. TrichCH4B, as SiliH-NOX inhibits SiliHK, thereby relieving the inhibitory effects of phosphorylation on SiliDGC. Thus, NO is expected to lead to an overall increase in c-di-GMP levels and biofilm formation (see **Figure 2.7**). Static biofilm assays with *Silicibacter* sp. TrichCH4B were performed in an anaerobic chamber, with NO introduced via DETA-NONOate added to the growth medium at 0 to 200 μM concentrations. DETA-NONOate is a slow-release NO donor, with a $t_{½}$ of 56 hours at 25°C at pH 7 (39). Before measuring biofilm formation, cell

density was measured by OD_{600}, and the cells grew to similar density under all conditions tested. NO addition resulted in a two-fold increase in biofilm formation with 200 μM DETA-NONOate compared with no NO added, as measured by crystal violet staining (**Fig. 2.6A**).

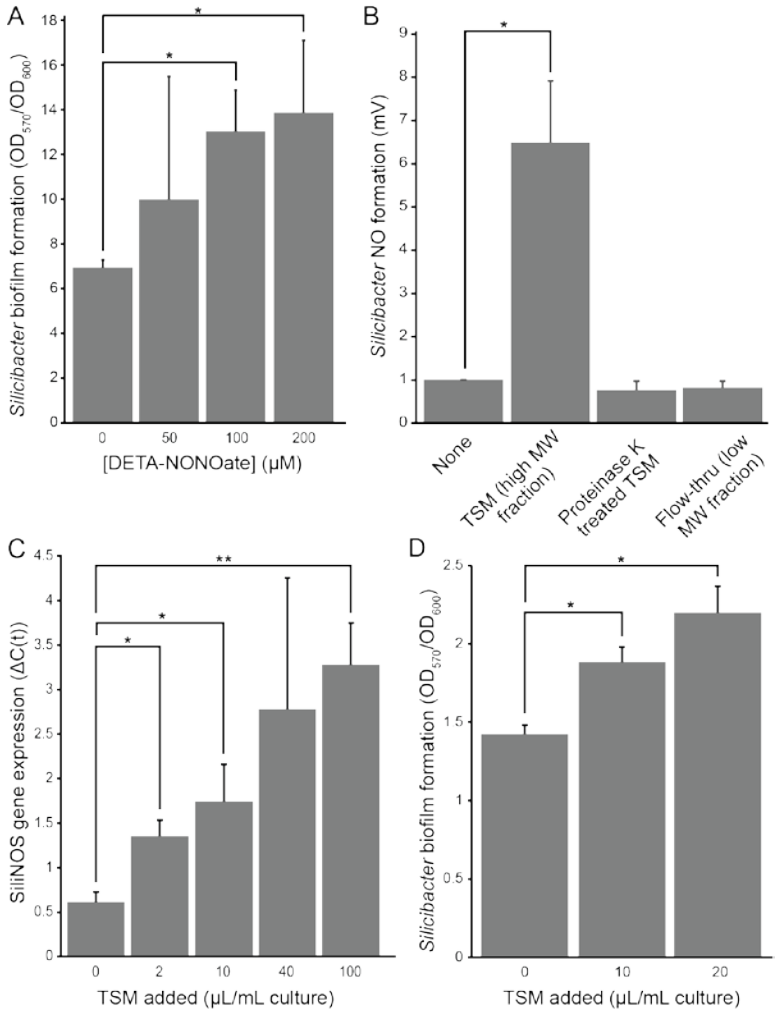

Figure 2.6. *Silicibacter* sp. TrichCH4B biological response to NO and *Trichodesmium erythraeum*. (**A**) Exogenous NO increases *Silicibacter* sp. TrichCH4B biofilm formation. Static biofilm assays were performed as described under Experimental Procedures. With increasing amounts of NO, *Silicibacter* sp. TrichCH4B formed more biofilm, as quantified by crystal violet staining (OD_{570}). Biofilm formation was normalize to growth (OD_{600}). (**B**) Addition of *T. erythraeum* spent media (TSM) increases *Silicibacter* sp. TrichCH4B NO formation. *Silicibacter* sp. TrichCH4B was grown anaerobically with TSM as described under Materials and Methods. To fully digest any proteins, TSM was also treated with Proteinase K before addition to *Silicibacter* sp. TrichCH4B. Only the TSM (high molecular weight fraction, or retentate, from a 5 kDa MWCO membrane filter) showed stimulation of NO formation by *Silicibacter* sp. TrichCH4B. (**C**) TSM addition increases *siliNOS* gene expression. *Silicibacter* sp. TrichCH4B was grown aerobically with varying amounts of TSM, and cDNA from *Silicibacter* sp. TrichCH4B mRNA was prepared as described under Materials and Methods. Expression of *siliNOS* (ΔC(t)) was calculated using BioRad CFX Manager with *rpoD* as a reference gene. *SiliNOS* gene expression increased with the amount of TSM added. (**D**) TSM addition increases *Silicibacter* sp. TrichCH4B biofilm formation. Static biofilm assays were

performed as described under Materials and Methods. *Silicibacter* sp. TrichCH4B biofilm increased upon increasing amount of TSM added, as quantified by crystal violet staining.
* indicates $p < 0.05$; ** indicates $p < 0.01$.

Silicibacter sp. TrichCH4B NO formation

To determine the factors that lead to NO synthesis and initiation of this novel bacterial signaling pathway, NO formation by *Silicibacter* sp. TrichCH4B was directly measured using a nitric oxide analyzer (**Fig. 2.6B**, first bar). The bacteria were grown anaerobically in sealed Hungate tubes, and before assaying the headspace for NO, a small volume of aerobic media was supplemented to provide sufficient oxygen for the O_2-dependent NOS reaction. Under anaerobic growth conditions in Seawater Complete media, *Silicibacter* sp. TrichCH4B produces NO. To confirm that the NO observed is produced by NOS, NO formation by two organisms that are closely related to *Silicibacter* sp. TrichCH4B, *Silicibacter* sp. TM1040 and *Dinoroseobacter shibae* FL-12 were also tested under the same conditions. These species do not encode a predicted NOS gene nor the NO-associated signaling pathway present in *Silicibacter* sp. TrichCH4B, and NO formation was not observed from either *Silicibacter* sp. TM1040 or *D. shibae* FL-12 (**Fig. A.5**).

T. erythraeum induces *Silicibacter* sp. TrichCH4B NO formation

Having established that NO regulates *Silicibacter* sp. TrichCH4B aggregation and biofilm formation, we next focused on the signal(s) that induce NO synthesis in *Silicibacter* sp. TrichCH4B. To determine the factors regulating SiliNOS activity, we turned to the natural habitat of the organism.

Silicibacter sp. TrichCH4B was originally isolated from colonies of the algae *T. erythraeum* as a symbiont (30). Therefore, we hypothesized that *T. erythraeum* regulates SiliNOS activity, and the effect of *T. erythraeum* on NO production by *Silicibacter* sp. TrichCH4B was tested. Cultures of *T. erythraeum* IMS101 were grown, and the cells were filtered over a 0.2 μm membrane to remove the *T. erythraeum* cells from the spent media, which was subsequently concentrated using a 5 kDa MWCO membrane. The concentrated *T. erythraeum* spent media (TSM) was added to *Silicibacter* sp. TrichCH4B cultures to test for stimulation of NOS activity. The high and low molecular weight fractions of the concentration (TSM, or retentate, and flow-through of the 5 kDa MWCO membrane, respectively) were added separately to *Silicibacter* sp. TrichCH4B cultures, and NO formation was measured using a nitric oxide analyzer. Cultures with the TSM, or high molecular weight fraction, exhibited a ~7-fold increase in NO formation over the samples with the flow-through (low molecular weight fraction), or without any additions (**Fig. 2.6B**, none vs. TSM). This demonstrates that *T. erythraeum* secretes a signaling agent captured in the TSM that induces NO production by SiliNOS.

To further characterize the stimulating factor of NO formation, TSM was treated with heat (95°C for 5 min) (data not shown) or protease (Proteinase K). *Silicibacter* sp. TrichCH4B cultures with TSM under both treatments did not show any stimulated NO formation (**Fig. 2.6B**). Thus, the stimulant of *Silicibacter* sp. TrichCH4B NO formation appears to be a secreted protein from the *T. erythaeum* culture that needs to be properly folded to stimulate NO formation.

T. erythraeum induces SiliNOS gene expression

To determine whether the stimulation of *Silicibacter* sp. TrichCH4B NO formation by *T. erythraeum* was regulated by gene expression or by direct activation of the SiliNOS enzyme, RT-qPCR was performed to examine the effect of TSM on *siliNOS* gene expression. Addition of increasing amounts of TSM correlated with increasing levels of *siliNOS* mRNA (**Fig. 2.6C**). The expression levels of a control gene, *rpoD* encoding RNA polymerase, were unchanged under all conditions. The observed increase in *siliNOS* gene expression correlated with the increase in NO formation by *Silicibacter* sp. TrichCH4B when grown with TSM (**Fig. 2.6B**), indicating that the stimulation of *Silicibacter* sp. TrichCH4B NO production occurs by inducing SiliNOS gene expression.

T. erythraeum spent media induces *Silicibacter* sp. TrichCH4B biofilm formation

Since TSM increases NO formation by *Silicibacter* sp. TrichCH4B, and NO induces biofilm formation, we tested whether TSM addition also increases *Silicibacter* sp. TrichCH4B biofilm formation. *Silicibacter* sp. TrichCH4B biofilm formation was quantified using the crystal violet staining assay as described above. Addition of TSM leads to increased *Silicibacter* sp. TrichCH4B biofilm formation in a concentration-dependent manner, confirming that *T. erythraeum* secreted protein(s) activate the NO signaling pathway and increase biofilm formation in *Silicibacter* sp. TrichCH4B (**Fig. 2.6D**).

Discussion

Silicibacter sp. TrichCH4B H-NOX signals through a conserved two-component signaling network

H-NOX signaling has been shown to regulate bacterial motility through control of cellular c-di-GMP levels, either by direct regulation of a diguanylate cyclase (11) or through a two-component signaling network (12, 14). In *Silicibacter* sp. TrichCH4B, NO-bound SiliH-NOX inhibits SiliHK autophosphorylation (**Fig. 2.3B**), as is the case with all other H-NOX-associated histidine kinases characterized thus far (8, 13). However, SiliHK is a hybrid histidine kinase that includes a receiver domain, and therefore requires an Hpt protein in order to complete phosphotransfer to the response regulator (**Fig. A.2**). The *Silicibacter* sp. TrichCH4B genome only encodes one annotated stand-alone Hpt protein, SiliHpt, which was found to be a phosphotransfer partner of SiliHK (**Fig. 2.4A**). The response regulator phosphorylated and controlled by SiliHK/SiliHpt was identified by examining the phosphotransfer kinetics between SiliHK/SiliHpt and a panel of twelve orphan response regulators in *Silicibacter* sp. TrichCH4B. To identify the cognate response regulator for SiliHK, we relied on the principle that *in vivo* cognate interaction partners are expected to exhibit fast (typically within 1 min) phosphotransfer kinetics *in vitro*, and only one orphan response regulator caused a rapid decrease in SiliHK/SiliHpt phosphorylation (**Fig. 2.4B**). This response regulator contains a GGDEF domain and was subsequently confirmed to be a diguanylate cyclase (SiliDGC) (**Fig. A.4**), and phosphorylation of the SiliDGC receiver domain inhibits SiliDGC diguanylate cyclase activity (**Fig. 2.5**). However, inhibition of SiliHK by NO-bound SiliH-NOX relieves the SiliDGC inhibition, resulting in higher c-di-GMP levels than when SiliHK is fully active (**Fig. 2.7**).

In *Shewanella oneidensis*, NO-bound H-NOX also inhibits the activity of its associated histidine kinase (13). In *S. oneidensis*, there are three cognate response regulators for the H-NOX-associated histidine kinase. One of the response regulators is an EAL-containing phosphodiesterase (PDE) that is responsible for hydrolyzing c-di-GMP. Phosphorylation was shown to stimulate PDE activity. Kinase inhibition by NO-bound H-NOX results in lower PDE phosphorylation and activity and, therefore, higher c-di-GMP levels (14). A similar signaling network was confirmed in *Vibrio cholerae*, in which the H-NOX-associated histidine kinase also phosphorylates a PDE (14). In the current study, the *Silicibacter* sp. TrichCH4B H-NOX/histidine kinase signaling network leads to the same overall response: NO signaling results in increased cellular c-di-GMP levels, through relief of phosphorylation-based inhibition of a diguanylate cyclase (SiliDGC).

Cyclic-di-GMP is an important bacterial second messenger, controlling various processes such as motility and biofilm formation (38). Typically, higher c-di-GMP levels result in increased biofilm formation, consistent with the phenotype exhibited by *Silicibacter* sp. TrichCH4B (**Fig. 2.6A** and **2.6D**), as well as *S. oneidensis* and *V. cholerae* (14). In addition to controlling a two-component signaling circuit, NO-bound H-NOX has been shown in *Legionella pneumophila* and *Shewanella woodyi* to directly control activity of an adjacent GGDEF and/or EAL-containing protein (11, 12). Thus, NO/H-NOX control of bacterial biofilm through c-di-GMP regulation may be more universal than previously thought, leading to increased understanding of factors governing bacterial communal behavior.

Silicibacter sp. TrichCH4B: first characterized bacterium with NOS-Dependent H-NOX pathway

Silicibacter sp. TrichCH4B is unique among the aforementioned bacteria in that, in addition to the NO-sensing H-NOX, the *Silicibacter* sp. TrichCH4B genome also encodes for a full-length nitric oxide synthase (SiliNOS). SiliNOS was identified through a BLAST search using the oxygenase domain of human iNOS, along with other predicted NOS homologues in bacteria and mammals, including the NOS from *S. cellulosum* (42% sequence identity), which shares the same domain architecture as SiliNOS (23) (**Fig. 2.1**). SiliNOS has a putative N-terminal reductase domain and a predicted NOS oxygenase domain at the C-terminus. The reductase domain contains the subdomains of a FAD and NAD(P)H binding ferredoxin reductase and a 2Fe-2S cluster-binding bacterioferritin-associated ferredoxin. In contrast, mammalian NOS reductase domains resemble cytochrome *c* reductase and other P450 reductases, with FAD, FMN, and NADPH-binding subdomains. Many bacterial NOS proteins (*e.g.* from *Bacillus*, *Staphylococcus*, and *Geobacillus* species) contain only the oxygenase domain without a fused reductase domain. In those organisms, an independent reductase protein is required for NO synthesis (18, 22). Thus, the oxygenase domain appears to be the common ancestor for bacterial and mammalian NOS, and variants have evolved to include different reductase domains, or remain without a fused reductase.

To date, NO signaling in NOS-containing bacteria is not well understood. Proposed functions for bacterial NOS proteins include protection against oxidative stress and antibiotics (20, 40–42), but in most bacteria, the biological role of NO synthesized by bacterial NOS is unknown. As mentioned above, bacterial H-NOX proteins regulate bacterial biofilm formation through

control of cellular c-di-GMP levels. For these H-NOX-containing bacteria, the source of NO is likely from the host immune system or the environment, such as surrounding soil (8).

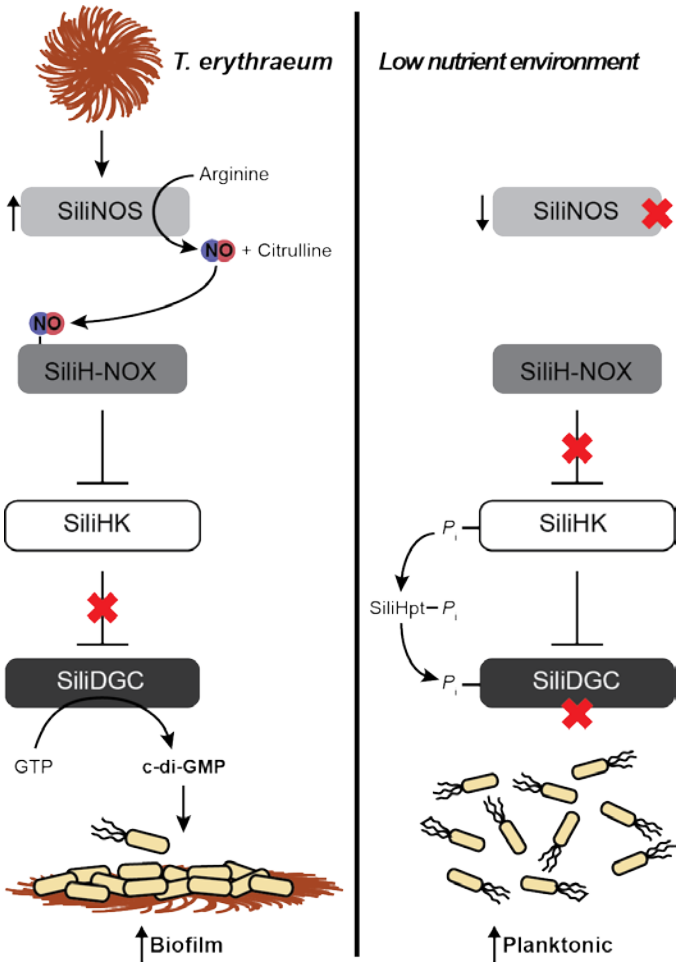

Figure 2.7. *Silicibacter* sp. TrichCH4B NO signaling summary. *Left*: SiliNOS is activated by a secreted *T. erythraeum* protein through a currently-unknown mechanism. NO-bound SiliH-NOX inhibits SiliHK autophosphorylation activity. Loss of phosphorylation on SiliDGC leads to increased diguanylate cyclase activity, resulting in higher c-di-GMP levels and biofilm formation. *Right*: In the absence of *T. erythraeum*, SiliNOS expression is reduced, which relieves inhibition of SiliHK autophosphorylation by SiliH-NOX. The resulting increase in SiliDGC phosphorylation via SiliHpt leads to decreased activity and lower c-di-GMP levels, and therefore less biofilm formation and more planktonic cells as a result.

In mammals, NO from NOS activates production of the mammalian second messenger cGMP by sGC. In *Silicibacter* sp. TrichCH4B, NO leads to increased levels of the bacterial second messenger c-di-GMP. *Silicibacter* sp. TrichCH4B is the first characterized bacteria with a complete NO signaling system, in which the bacterial H-NOX responds to NO synthesized by the bacteria, instead of NO from the environment. The clear parallels between mammalian and *Silicibacter* sp. TrichCH4B NO signaling pathways suggest a bacterial evolutionary origin for mammalian NO signaling. Although *Silicibacter* sp. TrichCH4B is the only organism so far with characterized NOS and H-NOX proteins, the large number of new bacterial genome sequences

will likely reveal additional organisms that have similar pathways, increasing our understanding of the emergence of current NO signaling systems in bacteria and mammals.

Silicibacter sp. TrichCH4B NO signaling is induced by *Trichodesmium erythraeum*

Silicibacter sp. TrichCH4B was originally isolated from colonies of the algae *Trichodesmium*, a filamentous cyanobacteria. The genus *Trichodesmium* has gained large scientific interest as one of the major diazotrophic (dinitrogen-fixing) species in the ocean (43) and is capable of doing so in a low-nutrient marine environment. Thus, *Trichodesmium* algae colonies provide a nutrient-rich environment that supports a variety of bacteria. The symbiotic interactions between *Trichodesmium* and associated bacteria are of great interest, as these bacteria are essential to the ecology of algae and N_2 fixation as well as maintaining a balanced ocean ecosystem (44–46).

Previous studies have shown that the bacteria, including *Silicibacter* sp. TrichCH4B, provide *Trichodesmium* with essential minerals and metals (such as iron), indicating a symbiotic relationship (46, 47). However, the specific signaling mechanisms between *Trichodesmium* and associated bacteria have not been explored. Here, we found that NO production by *Silicibacter* sp. TrichCH4B is stimulated by the presence of concentrated spent media from a growing *T. erythraeum* culture (TSM) (**Fig. 2.6B**). Accordingly, *Silicibacter* sp. TrichCH4B biofilm also increases with addition of TSM (**Fig. 2.6D**). Quantitative real-time PCR experiments show that TSM increases *siliNOS* gene expression (**Fig. 2.6C**), indicating induction at the transcription level. Protease and heat treatments of TSM remove any stimulation of *Silicibacter* sp. TrichCH4B NO production, suggesting that the activator of *Silicibacter* sp. TrichCH4B NO production is a secreted protein (**Fig. 2.6B**). Current efforts are directed at identification of this *T. erythraeum* signaling protein.

Other bacteria in the *Roseobacter* clade, which includes *Silicibacter* sp. TrichCH4B, are symbiotic with dinoflagellates and practice a “swim or stick” lifestyle, in which they switch from sessile to motile phases depending upon the presence of their algal symbiont (48, 49). *Silicibacter* sp. TrichCH4B and *T, erythraeum* appear to have a similar mechanism for symbiosis – when *Silicibacter* sp. TrichCH4B is in the vicinity of *T. erythraeum*, it senses a *T. erythraeum* secreted signaling protein that induces *siliNOS* gene expression and thus, increased NO formation. NO activates the H-NOX signaling pathway, leading to higher levels of cellular c-di-GMP and biofilm formation, most likely on the *T. erythraeum* colonies, poising the two species for nutrient exchange and improved growth and production processes (**Fig. 2.7**). The *Silicibacter* sp. TrichCH4B NO signaling pathway may be key to the symbiosis between the two organisms, revealing a new role for NO in bacterial signaling and communication.

References

1. Dinerman, J. L., Lowenstein, C. J., and Snyder, S. H. (1993) Molecular Mechanisms of Nitric Oxide Regulation - Potential Relevance to Cardiovascular Disease. *Circ. Res.* **73**, 217–222

2. Moncada, S., Palmer, R., and Higgs, E. (1991) Nitric oxide: physiology, pathophysiology, and pharmacology. *Pharmacol. Rev.* **43**, 109–142
3. Kerwin, J. F., Lancaster, J. R., and Feldman, P. R. (1995) Nitric Oxide: A New Paradigm for Second Messengers. *J. Med. Chem.* **38**, 4343–4362
4. Ignarro, L. J., Cirino, G., Casini, A., and Napoli, C. (1999) Nitric Oxide as a Signaling Molecule in the Vascular System: An Overview. *J. Cardiovasc. Pharmacol.* **34**, 879–886
5. Bredt, D. S., and Snyder, S. H. (1992) Nitric oxide, a novel neuronal messenger. *Neuron*. **8**, 3–11
6. Pellicena, P., Karow, D. S., Boon, E. M., Marletta, M. A., and Kuriyan, J. (2004) Crystal structure of an oxygen-binding heme domain related to soluble guanylate cyclases. *Proc. Natl. Acad. Sci. U. S. A.* **101**, 12854–12859
7. Karow, D. S., Pan, D., Tran, R., Pellicena, P., Presley, A., Mathies, R. A., and Marletta, M. A. (2004) Spectroscopic characterization of the soluble guanylate cyclase-like heme domains from Vibrio cholerae and Thermoanaerobacter tengcongensis. *Biochemistry*. **43**, 10203–10211
8. Plate, L., and Marletta, M. A. (2013) Nitric oxide-sensing H-NOX proteins govern bacterial communal behavior. *Trends Biochem. Sci.* **38**, 566–575
9. Alderton, W. K., Cooper, C. E., and Knowles, R. G. (2001) Nitric oxide synthases: structure, function and inhibition. *Biochem. J.* **357**, 593–615
10. Macmicking, J., Xie, Q., and Nathan, C. (1997) Nitric Oxide and Macrophage Function. *Annu. Rev. Immunol.* **15**, 323–350
11. Carlson, H. K., Vance, R. E., and Marletta, M. A. (2010) H-NOX regulation of c-di-GMP metabolism and biofilm formation in Legionella pneumophila. *Mol. Microbiol.* **77**, 930–942
12. Liu, N., Xu, Y., Hossain, S., Huang, N., Coursolle, D., Gralnick, J. A., and Boon, E. M. (2012) Nitric oxide regulation of cyclic di-GMP synthesis and hydrolysis in Shewanella woodyi. *Biochemistry*. **51**, 2087–2099
13. Price, M. S., Chao, L. Y., and Marletta, M. A. (2007) Shewanella oneidensis MR-1 H-NOX regulation of a histidine kinase by nitric oxide. *Biochemistry*. **46**, 13677–13683
14. Plate, L., and Marletta, M. A. (2012) Nitric Oxide Modulates Bacterial Biofilm Formation through a Multicomponent Cyclic-di-GMP Signaling Network. *Mol. Cell*. **46**, 449–460
15. Plate, L., and Marletta, M. A. (2013) Phosphorylation-dependent derepression by the response regulator HnoC in the Shewanella oneidensis nitric oxide signaling network. *Proc. Natl. Acad. Sci. U. S. A.* **110**, E4648–E4657
16. Hurshman, A. R., and Marletta, M. A. (2002) Reactions catalyzed by the heme domain of inducible nitric oxide synthase: evidence for the involvement of tetrahydrobiopterin in electron transfer. *Biochemistry*. **41**, 3439–3456
17. Marletta, M. A., Hurshman, A. R., and Rusche, K. M. (1998) Catalysis by nitric oxide synthase. *Curr. Opin. Chem. Biol.* **2**, 656–663
18. Adak, S., Bilwes, A. M., Panda, K., Hosfield, D., Aulak, K. S., McDonald, J. F., Tainer, J. A., Getzoff, E. D., Crane, B. R., and Stuehr, D. J. (2002) Cloning, expression, and characterization of a nitric oxide synthase protein from Deinococcus radiodurans. *Proc. Natl. Acad. Sci. U. S. A.* **99**, 107–112

19. Pant, K., Bilwes, A. M., Adak, S., Stuehr, D. J., and Crane, B. R. (2002) Structure of a nitric oxide synthase heme protein from Bacillus subtilis. *Biochemistry*. **41**, 11071–11079
20. Shatalin, K., Gusarov, I., Avetissova, E., Shatalina, Y., McQuade, L. E., Lippard, S. J., and Nudler, E. (2008) Bacillus anthracis-derived nitric oxide is essential for pathogen virulence and survival in macrophages. *Proc. Natl. Acad. Sci. U. S. A.* **105**, 1009–1013
21. Kuroda, M., Ohta, T., Uchiyama, I., Baba, T., Yuzawa, H., Kobayashi, I., Cui, L., Oguchi, A., Aoki, K., Nagai, Y., Lian, J., Ito, T., Kanamori, M., Matsumaru, H., Maruyama, A., Murakami, H., Hosoyama, A., Mizutani-Ui, Y., Takahashi, N. K., Sawano, T., Inoue, R., Kaito, C., Sekimizu, K., Hirakawa, H., Kuhara, S., Goto, S., Yabuzaki, J., Kanehisa, M., Yamashita, A., Oshima, K., Furuya, K., Yoshino, C., Shiba, T., Hattori, M., Ogasawara, N., Hayashi, H., and Hiramatsu, K. (2001) Whole genome sequencing of meticillin-resistant Staphylococcus aureus. *Lancet*. **357**, 1225–1240
22. Crane, B. R., Sudhamsu, J., and Patel, B. A. (2010) Bacterial nitric oxide synthases. *Annu. Rev. Biochem.* **79**, 445–470
23. Agapie, T., Suseno, S., Woodward, J. J., Stoll, S., Britt, R. D., and Marletta, M. A. (2009) NO formation by a catalytically self-sufficient bacterial nitric oxide synthase from Sorangium cellulosum. *Proc. Natl. Acad. Sci. U. S. A.* **106**, 16221–16226
24. Carlson, H. K., Plate, L., Price, M. S., Allen, J. J., Shokat, K. M., and Marletta, M. A. (2010) Use of a semisynthetic epitope to probe histidine kinase activity and regulation. *Anal. Biochem.* **397**, 139–143
25. Letunic, I., Doerks, T., and Bork, P. (2012) SMART 7: recent updates to the protein domain annotation resource. *Nucleic Acids Res.* **40**, D302–D305
26. Schultz, J., Milpetz, F., Bork, P., and Ponting, C. P. (1998) SMART, a simple modular architecture research tool: identification of signaling domains. *Proc. Natl. Acad. Sci. U. S. A.* **95**, 5857–5864
27. Yan, D., Cho, H. S., Hastings, C. A., Igo, M. M., Lee, S. Y., Pelton, J. G., Stewart, V., Wemmer, D. E., and Kustu, S. (1999) Beryllofluoride mimics phosphorylation of NtrC and other bacterial response regulators. *Proc. Natl. Acad. Sci. U. S. A.* **96**, 14789–14794
28. Lassak, J., Henche, A.-L., Binnenkade, L., and Thormann, K. M. (2010) ArcS, the cognate sensor kinase in an atypical Arc system of Shewanella oneidensis MR-1. *Appl. Environ. Microbiol.* **76**, 3263–3274
29. Sunda, W., Price, N., and Morel, F. (2005) Trace metal ion buffers and their use in culture studies. *Algal Cult. Tech.*
30. Roe, K. L. (2012) *Microbial iron cycling on Trichodesmium colonies: laboratory culture studies of Trichodesmium and associated model organisms*. Ph.D. thesis, UC San Diego, b7276570
31. West, A. H., and Stock, A. M. (2001) Histidine kinases and response regulator proteins in two-component signaling systems. *Trends Biochem. Sci.* **26**, 369–376
32. Laub, M. T., and Goulian, M. (2007) Specificity in two-component signal transduction pathways. *Annu. Rev. Genet.* **41**, 121–145
33. Podgornaia, A. I., and Laub, M. T. (2013) Determinants of specificity in two-component signal transduction. *Curr. Opin. Microbiol.* **16**, 156–162
34. Laub, M. T., Biondi, E. G., and Skerker, J. M. (2007) Phosphotransfer profiling:

systematic mapping of two-component signal transduction pathways and phosphorelays. *Methods Enzymol.* **423**, 531–48

35. Laub, M. T., Biondi, E. G., and Skerker, J. M. (2007) Phosphotransfer Profiling: Systematic Mapping of Two-Component Signal Transduction Pathways and Phosphorelays. *Methods Enzymol.* **423**, 531–548
36. Attwood, P. V., Besant, P. G., and Piggott, M. J. (2011) Focus on phosphoaspartate and phosphoglutamate. *Amino Acids*. **40**, 1035–1051
37. Ryjenkov, D. A., Tarutina, M., Moskvin, O. V, and Gomelsky, M. (2005) Cyclic Diguanylate Is a Ubiquitous Signaling Molecule in Bacteria: Insights into Biochemistry of the GGDEF Protein Domain. *J. Bacteriol.* **187**, 1792–1798
38. Hengge, R. (2009) Principles of c-di-GMP signalling in bacteria. *Nat. Rev. Microbiol.* **7**, 263–273
39. Hrabie, J. A. A., Klose, J. R. R., Wink, D. A. A., and Keefer, L. K. K. (1993) New nitric oxide-releasing zwitterions derived from polyamines. *J. Org. Chem.* **58**, 1472–1476
40. Gusarov, I., and Nudler, E. (2005) NO-mediated cytoprotection: instant adaptation to oxidative stress in bacteria. *Proc. Natl. Acad. Sci. U. S. A.* **102**, 13855–13860
41. Gusarov, I., Shatalin, K., Starodubtseva, M., and Nudler, E. (2009) Endogenous nitric oxide protects bacteria against a wide spectrum of antibiotics. *Science (80-.).* **325**, 1380–1384
42. Johnson, E. G., Sparks, J. P., Dzikovski, B., Crane, B. R., Gibson, D. M., and Loria, R. (2008) Plant-pathogenic Streptomyces species produce nitric oxide synthase-derived nitric oxide in response to host signals. *Chem. Biol.* **15**, 43–50
43. Bergman, B., Sandh, G., Lin, S., Larsson, J., and Carpenter, E. J. (2013) Trichodesmium - a widespread marine cyanobacterium with unusual nitrogen fixation properties. *FEMS Microbiol. Rev.* **37**, 286–302
44. Janson, S., Bergman, B., Carpenter, E. J., Giovannoni, S. J., and Vergin, K. (1999) Genetic analysis of natural populations of the marine diazotrophic cyanobacterium Trichodesmium. *FEMS Microbiol. Ecol.* **30**, 57–65
45. Hmelo, L., Van Mooy, B., and Mincer, T. (2012) Characterization of bacterial epibionts on the cyanobacterium Trichodesmium. *Aquat. Microb. Ecol.* **67**, 1–14
46. Thompson, A. W., and Zehr, J. P. (2013) Cellular interactions: lessons from the nitrogen-fixing cyanobacteria. *J. Phycol.* **49**, 1024–1035
47. Roe, K. L., Barbeau, K., Mann, E. L., and Haygood, M. G. (2012) Acquisition of iron by Trichodesmium and associated bacteria in culture. *Environ. Microbiol.* **14**, 1681–1695
48. Sule, P., and Belas, R. (2012) A novel inducer of Roseobacter motility is also a disruptor of algal symbiosis. *J. Bacteriol.* **195**, 637–646
49. Miller, T. R., and Belas, R. (2006) Motility is involved in Silicibacter sp. TM1040 interaction with dinoflagellates. *Environ. Microbiol.* **8**, 1648–59

CHAPTER 3:

NITRIC OXIDE-INDUCED CONFORMATIONAL CHANGES GOVERN H-NOX AND HISTIDINE KINASE INTERACTION AND REGULATION IN *SHEWANELLA ONEIDENSIS*[†]

Summary

In this chapter, the H-NOX and HK signaling pair from *Shewanella oneidensis* MR-1 was characterized. The N-terminal domain in *So* HK was determined as the site of H-NOX interaction, and the binding interface on *So* H-NOX was identified using a combination of hydrogen-deuterium exchange mass spectrometry and surface-scanning mutagenesis. Binding kinetics measurements and analytical gel filtration revealed that NO-bound *So* H-NOX has a tighter affinity for *So* HK compared with H-NOX in the unliganded state, correlating binding affinity with kinase inhibition. Kinase activity assays with binding-deficient H-NOX mutants further indicate that while formation of the H-NOX-HK complex is required to stabilize the HK, H-NOX conformational changes upon NO-binding are necessary for HK inhibition.

Introduction

Bacterial biofilm formation occurs when cells switch from motile, single-cell growth to a sessile, surface-attached lifestyle (1). Bacteria within biofilms are resistant to adverse environmental factors or antibiotics as a result of encapsulation within a robust extracellular polysaccharide matrix (2). Bacterial biofilm formation is directly correlated with intracellular levels of cyclic-di-GMP, which is synthesized by diguanylate cyclases (DGC) and hydrolyzed by phosphodiesterases (PDE) (3–6). Since biofilms play a key role in sustaining microbial infections, pathways affecting cyclic-di-GMP signaling have attracted interest as therapeutic targets (7).

Bacterial biofilm formation is influenced by several factors, including nitric oxide (NO) (8, 9). NO signaling in bacteria has been shown to contribute to regulation of cyclic-di-GMP levels that activate biofilm formation. Although NO is a required signaling molecule for processes such as vasodilation and neurotransmission in mammals (10–12), it is also utilized in large amounts as a cytotoxic agent released by macrophages during the host response to infection (13). As such, it

[†] The work described in this chapter was performed in collaboration with Mark A. Herzik, Ph.D. in Professor Michael A. Marletta's laboratory (UC Berkeley), and Anthony T. Iavarone, Ph.D. at the QB3 Institute (UC Berkeley). M.A.H. and A.T.I. performed the hydrogen-deuterium exchange mass spectrometry experiments, and M.A.H. created and tested histidine kinase truncations for H-NOX binding. Part of this study was described in the dissertation of Mark A. Herzik, Ph.D. entitled "Structural Insights into Gas Binding and Signal Transduction in the H-NOX Family of Heme Proteins".

has been hypothesized that pathogenic microbes may utilize biofilm formation as a defense mechanism against the innate immune response (9).

Heme-nitric oxide/oxygen binding (H-NOX) proteins are small (~20 kDa), isolable heme-containing proteins that have been identified as selective NO sensors in several species of bacteria. In *Legionella pneumophila* and *Shewanella woodyi*, H-NOX proteins directly control the activity of a DGC and PDE, influencing cyclic-di-GMP levels and biofilm dispersal (14, 15). In *Silicibacter* sp. TrichCH4B, *Vibrio cholerae*, and *Shewanella oneidensis*, H-NOX proteins are an important part of bacterial two-component / histidine-aspartate phosphorelay signaling systems by regulating the autophosphorylation of histidine kinases (HK) in response to NO, which in turn govern activity of downstream response regulators, including DGC or PDE, that fine-tune cyclic-di-GMP levels. In *S. oneidensis*, HK-mediated phosphorylation of specific response regulators increases PDE activity and thus decreases cyclic-di-GMP levels. In the presence of NO, the H-NOX protein inhibits HK autophosphorylation activity, thereby abolishing phosphotransfer between the kinase and the respective cognate response regulators, leading to increased cyclic-di-GMP levels and biofilm formation (16–19).

Although the H-NOX-dependent NO response has been characterized in several bacterial species, the structural mechanism(s) by which H-NOX proteins regulate signaling partners have been less well characterized. Structures of H-NOX proteins from different bacterial species reveal a similar overall fold comprised of a monomer with two subdomains, termed the distal and proximal subdomains, with the heme located at the interface between these subdomains (20–22). Structural studies using the H-NOX from *S. oneidensis* (*So* H-NOX) have shown that NO binding causes cleavage of the heme iron-histidine bond, which in turn leads to a shift of the heme-ligating histidine (H103) along the helix on which it is located (22, 23). In addition, the highly distorted heme in the unliganded H-NOX relaxes to a more planar conformation, and as a result of these structural rearrangements in the heme binding pocket, the distal subdomain of the protein is displaced relative to the proximal subdomain (**Fig. 3.1**) (22). Thus, it has been proposed that this NO-induced conformational change is the mechanism by which H-NOX proteins translate the binding of NO to regulation of signaling partner proteins.

In the present study, the mechanism of molecular recognition and NO-dependent H-NOX regulation of histidine kinase activity in *S. oneidensis* are detailed. Specifically, a combination of pull-down assays and hydrogen-deuterium exchange mass spectrometry identified putative sites of interaction on both the H-NOX and HK proteins. Site-directed mutagenesis coupled with binding assays confirm the HK binding interface on the H-NOX protein. Furthermore, binding kinetics measurements and kinase activity assays were employed to further understand the effect of ligand binding on kinase inhibition. Together, this chapter probes the specific interaction between the H-NOX and HK as an important step towards understanding the mechanism of HK inhibition by H-NOX proteins.

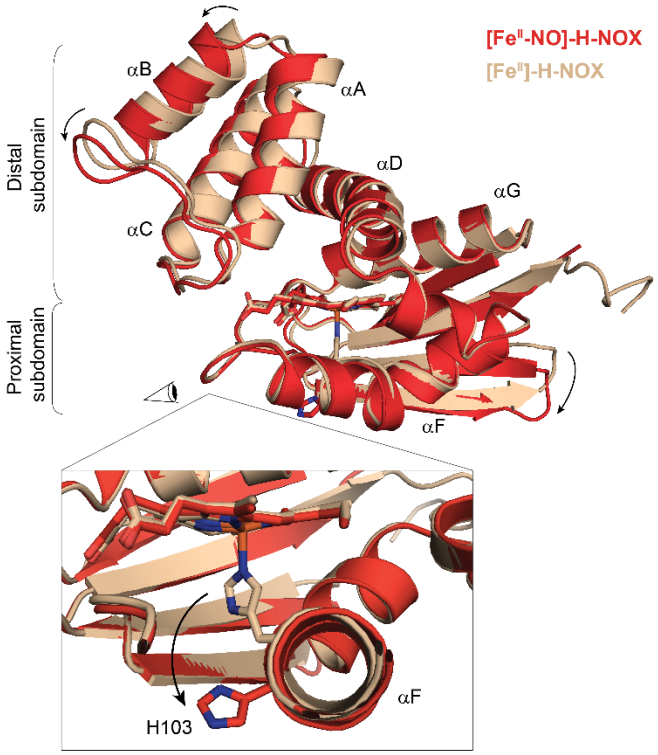

Figure 3.1. Conformational change of *So* H-NOX upon NO binding. Superimposition of the [Fe^{II}] and [Fe^{II}-NO] *So* H-NOX crystal structures (PDB IDs 4U9B and 4U99, respectively). Arrows highlight the conformational changes in the protein upon NO binding, which include a downward shift of the distal subdomain, rotation of the αF signaling helix, and β sheet shift. Inset: comparison of [Fe^{II}] and [Fe^{II}-NO] *So* H-NOX αF signaling helix, from the indicated perspective looking "into" the helix. In the [Fe^{II}] state, H103 is ligated to the heme iron. In the NO-bound structure, H103 swings and points towards the heme to the left side of the protein, corresponding to rotation of the αF helix.

Experimental Procedures

Protein Expression and Purification

So H-NOX. *So* H-NOX constructs were expressed and purified as previously described (22). *So* H-NOX point mutations were introduced by site-directed mutagenesis using a pET20b vector containing wild-type *So* H-NOX as template. Mutagenesis products were transformed into *E. coli* DH5α cells for propagation. Mutations were confirmed by DNA sequencing (Quintara Biosciences; Eton Bioscience). Constructs were expressed and purified as described for wild-type *So* H-NOX (22).

So HK. The gene for *So* HK (SO2145) was cloned into either pHMGWA, which appends an N-terminal maltose binding protein with hexahistidine (His_6-MBP) tag, or pET-GSTx, which appends an N-terminal glutathione-*S*-transferase (GST) tag. GST-fusions of *So* HK truncations, termed GST-N-Term (residues 1-60) and GST-C-Term (residues 61-311) were generated by

cloning the desired *So* HK domain(s) into a pGEX-2T vector (GE Healthcare). *So* HK constructs were transformed into *E. coli* BL21(DE3) cells for protein expression. Cells were grown at 37 °C in 2XYT Broth in the presence of 100 μg/mL ampicillin. Protein expression was induced at OD_{600} ~0.6 with 400 μM IPTG, and cells were grown at 18 °C for 20 to 22 h. Cells were pelleted and resuspended in Buffer A (50 mM Tris [pH 8.0], 150 mM NaCl, 10 mM $MgCl_2$, 25 mM L-glutamate, 5 mM β-mercaptoethanol, 10% [v/v] glycerol, 1 mM benzamidine, and 1 mM Pefabloc® SC (Sigma-Aldrich)) and lysed by passage through a high-pressure homogenizer (Avestin). Cell debris was removed by centrifugation at 100,000 × *g* for 30 min using an Optima XL-100K ultracentrifuge with a Ti-45 rotor (Beckman). For MBP-*So* HK, the supernatant was loaded onto amylose resin (NEB) pre-equilibrated with Buffer B (50 mM Tris [pH 8.0], 150 mM NaCl, 10 mM $MgCl_2$, 25 mM L-glutamate, 5 mM β-mercaptoethanol, and 10% [v/v] glycerol). The resin was washed with 20 column volumes of Buffer B, and the protein was eluted in Buffer B containing 10 mM maltose. Eluted protein was mixed with TEV protease and dialyzed overnight at 4 °C against Buffer B. Cleaved His_6-MBP and uncleaved protein were removed by subtractive nickel affinity, and cleaved *So* HK was then subjected to size-exclusion chromatography using a HiLoad 16/60 Superdex 200 column (GE Healthcare) that had been equilibrated with Buffer C (50 mM Tris [pH 8.0], 150 mM NaCl, 10 mM $MgCl_2$, 25 mM L-glutamate, 5 mM DTT, and 10% [v/v] glycerol. Fractions containing the highest purity *So* HK, as determined by SDS-PAGE, were pooled, concentrated, and either used immediately or flash frozen in liquid nitrogen and stored at -80 °C.

For GST-*So* HK variants, the supernatant was loaded onto glutathione resin (GE Healthcare) pre-equilibrated with Buffer B. The resin was washed with 20 column volumes of Buffer B, and the protein was eluted with Buffer B containing 10 mM reduced glutathione. Eluted proteins were subjected to size-exclusion chromatography and stored in the same manner as described above.

Hydrogen-Deuterium Exchange

Exchange time courses. Exchange experiments were performed with slight modifications of a previously described procedure (24). Exchange time courses were performed in triplicate with the following time points: 1, 2, 5, 10, 30, 60, and 1440 min. Protein samples consisted of 1 nmol of *So* H-NOX-His_6 and 5 nmol of full-length, untagged *So* HK (H72A) (ATP-bound). To initiate exchange, protein samples were diluted with D_2O buffered with 50 mM Tris [pD 8.0], 150 mM NaCl, 10 mM $MgCl_2$, 5% [v/v] glycerol, and 1 mM TCEP. At each time point, 150 μL of the reaction was quenched by addition of 2.5% [v/v] trifluoroacetic acid (TFA) to a final pH of ~2.5, followed by immediate freezing in liquid nitrogen. For protease digestion, immobilized pepsin (Pierce) was pre-washed in deionized H_2O/0.025% TFA/4 M urea [pH 2.5]. Time point samples were thawed quickly and added to 150 μL immobilized pepsin slurry. Digestion proceeded at 4 °C with rotation for 2.5 min. Pepsin was removed by brief centrifugation, and the digested sample was immediately frozen in liquid nitrogen. Samples were maintained at -80 °C until analysis.

MS Analysis. Liquid chromatography tandem mass spectrometry (LC-tandem MS) for the identification of pepsin digestion products and liquid chromatography mass spectrometry (LC-MS)

for analysis of peptides following hydrogen/deuterium exchange were performed as previously described (24). The mean percent deuteration for each peptide was calculated from at least three replicates with error bars representing the standard deviation.

Data analysis. Hydrogen/deuterium exchange MS (HDX-MS) data for *So* H-NOX in the presence of excess *So* HK were analyzed using the HX Express macro for Microsoft Excel (25). Deuteron incorporation was measured according to equation S1, as described by Underbakke *et al* (24). Back-exchange was estimated to be ~15% from representative maximally deuterated control *So* H-NOX peptides. Maximally deuterated samples were generated by denaturing *So* H-NOX in 100% D_2O with 4 M deuterated urea followed by digestion with an equal volume of 50% immobilized pepsin slurry pre-washed in deionized H_2O/0.025% TFA [pH 2.5].

Analysis of Complex Formation by Analytical Gel Filtration

The ferrous-unliganded (Fe^{II}) and ferrous-nitrosyl (Fe^{II}-NO) states of wild-type or mutant *So* H-NOX were generated as previously described (16, 22). GST-*So* HK was mixed with a 3.5-fold excess of [Fe^{II}] or [Fe^{II}-NO] *So* H-NOX. Protein complexes were then analyzed on a Superdex 200 10/300 GL size-exclusion column equilibrated with Buffer C. Proteins were eluted at a flow rate of 0.5 mL/min, and peaks were analyzed by SDS-PAGE.

Pull-Down Assays

To map the binding of *So* H-NOX onto different domains of *So* HK, [Fe^{II}-NO]-H-NOX-His_6 was immobilized on magnetic Ni^{2+} NTA beads equilibrated in Buffer B. Beads were washed with Buffer B to remove unbound H-NOX-His_6. GST, GST-N-Term HK, GST-C-Term HK, untagged full-length *So* HK, or no other proteins were incubated with immobilized H-NOX for 1 h at 4 °C under gentle, frequent mixing. Beads were pelleted using a magnetic tray and washed with Buffer B supplemented with 500 mM NaCl. Immobilized proteins were eluted using Buffer B supplemented with 250 mM imidazole and analyzed by SDS-PAGE.

To test the binding of *So* H-NOX surface mutants with *So* HK, 5, 10, and 20 μM of each H-NOX mutant were incubated with 1 μM GST-*So*HK for 1 h at 4 °C under gentle, frequent mixing. Magnetic glutathione beads equilibrated in Buffer B were added to the protein mix and incubated for 15 min at 4 °C with gentle, frequent mixing. Beads were pelleted using a magnetic tray, and beads were washed with Buffer B supplemented with 500 mM NaCl. Immobilized proteins were eluted using Buffer B supplemented with 10 mM reduced glutathione and analyzed by SDS-PAGE. Gel bands corresponding to H-NOX in each lane were quantified by Image Lab software (Bio-Rad Laboratories) and normalized relative to the intensity of WT H-NOX.

Measurement of Binding Kinetics with Bio-Layer Interferometry

The kinetics of interactions between *So* H-NOX and GST-*So* HK were measured by Bio-Layer Interferometry (BLI) on a BLItz instrument (ForteBio) in Advanced Kinetics mode. Anti-

GST biosensors (ForteBio) were hydrated in Buffer B for at least 10 min prior to each run. 200 μL of Buffer B was used for baseline measurements and dissociation. GST-*So* HK (4 μL) was used for loading, and 4 μL of *So* H-NOX at varying concentrations from 5 to 75 μM was used for association. At least 3 H-NOX concentrations were used for each experiment. All runs were performed with the following steps: (1) initial baseline, 30 s; (2) loading of 50 ng/μL GST-*So* HK, 120 s; (3) baseline, 30 s; (4) association of *So* H-NOX variant, 120 s; (5) dissociation of *So* H-NOX, 120 s. For each run, a new biosensor was prepared (i.e. biosensors were not re-used). On-rates (k_a), off-rates (k_d), and binding constants (K_D) were calculated using BLItz software with a global fitting mode.

Histidine Kinase Activity Assays

Histidine kinase activity was measured with slight modifications of a previously described procedure (17). Purified GST-*So* HK (4 μM) was incubated with 40 μM of wild-type *So* H-NOX in either the Fe^{II} or Fe^{II}-NO state, or mutant *So* H-NOX in the Fe^{II}-NO state, for 30 min at room temperature in an anaerobic glove bag (Coy Laboratory Products). Reactions were initiated by the addition of 5 μCi of [γ-^{32}P] ATP and 500 μM ATP. Assays were quenched at 30 min with SDS-PAGE loading buffer and 50 mM EDTA (final concentration). Reactions were analyzed by SDS-PAGE, and data were collected as described previously (17, 18). Bands were quantified by ImageJ software, and experiments were run in triplicate.

Results

H-NOX ligation state affects histidine kinase binding affinity

To determine the effect of NO on the binding interaction between *So* H-NOX and *So* HK, H-NOX–HK complexes were prepared with Fe^{II} and Fe^{II}-NO states of the H-NOX and analyzed by analytical gel filtration (AGF) (**Fig. 3.2A**). For each ligation state, H-NOX was incubated with the HK at a ~3.5-fold molar excess prior to analysis by AGF. Although complex formation was observed with *So* H-NOX in both ligation states, the [Fe^{II}-NO]-H-NOX exhibited a markedly tighter binding affinity than the unliganded protein. [Fe^{II}]-H-NOX traces displayed an additional peak corresponding to free HK, suggesting that not all of the HK was complexed with [Fe^{II}]-H-NOX. These results indicate the [Fe^{II}-NO]-H-NOX forms a tighter complex with the HK.

To further characterize the effects of H-NOX ligation state on HK affinity, *So* HK and [Fe^{II}]-H-NOX or [Fe^{II}-NO]-H-NOX binding kinetics were determined by Bio-Layer Interferometry (BLI). For these experiments, *So* HK containing an N-terminal GST tag was immobilized onto anti-GST biosensors, then association and dissociation rates of *So* H-NOX in the two different ligation states were measured. [Fe^{II}-NO]-H-NOX with GST-*So* HK has a binding constant of 8.3 nM. In contrast, [Fe^{II}]-H-NOX with GST-*So* HK has a binding constant of 196 nM, nearly two orders of magnitude weaker in affinity (**Table 3.1**; **Fig. B.1**). Therefore, the H-NOX ligation state is directly correlated with binding affinity, namely, NO binding to the H-NOX yields a conformation that promotes a tighter H-NOX-HK complex.

Localization of the H-NOX binding interface on the histidine kinase

A Conserved Domain Database search (26) revealed that *So* HK is comprised of three domains: an N-terminal coiled-coil region (as estimated by secondary structure prediction servers), followed by a dimerization and histidine phosphorylation domain (DHp), which contains the phospho-accepting histidine (H72), and the catalytic and ATP-binding (CA) domain at the C-terminus (**Fig. B.2**). The observation that [Fe^{II}]-H-NOX forms a weak but observable complex with the HK without affecting kinase autophosphorylation activity may indicate that the protein-protein interaction site is distant from the phospho-accepting histidine and the catalytic site.

Table 3.1. H-NOX and HK Binding Kinetics from BLItz

Construct	Ligation State	k_a (× 10^3 M^{-1} s^{-1})	k_d (× 10^{-4} s^{-1})	K_D (nM)
WT	Fe^{II}	44.1 ± 5.0	79.1 ± 18.0	196.0 ± 45.6
WT	Fe^{II}-NO	30.6 ± 3.7	2.5 ± 1.7	8.3 ± 5.6
K108A	Fe^{II}	36.3 ± 3.0	40.5 ± 7.1	112.0 ± 21.6
K108A	Fe^{II}-NO	6.0 ± 0.2	64.0 ± 3.4	1100.0 ± 6.7
S20E	Fe^{II}-NO	4.8 ± 0.5	5.4 ± 1.6	110.0 ± 35.3
E27K	Fe^{II}-NO	28.0 ± 3.0	7.8 ± 2.8	28.0 ± 10.4
R34E	Fe^{II}-NO	3.0 ± 0.01	11.0 ± 1.1	370.0 ± 36.7
V35E	Fe^{II}-NO	4.4 ± 0.2	7.0 ± 1.3	160.0 ± 30.4
S38E	Fe^{II}-NO	10.0 ± 0.5	17.0 ± 2.1	170.0 ± 22.7
S79N	Fe^{II}-NO	140.0 ± 9.0	9.8 ± 2.6	7.2 ± 1.9
D83K	Fe^{II}-NO	130.0 ± 15.0	640.0 ± 78.0	480.0 ± 82.8
D89K	Fe^{II}-NO	53.0 ± 3.3	110.0 ± 14.0	210.0 ± 29.4
R131E	Fe^{II}-NO	570.0 ± 95.0	18.0 ± 8.9	3.1 ± 1.6

Grey boxes: K_D is at least 2 orders of magnitude higher than WT [Fe^{II}-NO]-H-NOX with HK.
k_a: association rate; k_d: dissociation rate; K_D: dissociation constant

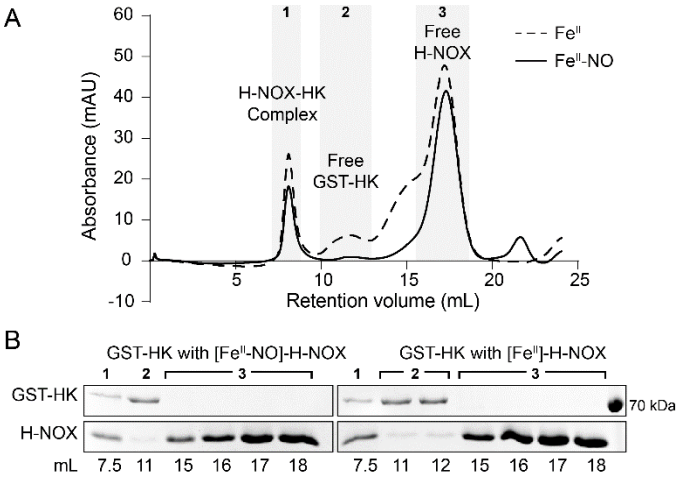

Figure 3.2. Analytical gel filtration of GST-*So* HK and *So* H-NOX variants. (A) Gel filtration chromatogram of GST-tagged *So* HK with *So* H-NOX in either Fe^{II} (dashed line) or Fe^{II}-NO (solid line) ligation states. Complex formation utilized a 3.5-fold excess of H-NOX. (B) SDS-PAGE analysis of analytical gel filtration fractions corresponding to collected peaks.

To test this hypothesis, *So* HK domain truncations were generated as GST-tagged fusion proteins with either the N-terminal domain or the DHp and CA domains (**Fig. 3.3A**). [Fe^{II}-NO]-H-NOX with a C-terminal His_6 tag was incubated with the truncated constructs and full-length kinase and immobilized with Ni^{2+} magnetic beads. *So* H-NOX and any binding partners were then eluted from the beads and analyzed via SDS-PAGE. Analysis of the eluates indicates that *So* H-NOX shows no appreciable affinity towards GST or the DHp/CA domains. However, the GST-N-terminal domain and full-length kinase were pulled down by the immobilized H-NOX (**Fig. 3.3B**). From these data, it is clear that *So* H-NOX binds to elements within the predicted N-terminal domain of *So* HK.

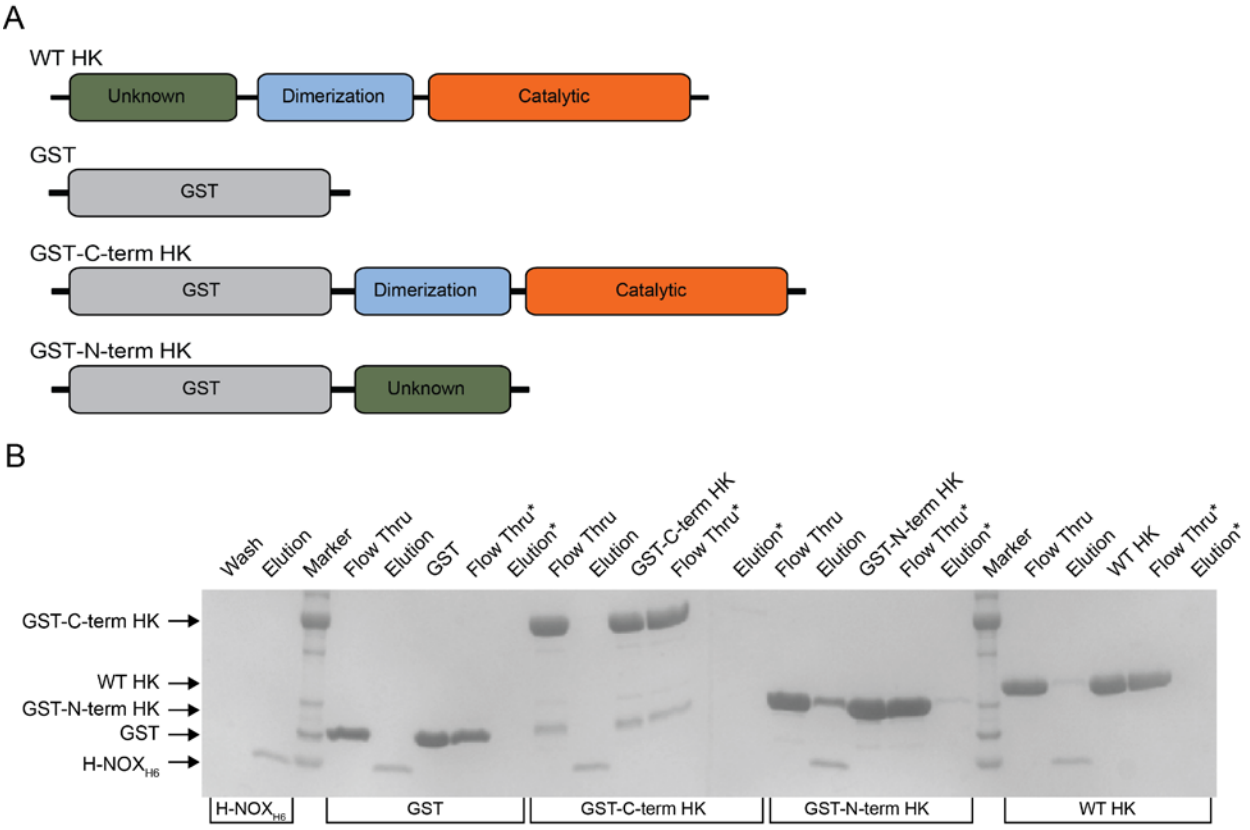

Figure 3.3. *So* HK domain organization and pull-down assays. (**A**) Domain architecture for *So* HK constructs used in the H-NOX-His_6 pull-down assay shown in (**B**). (**B**) Pull-down assay using [Fe^{II}-NO]-H-NOX-H_6 as the bait. For each construct, the flow-thru (FT), wash (W), elution (E), and bead-only controls were analyzed by SDS-PAGE.

Mapping of histidine kinase interface on H-NOX by HDX-MS

The H-NOX-HK binding interface was mapped using hydrogen-deuterium exchange mass spectrometry (HDX-MS), a powerful technique for studying protein-protein interactions and conformational changes (27). Briefly, [Fe^{II}-NO]-H-NOX in the presence of excess HK was diluted with >99% D_2O to initiate the exchange reaction. After the desired incubation time, reactions were quenched and digested with the acid-stable protease pepsin, and peptides were then analyzed by LC-MS (24). Optimization of the pepsin digestion step yielded multiple overlapping peptides with 89% sequence coverage for the H-NOX (**Fig. B.3**). No digestion time course yielded robust observation of the αB-αC loop.

Regions of the H-NOX that are either involved in the H-NOX-HK interface or experience decreased protein dynamics upon complex formation with the HK are expected to exhibit decreased rates of deuteron incorporation. Several regions of the H-NOX meet these criteria when in the presence of the HK. For example, the peptide corresponding to amino acids 1-6 in helix αA exhibits 31-35% fewer deuterons incorporated in the presence of the kinase. Additionally, an overlapping peptide comprised of residues 1-11 also displays decreased exchange in the presence of the kinase, indicating that the N-terminal portion of helix αA is potentially involved in the interaction with the histidine kinase (**Fig. 3.4A**; **Fig. B.3**). Global analysis of the H-NOX HDX-MS data revealed numerous overlapping peptides that display significantly decreased exchange rates in the presence of the HK. More importantly, these residues map to a single face of the H-NOX, spanning the distal and proximal subdomains while the opposing face of the H-NOX shows no difference in exchange rates in the presence of the HK. Specifically, residues within helices αA, αB, and the αG-αF loop experience the most significant decrease in exchange rates (**Fig. 3.4**). Although no information was obtained for the αB-αC or αF-β1 loops, it is reasonable to assume that these loops are also involved in the HK-binding interface as the helices flanking these loops all experienced kinase-dependent decreased exchange rates.

H-NOX scanning mutagenesis of the histidine kinase interface

To validate the putative kinase-binding interface observed by HDX-MS, *So* H-NOX point mutations were generated in the regions that exhibited kinase-dependent decreased exchange. Several mutants were also chosen in the solvent-exposed residues in the αB-αC loop, which was not covered by HDX-MS but directly adjacent to the protected region identified. In addition, parts of the *So* H-NOX αB and αF helices were identified by HDX-MS to be protected in the presence of *So* HK. Hence, mutations were made in areas of these helices without peptide coverage in order to identify a more comprehensive interface on the H-NOX responsible for HK interaction. Residues chosen for mutation are capable of either hydrogen bonding or electrostatic interactions (*e.g.* serine, glutamate, aspartate, and lysine). Additionally, R131, located in the β2 strand distant from the putative kinase interface, was also chosen as a control mutation (**Fig. 3.5A**). Each residue was mutated to either an alanine or a more disruptive mutation (*i.e.* serine/valine/arginine to glutamate; aspartate/glutamate to lysine; see **Table 3.1**). The mutations did not have a deleterious effect on folding, as all mutants displayed very similar ligand-binding properties and gel filtration elution times as wild-type H-NOX (**Fig. B.4**).

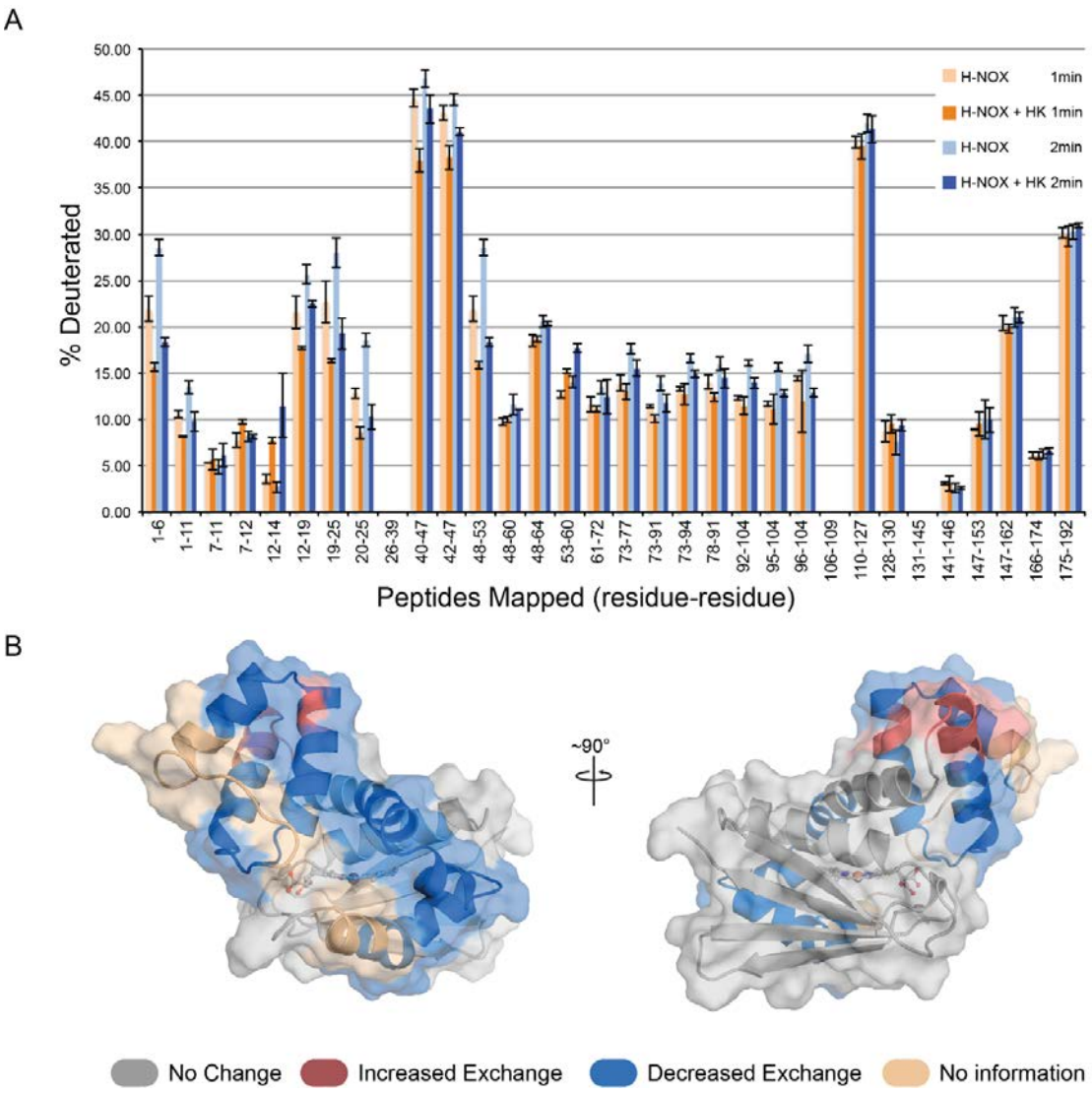

Figure 3.4. Hydrogen-deuterium exchange mass spectrometry (HDX-MS) analysis of HK binding to H-NOX. (**A**) Percent deuteration of *So* H-NOX in the absence (light orange and orange) or in complex with *So* HK (light blue and blue). For each peptide, values are averaged across at least 3 replicates. Percent deuteration was determined as the ratio of the number of deuterons incorporated into the peptide versus the number of possible exchangeable amide protons. (**B**) Color coded HDX-MS results mapped to the crystal structure of *So* H-NOX. Peptides that exhibit statistically significant differences in HDX-MS exchange rates are colored accordingly. Regions that do not display differences in exchange rates are colored gray. Regions for which no sequence coverage was obtained are colored wheat.

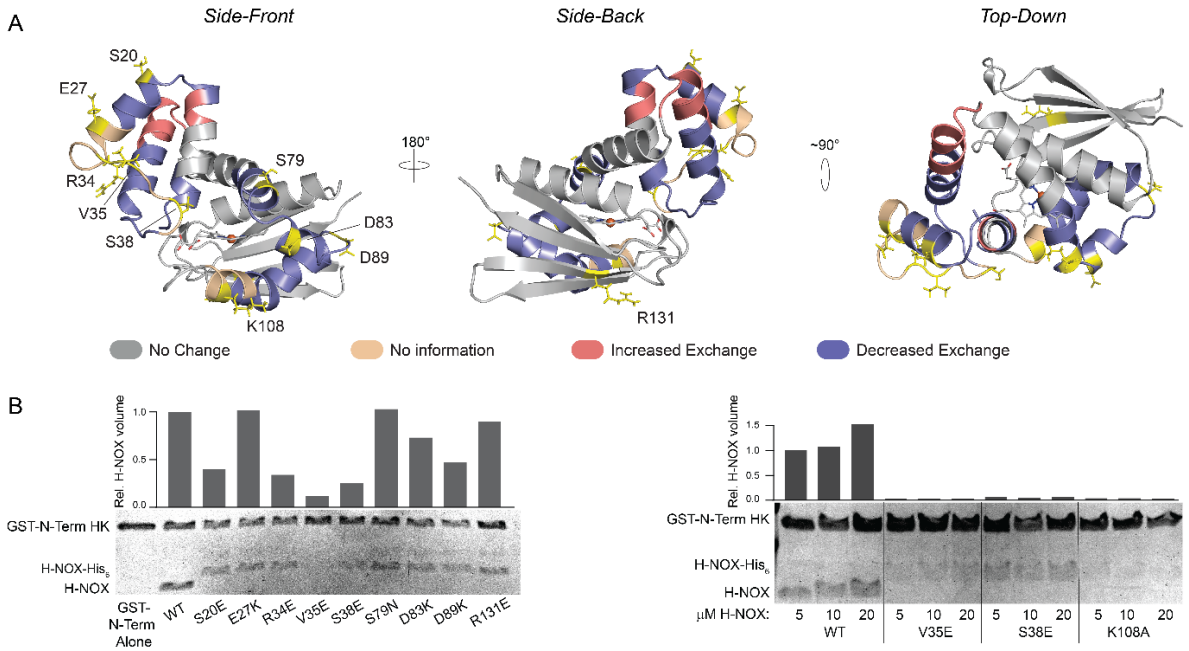

Figure 3.5. *So* H-NOX surface-scanning mutations. **(A)** Structure of *So* H-NOX color-coded according to observed changes in deuteration rates in the presence of *So* HK as determined by HDX-MS. Residues chosen for mutagenesis are shown as yellow sticks. **(B)** The GST-N-terminal domain of *So*HK was incubated with varying concentrations of wild-type or mutant *So* H-NOX. Magnetic glutathione beads were then added to the protein mix to pull GST-*So* HK and any bound H-NOX out of solution. Beads were washed extensively before the proteins were eluted and analyzed by SDS-PAGE followed by Coomassie staining. H-NOX bands from each gel were quantified and normalized to wild-type H-NOX.

The GST-N-terminal HK domain was then used as bait against each of these mutants to test whether any of the mutations had an effect on binding. From the pull-down assays, the S20E, R34E, V35E, S38E, and K108A mutants had decreased binding affinity (**Fig. 3.5B**). These residues are located along the interface identified by HDX-MS, further supporting the involvement of this putative interface in kinase recognition. The R131E mutant displayed similar complex-formation properties with *So* HK as wild-type H-NOX, consistent with the expectation that R131 is not part of the putative binding interface.

Binding kinetics of histidine kinase and H-NOX

To further characterize the effects of *So* H-NOX point mutations on HK complex formation, binding kinetics between *So* HK and *So* H-NOX mutants were measured. GST-tagged HK was immobilized onto anti-GST biosensors, and association and dissociation rates of [Fe^{II}-NO]-H-NOX mutants were measured using BLI. Wild-type [Fe^{II}-NO]-H-NOX with GST-*So* HK has a binding constant (K_D) of 8.3 nM, with an association rate (k_a) of 3.1×10^4 M^{-1} s^{-1} and dissociation rate (k_d) of 2.5×10^{-4} s^{-1}. All [Fe^{II}-NO]-H-NOX mutants except for S79N displayed decreased affinity for GST-HK (**Table 3.1**; **Fig. B.1**). Most of the mutants displayed 2 orders of magnitude decreased binding affinity, and the K108A mutant had the lowest affinity for the HK at 1.1 μM.

For most of the surface mutants, a slower association rate contributed to the overall higher K_D. However, the D83K mutant exhibited a faster on-rate, D89K exhibited comparable on-rate as wild-type, and both D83K and D89K mutants exhibited a much faster off-rate compared with wild-type H-NOX or other surface mutants. These data confirm that the putative binding interface identified by HDX-MS as well as the solvent-exposed region in the αB-αC and αF-β1 loops indeed comprise the site of *So* H-NOX and *So* HK interaction.

Interestingly, the K108A mutant in the [Fe^{II}] unliganded state had an affinity of 112 nM, which is similar to that of the wild-type [Fe^{II}]-H-NOX (196 nM), and both form a tighter complex than that of [Fe^{II}-NO]-H-NOX K108A (1.1 μM). Thus, the K108 residue appears to be important for the H-NOX-HK complex formation when the H-NOX is bound to NO, but not in the unliganded state.

Effect of H-NOX binding-deficient mutants on histidine kinase activity

The Fe^{II}-NO state of *So* H-NOX has been demonstrated to inhibit the autophosphorylation activity of *So* HK (17). Since formation of the H-NOX-HK complex is presumably required for kinase inhibition, the binding-deficient H-NOX mutants should also exhibit less inhibitory effects on the histidine kinase autophosphorylation activity. [Fe^{II}-NO]-H-NOX wild-type and mutants were incubated with *So* HK, and autophosphorylation activity was measured with [γ-^{32}P] ATP as the substrate. As expected, *So* HK incubated with wild-type [Fe^{II}-NO]-H-NOX had the lowest autophosphorylation activity, and similar results were obtained with the control mutant, R131E. HK with binding-deficient mutants V35E, S38E, D83K, and K108A had 1.5~2-fold higher activity, which is attributed to the lack of a sufficiently stable H-NOX-HK complex required for inhibition. *So* HK alone (without any H-NOX) was previously reported to have activity levels comparable to that of the protein when incubated with [Fe^{II}]-*So* H-NOX (17), but this result could not be reproduced here. Here, free *So* HK exhibited very little activity. In the presence of excess [Fe^{II}]-H-NOX, the kinase has increased activity compared to the activity without H-NOX (**Fig. 3.6**). In the case of *So* H-NOX binding-deficient mutants, we conclude that there is *sufficient* interaction with *So* HK to increase kinase activity compared with free HK, but *insufficient* complex formation to inhibit kinase activity at the level of wild-type [Fe^{II}-NO]-H-NOX. Thus, formation of the H-NOX-HK complex is insufficient for inhibition, and the H-NOX conformational changes upon NO binding are required for inhibiting HK activity.

DISCUSSION

Two-component signal transduction is a key strategy for bacteria to respond to environmental stimuli, including NO (28). The regulation of histidine kinase activity by H-NOX proteins in two-component signaling systems is important for various processes including motility, cellular aggregation, and bioluminescence (9, 18, 29). Across a diverse range of bacteria, genes encoding H-NOX and HK proteins are found directly adjacent to each other on the same operon, and the response regulators of these H-NOX-associated HKs have been found to be either DNA-binding domains, or cyclic-di-GMP-processing enzymes such as diguanylate cyclases or

phosphodiesterases. In pathogens such as *Vibrio cholerae*, biofilm formation mediated by the NO/H-NOX signaling pathway may be directly involved in virulence (9, 16–18, 30, 31). In each of these cases, NO binding to H-NOX displays inhibitory effects on the autophosphorylation activity of its associated HK, which prevents any subsequent phosphotransfer to downstream effector proteins. Despite all that has been uncovered, the mechanism by which H-NOX proteins regulate the activity of signaling partner proteins remained largely uncharacterized.

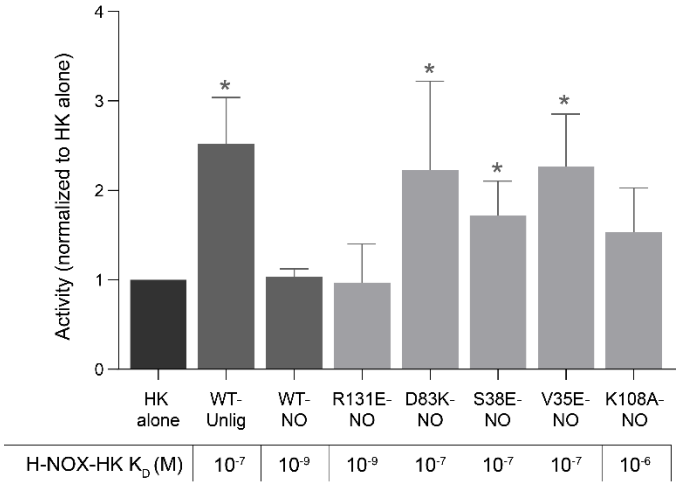

Figure 3.6. Measurement of *So* HK autophosphorylation with *So* H-NOX variants. Black: HK alone; dark grey: WT H-NOX; light grey: H-NOX mutants. For each reaction, 4 μM of GST-*So* HK was incubated with 40 μM *So* H-NOX for 30 min, and reactions initiated with 5 μCi [γ-^{32}P] ATP and quenched at 30 min. Activity was normalized to the kinase-only control reaction. The K_D for each H-NOX variant for the HK, from BLItz experiments, are indicated below the graph.
* $p < 0.05$ compared with HK alone (first bar).

Two possible mechanisms of histidine autophosphorylation inhibition are: (i) steric hindrance, where the inhibitor physically blocks the site of HK phosphorylation, or (ii) allosteric regulation, where inhibition occurs without directly blocking the phosphorylation site. The sporulation regulator KinA from *Bacillus subtilis* illustrates the first possibility: the kinase inhibitor protein Sda binds near the site of the phospho-accepting histidine, and thereby sterically hinders KinA autophosphorylation as well as phosphotransfer from KinA to the cognate response regulator Spo0F (32). The second case involves the inhibitor inducing a conformational change in the kinase via binding to a site distant from the phospho-accepting histidine. The results here show that *So* H-NOX is likely to regulate histidine kinase activity via allosteric regulation, and mapping the sites of interaction between these two proteins supports this conclusion.

The *S. oneidensis* histidine kinase is comprised of three domains, the canonical histidine kinase DHp and CA domains with a previously uncharacterized N-terminal domain of unknown function that is predicted to be a coiled-coil. Pull-down assays using various HK domain truncations indicate that this N-terminal domain is the primary binding site of *So* H-NOX. As discussed above, H-NOX binding to *So* HK is not at the catalytic domain but at a site distant from

ATP binding and phosphorylation. Notably, this N-terminal domain is conserved in other H-NOX-associated HKs from *Pseudoalteromonas* and *Vibrio* species, including *V. cholerae*, suggesting that it could also be the H-NOX-binding domain in these organisms. However, H-NOX-associated HKs have a diverse range of domain architectures, many of which do not contain this binding domain, suggesting that these HKs have diverged in their mechanism of binding to their partner H-NOX proteins.

HDX-MS revealed several regions of *So* H-NOX that exhibited decreased rates of deuteron incorporation in the presence of *So* HK. Notably, these regions of slowed exchange map to a single contiguous face of the H-NOX, spanning the distal and proximal subdomains. Point mutations were generated in the region covered by HDX-MS, as well as in adjacent regions, in order to map the *So* H-NOX:HK interface. S20 is located on the N-terminal αB helix, which has been shown to be the signaling helix in other bacterial H-NOX proteins (33). R34, V35, and S38 lie on the αB-αC loop, which was not covered from the peptide mapping of HDX-MS. K108, which is positioned on the αF helix almost directly opposite of the heme-ligating histidine (H103), is also in a region with poor peptide coverage. Of the H-NOX point mutations, all but the S79E mutation had decreased affinity for *So* HK, with the K108A mutation on the αF helix displaying the lowest affinity. This confirms that the area identified by HDX-MS, as well as the adjacent αB-αC loop and the αB and αF helices, a potentially buried surface area of ~1640 - 2100 $Å^2$, are part of the H-NOX-HK interface.

Interestingly, two of the H-NOX point mutants on this interface, D83K and D89K, exhibited faster on-rates *and* faster off-rates and an overall decreased affinity compared with wild-type. These residues lie on the αD-αF loop, which extends farther outward than the rest of the interaction surface and may be more accessible to the HK, contributing to a faster on-rate. However, the off-rate is also faster than wild-type H-NOX, possibly due to the mutations' disruption of the proper surface contacts, resulting in an overall weaker affinity for *So* HK.

In pull-down assays performed to validate the kinetics results, the V35E, S38E, and K108A mutants showed almost no binding to the GST-tagged HK N-Term. Interestingly, a sequence alignment of 29 different bacterial H-NOX proteins, all of which have HK partners, revealed that the V35, S38, and K108 residues are fairly conserved (numbering based on *S. oneidensis*). Of the aligned sequences, 38% contain a valine at position 35, and 88% contain a small, hydrophobic residue (*i.e.* valine, alanine, or isoleucine) at that position. At position 38, 59% of sequences contain a serine, and the residue immediately preceding it is a conserved threonine, suggesting that hydrogen bonding may play a role in the H-NOX/HK interaction in this region. Finally, the K108 position is either a lysine or arginine in 85% of the included sequences, including three organisms from the Clostridia family that have H-NOX domains fused to methyl-accepting chemotaxis proteins (Fig. S5). In fact, the H-NOX domain from *Caldanaerobacter subterraneus* (*Cs* H-NOX), which holds the mostly conserved valine and lysine residues from *So* H-NOX, is able to also regulate an orthogonal histidine kinase from *V. cholerae*. Structural analyses of *So* H-NOX and *Cs* H-NOX reveal that they undergo analogous conformational changes, though in the presence of different ligands.(34) These observations suggest that there is sufficient conservation at the H-

NOX-HK binding interface across these two species for interaction, and also sufficient similarity in H-NOX conformational changes for signal transduction between the orthogonal proteins.

The location of K108 on the αF signaling helix provides insight into the signal transduction between the H-NOX and HK. Previous structural studies of H-NOX proteins have shown that upon NO binding to [Fe^{II}]-H-NOX, the iron-histidine bond between the heme and H103 is cleaved, and the αF helix containing K108 rotates ~45° along the length of the helix (**Fig. 3.1** inset; **Fig 3.5A**, top-down view) (22). Kinetic measurements indicate a large affinity difference for *So* HK between wild-type and the K108A mutant *So* H-NOX in the NO bound state, but virtually no difference in affinity in the unliganded state. Thus, the rotation of the αF signaling helix upon NO binding appears to be crucial for stabilizing the H-NOX-HK complex. This could partially explain the overall higher affinity of NO-bound *So* H-NOX for *So* HK as compared to unliganded *So* H-NOX.

Prolonged lifetime of a protein complex is important for regulation of HK activity by the H-NOX. Previous studies with *So* HK as well as studies on H-NOX-associated HKs from other organisms indicate that HK activity alone should be comparable to HK with [Fe^{II}]-H-NOX (17); however, this was not observed in our *in vitro* kinase assays with *So* HK. *So* H-NOX and HK are located on the same operon and are expected to be co-transcribed and expressed *in vivo*; therefore, HK activity with [Fe^{II}]-H-NOX is assumed to be the "basal" state, which is higher than activity of HK alone. *So* HK shows markedly decreased activity in the presence of [Fe^{II}-NO]-H-NOX, which appears related to binding affinity, *i.e*. tighter affinity leads to greater inhibition. In the presence of the binding-deficient *So* H-NOX mutants in the [Fe^{II}-NO] state, *So* HK was restored to the comparable levels as [Fe^{II}]-H-NOX, suggesting that lack of the contacts required for a tight complex formation prevents the NO-dependent H-NOX inhibition of HK activity. Interestingly, the binding kinetics of the V35E, S38E, and D83K [Fe^{II}-NO]-H-NOX mutants were comparable to that of [Fe^{II}] wild-type *So* H-NOX, indicating that the weaker complex can mimic *So* H-NOX and HK in the basal state, but is insufficient for inhibition even though the H-NOX is in the NO-bound, HK-inhibitory conformation (**Fig. 3.6**).

The results in this study lead to a model for *So* H-NOX-HK complex formation and regulation of kinase activity. *In vivo*, the H-NOX and HK are expected to be expressed at similar levels, and the H-NOX to be in the Fe^{II} unliganded state. Under these conditions, [Fe^{II}]-H-NOX and HK form a relatively weak complex, and HK autophosphorylation is active. When NO binds to the H-NOX, conformational shifts occur in the N-terminal domain and the signaling helix, and [Fe^{II}-NO]-H-NOX forms a relatively tight interaction with the HK and is inhibitory of kinase activity (**Fig. 3.7**). The H-NOX residue contacts resulting in strong affinity for *So* HK are required for H-NOX inhibition, as evidenced by the kinase assays with *So* H-NOX binding-deficient mutants that were unable to inhibit *So* HK even while in the Fe^{II}-NO state. Thus, the results of this study suggest that while complex formation is important for stabilizing *So* HK, the H-NOX conformational changes upon NO binding, resulting in tight binding affinity, are necessary for HK inhibition. While the molecular details of HK inhibition as transduced by conformational changes in the H-NOX are yet unknown, this study represents an important step towards understanding the mechanism of NO-mediated regulation of histidine kinases.

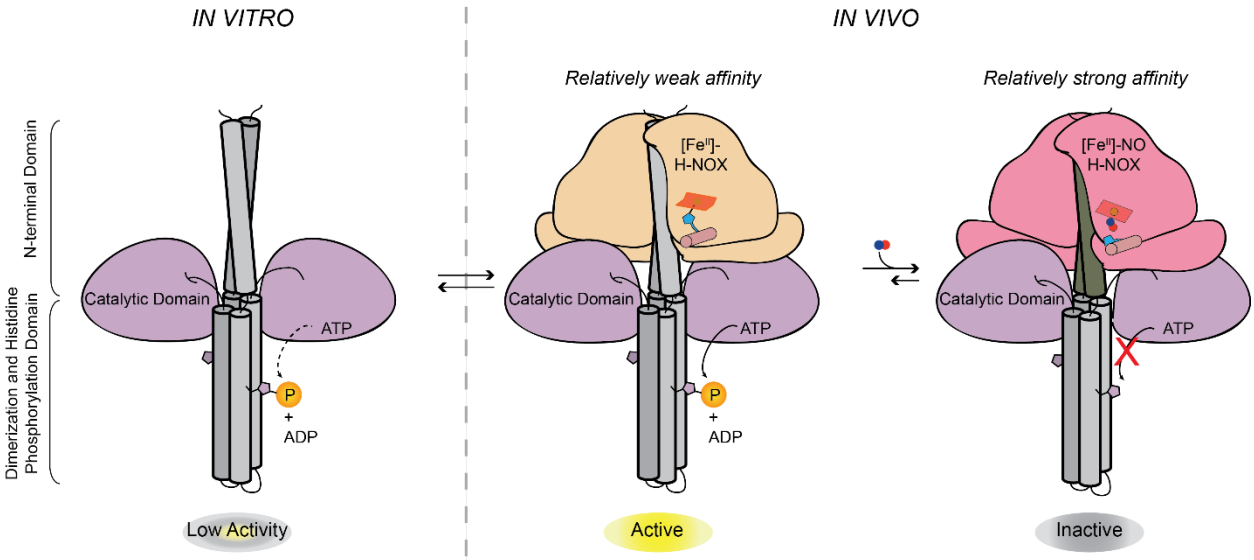

Figure 3.7. Proposed model for H-NOX-dependent inhibition of HK activity in *Shewanella oneidensis.* In the basal state (without H-NOX), the HK is weakly active. When complexed with [Fe^{II}]-H-NOX, kinase activity is increased, presumably due to stabilization of the HK by the H-NOX. Upon NO binding, the [Fe^{II}-NO]-H-NOX:HK complex has a stronger affinity ($K_D \sim 10^{-9}$ M), compared with [Fe^{II}]-H-NOX:HK ($K_D \sim 10^{-7}$ M). The NO-induced conformational changes in *So* H-NOX are transduced to the HK, inhibiting kinase autophosphorylation.

References

1. Donlan, R. M., and Costerton, J. W. (2002) Biofilms: Survival Mechanisms of Clinically Relevant Microorganisms. *Clin. Microbiol.* 15, 167–193
2. Costerton, J. W., Stewart, P. S., and Greenberg, E. P. (1999) Bacterial biofilms: a common cause of persistent infections. *Science (80-.).* 284, 1318–1322
3. Ryjenkov, D. A., Tarutina, M., Moskvin, O. V, and Gomelsky, M. (2005) Cyclic Diguanylate Is a Ubiquitous Signaling Molecule in Bacteria: Insights into Biochemistry of the GGDEF Protein Domain. *J. Bacteriol.* 187, 1792–1798
4. Hengge, R. (2009) Principles of c-di-GMP signalling in bacteria. *Nat. Rev. Microbiol.* 7, 263–273
5. Galperin, M. Y., Nikolskaya, A. N., and Koonin, E. V. (2001) Novel domains of the prokaryotic two-component signal transduction systems. *FEMS Microbiol. Lett.* 203, 11–21
6. Schmidt, A. J., Ryjenkov, D. A., and Gomelsky, M. (2005) The ubiquitous protein domain EAL is a cyclic diguanylate-specific phosphodiesterase: Enzymatically active and inactive EAL domains. *J. Bacteriol.* 187, 4774–4781
7. Römling, U., and Balsalobre, C. (2012) Biofilm infections, their resilience to therapy and innovative treatment strategies. *J. Intern. Med.* 272, 541–561

8. Stanley, N. R., and Lazazzera, B. A. (2004) Environmental signals and regulatory pathways that influence biofilm formation. *Mol. Microbiol.* 52, 917–924
9. Plate, L., and Marletta, M. A. (2013) Nitric oxide-sensing H-NOX proteins govern bacterial communal behavior. *Trends Biochem. Sci.* 38, 566–575
10. Dinerman, J. L., Lowenstein, C. J., and Snyder, S. H. (1993) Molecular Mechanisms of Nitric Oxide Regulation - Potential Relevance to Cardiovascular Disease. *Circ. Res.* 73, 217–222
11. Bredt, D. S., and Snyder, S. H. (1992) Nitric oxide, a novel neuronal messenger. *Neuron*. 8, 3–11
12. Moncada, S., Palmer, R. M. J., and Higgs, E. A. (1991) Nitric oxide: physiology, pathophysiology, and pharmacology. *Pharmacol. Rev.* 43, 109–142
13. Macmicking, J., Xie, Q., and Nathan, C. (1997) Nitric Oxide and Macrophage Function. *Annu. Rev. Immunol.* 15, 323–350
14. Carlson, H. K., Vance, R. E., and Marletta, M. A. (2010) H-NOX regulation of c-di-GMP metabolism and biofilm formation in Legionella pneumophila. *Mol. Microbiol.* 77, 930–942
15. Liu, N., Xu, Y., Hossain, S., Huang, N., Coursolle, D., Gralnick, J. A., and Boon, E. M. (2012) Nitric oxide regulation of cyclic di-GMP synthesis and hydrolysis in Shewanella woodyi. *Biochemistry*. 51, 2087–2099
16. Plate, L., and Marletta, M. A. (2012) Nitric Oxide Modulates Bacterial Biofilm Formation through a Multicomponent Cyclic-di-GMP Signaling Network. *Mol. Cell*. 46, 449–460
17. Price, M. S., Chao, L. Y., and Marletta, M. A. (2007) Shewanella oneidensis MR-1 H-NOX regulation of a histidine kinase by nitric oxide. *Biochemistry*. 46, 13677–13683
18. Rao, M., Smith, B. C., and Marletta, M. A. (2015) Nitric Oxide Mediates Biofilm Formation and Symbiosis in Silicibacter sp. Strain TrichCH4B. *MBio*. 6, 1–10
19. Mukhopadhyay, R., Sudasinghe, N., Schaub, T., and Yukl, E. T. (2016) Heme-Independent Redox Sensing by the Heme-Nitric Oxide/Oxygen Binding Protein (H-NOX) from Vibrio cholerae. *J. Biol. Chem.* 291, 17547–17556
20. Winter, M. B., Herzik, M. A., Kuriyan, J., and Marletta, M. A. (2011) Tunnels modulate ligand flux in a heme nitric oxide/oxygen binding (H-NOX) domain. *Proc. Natl. Acad. Sci. U. S. A.* 108, E881-889
21. Pellicena, P., Karow, D. S., Boon, E. M., Marletta, M. A., and Kuriyan, J. (2004) Crystal structure of an oxygen-binding heme domain related to soluble guanylate cyclases. *Proc. Natl. Acad. Sci. U. S. A.* 101, 12854–12859
22. Herzik, M. A., Jonnalagadda, R., Kuriyan, J., and Marletta, M. A. (2014) Structural insights into the role of iron-histidine bond cleavage in nitric oxide-induced activation of H-NOX gas sensor proteins. *Proc. Natl. Acad. Sci. U. S. A.* 111, E4156-4164
23. Erbil, W. K., Price, M. S., Wemmer, D. E., and Marletta, M. A. (2009) A structural basis for H-NOX signaling in Shewanella oneidensis by trapping a histidine kinase inhibitory conformation. *Proc. Natl. Acad. Sci. U. S. A.* 106, 19753–19760
24. Underbakke, E. S., Iavarone, A. T., and Marletta, M. A. (2013) Higher-order interactions bridge the nitric oxide receptor and catalytic domains of soluble guanylate cyclase. *Proc. Natl. Acad. Sci. U. S. A.* 110, 6777–6782

25. Weis, D. D., Engen, J. R., and Kass, I. J. (2006) Semi-Automated Data Processing of Hydrogen Exchange Mass Spectra Using HX-Express. *J. Am. Soc. Mass Spectrom.* 17, 1700–1703

26. Marchler-Bauer, A., Derbyshire, M. K., Gonzales, N. R., Lu, S., Chitsaz, F., Geer, L. Y., Geer, R. C., He, J., Gwadz, M., Hurwitz, D. I., Lanczycki, C. J., Lu, F., Marchler, G. H., Song, J. S., Thanki, N., Wang, Z., Yamashita, R. A., Zhang, D., Zheng, C., and Bryant, S. H. (2015) CDD: NCBI's conserved domain database. *Nucleic Acids Res.* 43, D222–D226

27. Engen, J. R. (2009) Analysis of Protein Conformation and Dynamics by Hydrogen/Deuterium Exchange MS. *Anal. Chem.* 81, 7870–7875

28. Stock, A. M., Robinson, V. L., and Goudreau, P. N. (2000) Two-component signal transduction. *Annu. Rev. Biochem.* 69, 183–215

29. Arora, D. P., Hossain, S., Xu, Y., and Boon, E. M. (2015) Nitric Oxide Regulation of Bacterial Biofilms. *Biochemistry*. 45, 3717–3728

30. Henares, B., Xu, Y., and Boon, E. (2013) A Nitric Oxide-Responsive Quorum Sensing Circuit in Vibrio harveyi Regulates Flagella Production and Biofilm Formation. *Int. J. Mol. Sci.* 14, 16473–16484

31. Wang, Y., Dufour, Y. S., Carlson, H. K., Donohue, T. J., Marletta, M. A., and Ruby, E. G. (2010) H-NOX-mediated nitric oxide sensing modulates symbiotic colonization by Vibrio fischeri. *Proc. Natl. Acad. Sci. U. S. A.* 107, 8375–8380

32. Cunningham, K. A., and Burkholder, W. F. (2009) The histidine kinase inhibitor Sda binds near the site of autophosphorylation and may sterically hinder autophosphorylation and phosphotransfer to Spo0F. *Mol. Microbiol.* 71, 659–677

33. Lahiri, T., Luan, B., Raleigh, D. P., and Boon, E. M. (2014) A Structural Basis for the Regulation of an H-NOX-Associated Cyclic-di-GMP Synthase/Phosphodiesterase Enzyme by Nitric Oxide-Bound H-NOX. *Biochemistry*. 53, 2126–2135

34. Hespen, C. W., Bruegger, J. J., Phillips-Piro, C. M., and Marletta, M. A. (2016) Structural and Functional Evidence Indicates Selective Oxygen Signaling in Caldanaerobacter subterraneus H-NOX. *ACS Chem. Biol.* 11, 2337–2346

CHAPTER 4:

CHARACTERIZATION OF A GLOBIN-CONTAINING NITRIC OXIDE SYNTHASE FROM *SYNECHOCOCCUS* SP. PCC 7335

Summary

In this chapter, a novel nitric oxide synthase from *Synechococcus* sp. PCC 7335 (SynNOS) was characterized. SynNOS is a full-length bacterial NOS containing both heme/oxidase and reductase domains, resembling mammalian NOS. The oxidase domain of SynNOS was shown to be active under single-turnover conditions. Additionally, SynNOS is the first predicted NOS to also contain a globin domain resembling bacterial flavohemoglobins, representing a previously uncharacterized class of bacterial nitric oxide synthases. Spectroscopic characterization of the SynNOS globin domain reveal a rapid autoxidation rate compared with other globins, suggesting a role in redox communication rather than gas storage and transport. The globin heme midpoint potential was also measured in an attempt to determine the role of the globin domain.

Introduction

Nitric oxide synthase (NOS) proteins are heme-containing monooxygenase enzymes that convert L-arginine (L-Arg) to L-citrulline (L-Cit) and nitric oxide (NO) (**Scheme 4.1**). NO regulates various mammalian processes such as vasodilation, hormone regulation, nerve cell transmission, and angiogenesis, and NO is released by macrophages as a first line of defense against pathogens (1–3).

Scheme 4.1. Reaction catalyzed by nitric oxide synthase.

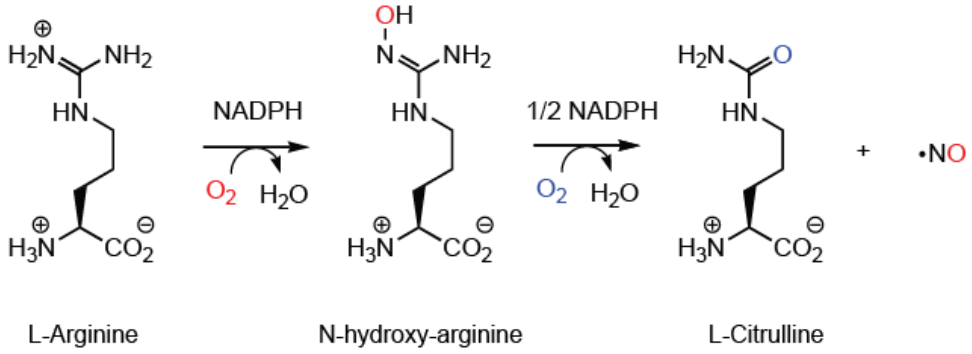

NO synthesis occurs in two distinct catalytic steps. The first step is a hydroxylation that converts L-Arg to the stable intermediate N^{ω}-hydroxy-L-arginine (NHA), and the second step converts NHA to L-Cit and NO. There are three mammalian NOS (mNOS) isoforms, each with its specific localization and function: inducible NOS (iNOS), neuronal NOS (nNOS), and endothelial

NOS (eNOS). All mNOS isoforms are active as homodimers and comprised of two primary domains: an N-terminal heme-containing oxidase domain (NOS_{ox}) and a C-terminal reductase domain (NOS_{red}), which is further divided into FMN-binding and FAD/NADPH-binding subdomains (**Figure 4.1**). A calmodulin (CaM)-binding interface spans the two domains and mediates electron transfer. NOS_{ox} binds the L-Arg substrate, heme, and the redox-active cofactor 6*R*-tetrahydrobiopterin (H_4B), all of which are required for NO synthesis. During catalysis, NOS_{red} transfers electrons from reduced NADPH through the FAD and FMN cofactors, and ultimately to the heme in NOS_{ox} (4, 5).

In recent years, NOS proteins have been discovered in bacteria, but the purpose for NO production within these organisms varies considerably compared to mNOS functions. Bacterial NOS proteins were initially isolated from *Deinococcus radiodurans* and *Bacillus subtilis*, which were found through sequence searching to contain open reading frames coding for proteins with high sequence similarity to the oxidase domain of mNOS (6, 7). Similar bacterial NOS proteins were subsequently discovered in the pathogens *Staphylococcus aureus* and *Bacillus anthracis* (8, 9). Bacterially-derived NO from these organisms has been proposed to protect against oxidative stress, radiation, and antibiotics (10–12).

As these bacterial NOS proteins only contain the oxidase domain, they require a separate flavin-containing reductase protein for NOS activity (10). Full-length bacterial NOS proteins containing a fused oxidase and reductase domain in one polypeptide sequence have been characterized from *Sorangium cellulosum* (scNOS) and *Silicibacter* sp. TrichCH4B (SiliNOS) (13, 14). **Chapter 2** details *Silicibacter* sp. TrichCH4B as the first characterized example of a bacterial organism with both a full-length NOS and an H-NOX/NO signaling system, in which NOS-derived NO binds to the H-NOX to activate downstream signaling, resembling the mammalian NOS/sGC signaling system. The biological function of NOS in *S. cellulosum* has yet to be determined. For both SiliNOS and scNOS, the reductase domains are at the N-terminus of the protein, and the cofactors are FAD and an iron-sulfur cluster, one of the diverse ways that bacteria have evolved electron source for the NOS reaction.

Recently, a full-length bacterial NOS from *Synechococcus* sp. PCC 7335 (SynNOS) was discovered to have a different domain architecture from mNOS and previously-characterized bacterial NOS proteins. SynNOS conserves the fused NOS_{ox} and NOS_{red} found in mNOS; however, the other features of SynNOS are distinctly different from mNOS isoforms. SynNOS lacks the CaM-binding sequence found to regulate redox communication between the NOS_{ox} and NOS_{red} domains, but includes a globin domain (NOS_{glb}). The inclusion of a globin domain in NOS is not unique to *Synechococcus* sp. PCC 7335; there are three other sequenced organisms found to contain an NOS with the same domain arrangement: *Spirosoma linguale* DSM 74, *Nostoc* sp. PCC 7107, and *Crinalium epipsammum* (**Figure 4.1**). This chapter details the characterization of the globin domain from SynNOS, and its possible roles in regulation or participation in the NO catalytic cycle, as an effort towards understanding this new subdivision of NOS enzymes.

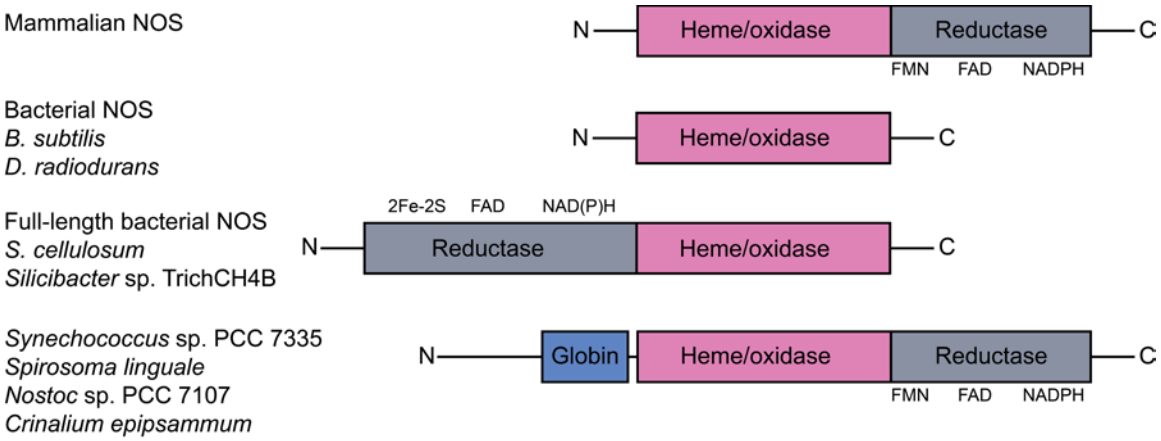

Figure 4.1. Domain arrangement of mammalian and three classes of bacterial NOS enzymes. Mammalian NOS has an N-terminal heme/oxidase domain (NOS_{ox}) and a C-terminal reductase domain (NOS_{red}). Bacterial NOS were initially discovered in *B. subtilis* and *D. radiodurans*, which contain only the oxidase domain. NOS from *S. cellulosum* and *Silicibacter* sp. TrichCH4B contain both the reductase and oxidase domains, but with a different domain organization than mNOS. SynNOS is a full-length bacterial NOS that contains both the oxidase and reductase domains like mNOS, but also contains a novel globin domain with sequence homology to bacterial flavohemoglobin proteins.

Experimental Procedures

Protein Expression and Purification

Full-length SynNOS was cloned into pET28b. The globin domain of SynNOS (amino acid residues 1-472; $SynNOS_{glb}$) was cloned into pSV272, which contains an N-terminal His_6-MBP tag and TEV recognition site. The oxidase domain of SynNOS (amino acid residues 473-855; $SynNOS_{ox}$) was cloned into pET28b. All primers are listed in **Table 4.1**. All plasmids were transformed into *E. coli* RP523(DE3) cells (15). $SynNOS_{ox}$ was co-transformed into RP523(DE3) containing pGroELS for co-expression with the groEL and groES chaperone proteins to increase proper folding and stability. For expression, cultures were grown at 37 °C in Terrific Broth supplemented with 30 μg/mL hemin (Frontier Scientific). At OD_{600} ~0.6, cells were induced with 1 mM isopropyl-β-D-thiogalactopyranoside (IPTG) and grown at 18 °C for 20 to 22 h. Cells were pelleted and resuspended in lysis buffer (50 mM sodium phosphate [pH 8.0], 150 mM NaCl, 10% [vol/vol] glycerol, 10 mM imidazole, 5 mM β-mercaptoethanol, 1 mM Pefabloc, 1 mM benzamidine), and lysed by passage through a high-pressure homogenizer (Avestin). Cell debris was removed by centrifugation at 100,000 × *g* for 30 min using an Optima XL-100K ultracentrifuge with a Ti-45 rotor (Beckman). The supernatant was applied to either a Ni-NTA (SynNOS full-length or $SynNOS_{ox}$) or an amylose column ($SynNOS_{glb}$) equilibrated with wash buffer (50 mM sodium phosphate [pH 8.0], 150 mM NaCl, 10% [vol/vol] glycerol, 10 mM imidazole, 5 mM β-mercaptoethanol). The resin was washed with 20 column volumes of wash buffer, and protein was eluted with wash buffer supplemented with 250 mM imidazole (Ni-NTA column) or 10 mM maltose (amylose column). To cleave the N-terminal His_6-MBP tag in

$SynNOS_{glb}$, TEV protease was added to the eluted protein at a ratio of 1:10 TEV:$SynNOS_{glb}$, and the mixture was dialyzed overnight at 4 °C against 2 L of wash buffer. The dialyzed protein solution was then applied to a Ni-NTA column equilibrated with wash buffer, and untagged $SynNOS_{glb}$ was collected as flow-through. All proteins were concentrated and buffer exchanged into storage buffer (50 mM HEPES [pH 8.0], 150 mM NaCl, 1 mM DTT, and 5% [vol/vol] glycerol), and flash frozen for storage at -80 °C.

Table 4.1. Primers used in this chapter.

Primer Name	Sequence
SynNOS-NdeI-1 F	GGAATTCCATATGCTTGTCAACGACTCTCGTCC
SynNOS-BamHI-1 F	GGAATTCGGATCCATGCTTGTCAACGACTCTCGTCC
SynNOS-XhoI-472 stop R	CCGCTCGAGCTAGGGTAGCTTAATCACGTTGCTAACC
SynNOS-XhoI-472 no stop R	CCGCTCGAGGGGTAGCTTAATCACGTTGCTAACC
SynNOS-NdeI-473 F	GGAATTCCATATGAAGCTTAACGAAGAACGGCT
SynNOS-XhoI-855 stop R	CCGCTCGAGCTATCATGCGTGGTTTGAACAAA
SynNOS-XhoI-1468 stop R	CCGCTCGAGCTACAAGTTGGCTAGCCATTTTTCGGC

UV-Vis Spectroscopy

For all protein constructs (full length SynNOS, $SynNOS_{ox}$, and $SynNOS_{glb}$), absorption spectra were recorded in an anaerobic cuvette on a Cary 3E or 300 spectrophotometer (Agilent). Protein samples were prepared in an anaerobic glove bag (Coy Laboratory Products). Ferric (Fe^{III}) $SynNOS_{glb}$ was prepared by addition of potassium ferricyanide, and excess oxidant was removed using a PD-10 desalting column (GE Healthcare) pre-equilibrated with storage buffer. Ferrous (Fe^{II}) proteins were prepared with addition of sodium hydrosulfite (dithionite). Excess reductant was removed using a PD-10 desalting column. For CO-binding, CO (Praxair, 99.99% purity) was added to the headspace of a sealed Reacti-Vial (Pierce) containing ferrous SynNOS full-length, $SynNOS_{ox}$, or $SynNOS_{glb}$. For NO-binding, an anaerobic solution of diethylamine NONOate (DEA-NONOate) (Cayman Chemicals) in 10 mM NaOH was added to ferrous $SynNOS_{glb}$.

Stopped-Flow Spectroscopy of $SynNOS_{glb}$

Autoxidation rates for $SynNOS_{glb}$ were determined at 25 °C as described previously (16) using a HiTech KinetAsyst stopped-flow instrument equipped with a diode-array detector. Sample preparations were prepared in the anaerobic glove bag as described above. Briefly, $SynNOS_{glb}$ was reduced with ~100 molar equivalent of dithionite for 10 minutes at room temperature. The protein was then exchanged into a buffer for spectral measurements (50 mM HEPES [pH 7.4] and 150 mM NaCl) using a PD-10 desalting column. [Fe^{II}]-$SynNOS_{glb}$ was loaded into a tonometer attached to a three-way joint that was also connected to a 30 mL Luer-Lok syringe filled with anaerobic buffer. Prior to data acquisition, the stopped-flow sample syringe was incubated with dithionite (~10 mM) for >15 min, and the dithionite was subsequently flushed from the syringe with ~15 mL of anaerobic buffer. Autoxidation reactions were initiated by equaling mixing on the stopped-flow instrument of the anaerobic [Fe^{II}]-$SynNOS_{glb}$ with aerobic buffer solution. UV-vis spectra were recorded for 4.5 s (300 scans, 1.5 ms integration time) from 300 to 700 nm using

Kinetic Studio (TgK Scientific). The spectral transition from 425 to 416 nm, then from 416 to 411 nm were fit to a three-state model using SPECFIT Global Analysis System (version 3.0.14).

Spectrochemical Redox Titration of $SynNOS_{glb}$

$SynNOS_{glb}$ potentiometric titrations were performed as previously described (16) using an Oakton pH 1100 Series potentiometer. Briefly, titrations were performed at 25 °C while stirring in the presence of a redox mediator mix solution (midpoint potentials indicated in parentheses): methyl viologen (-440 mV), anthraquinone-2,6-disulfonic acid (-184 mV), 2-hydroxy-1,4-naphthoquinone (-137 mV), 2,5-dihydroxyl-1,4-benzoquinone (-60 mV), tetramethyl-*p*-benzochinon (Duroquinone) (5 mV), 1,2-naphthoquinone (157 mV), and ferricyanide (356 mV). O_2 was removed from the cuvette by flushing continuously with argon. Oxidative titrations were performed by stepwise addition of 1H-[1,2,4]oxadiazolo[4,3-a]quinoxalin-1-one (ODQ; Cayman Chemicals). The change in the heme oxidation state was monitored by the absorbance change in the α-band at 560 nm. A_{560} of $[Fe^{II}]$-$SynNOS_{glb}$ (the α-band maximum) minus A_{560} of $[Fe^{III}]$-$SynNOS_{glb}$ was normalized and plotted against ambient potential.

Single Turnover Experiments of $SynNOS_{ox}$

$SynNOS_{ox}$ co-expressed with chaperones groEL and groES was used in NO formation studies due to the larger proportion of enzyme in the P450 state. NO formation was detected using a Nitric Oxide Analyzer (NOA) (Sievers model 270; GE Analytical Instruments). Reactions were prepared in an anaerobic glove bag, and $[Fe^{II}]$-$SynNOS_{ox}$ was prepared as described above. A 100-µL assay mix contained 500 µM substrate (NHA), 0 or 200 µM H_4B or tetrahydrofolate (H_4F), 60-100 µM $[Fe^{II}]$-$SynNOS_{ox}$ in assay buffer (50 mM Tris [pH 9.0] and 150 mM NaCl). Reactions were initiated with aerobic buffer. All reactions were performed at room temperature in sealed Reacti-Vials. NO formation was measured by sampling 200 µL of Reacti-Vial headspace and injecting into the NOA reaction vessel.

Results

Protein Expression Constructs

Full-length SynNOS (1468 amino acids) was expressed recombinantly in *E. coli* at very low levels and with limited heme incorporation. Thus, smaller constructs containing the separate domains were created with the goal of obtaining better protein expression and cofactor incorporation (**Figure 4.2A**). Constructs were designed based upon sequence alignments with other NOS enzymes. The $SynNOS_{ox}$ domain truncation (amino acids 473-855) was designed based on sequence similarity to other bacterial NOS proteins, in particular *B. subtilis* NOS. The $SynNOS_{glb}$ domain truncation (amino acids 1-472) includes the entire N-terminal region of the protein as well as the predicted globin domain (residues 344-472). Truncations that did not include the 1-344 N-terminal residues did not yield stable protein expression, and it is possible that some

portion of the N-terminal sequence provides additional stabilization to the globin domain. $SynNOS_{red}$ constructs were not successfully expressed in *E. coli*.

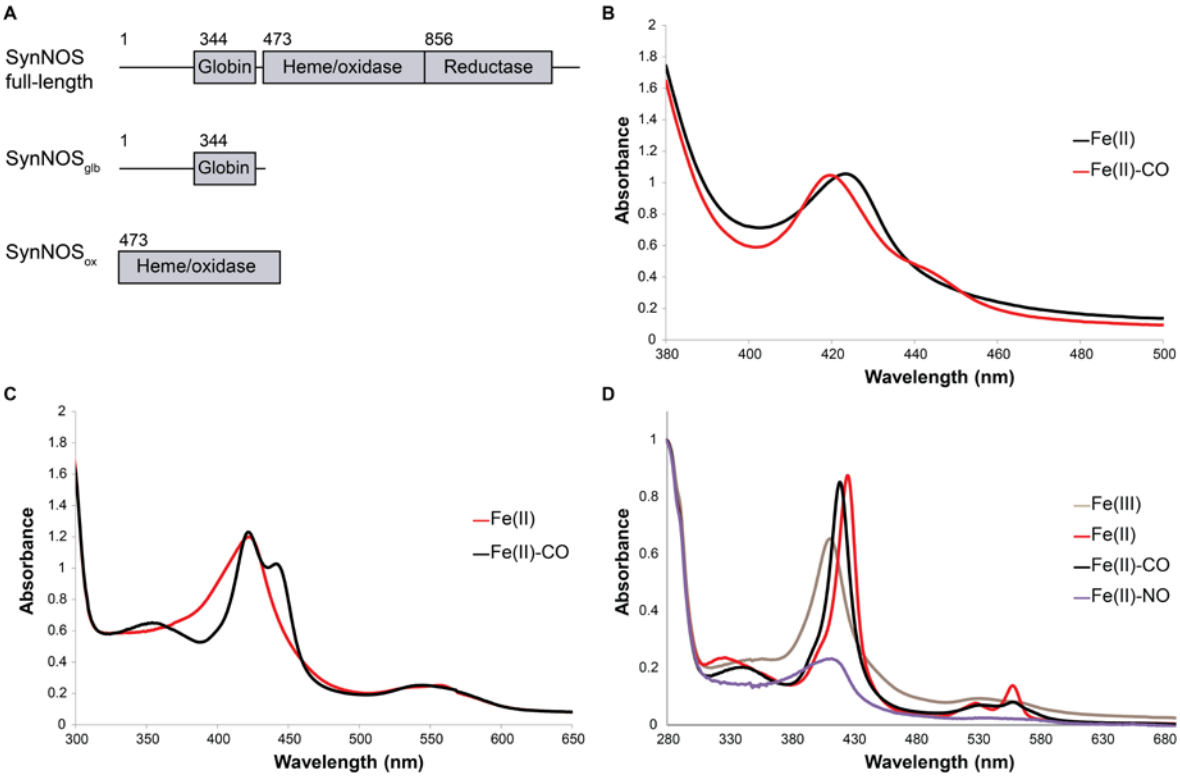

Figure 4.2. Spectroscopic characterization of $SynNOS_{ox}$ and $SynNOS_{glb}$. **(A)** SynNOS domain truncations. Amino acid residue numbers for the domains are indicated. **(B)** UV-vis absorption spectra for full-length SynNOS in the Fe^{II} and Fe^{II}-CO ligation states. Soret maxima: Fe^{II}: 424 nm; Fe^{II}-CO: 420 nm; minor shoulder at 446 nm. **(C)** UV-vis absorption spectra for $SynNOS_{ox}$ in the Fe^{II} and the Fe^{II}-CO ligation states. Soret maxima: Fe^{II}: 424 nm; Fe^{II}-CO: 420 nm, 446 nm. **(D)** UV-vis absorption spectra for $SynNOS_{glb}$ in the Fe^{III}, Fe^{II}, Fe^{II}-CO, and Fe^{II}-NO ligation states. Soret maxima: Fe^{III}: 411 nm; Fe^{II}: 425 nm; Fe^{II}-CO: 420 nm; Fe^{II}-NO: 417 nm.

Spectroscopic Characterization of $SynNOS_{ox}$ and $SynNOS_{glb}$

A spectroscopic signature of enzymes in the P450 family, including NOS enzymes, is the wavelength of the Soret absorption band of the Fe^{II}-CO complex of active enzyme, which typically shows a maximum at ~450 nm. This spectral species sometimes spontaneously converts to aform with a Soret band at ~420 nm (P420 species) often associate with inactive enzyme. The transition from P450 to P420 has been attributed to the protonation of the heme cysteine thiolate ligand. The UV-vis spectra of both full-length SynNOS and $SynNOS_{ox}$ exhibited mostly the P420 species, with only a minor species of P450 (**Figure 4.2B**). It has been shown that the conversion of P450 to P420 in $SynNOS_{ox}$ is pH-dependent, with the enzyme shifting to a more active form at pH values above 8.7 (**Figure 4.2C**). It is unclear whether the natural habitat of *Synechococcus* sp. PCC 7335 has pH values above 8.7; however, laboratory culture conditions call for a growth medium at pH

8.5, suggesting that the organism may survive in higher pH environments, and that SynNOS may be present in the active P450 form in the organism.

Ligand binding experiments were performed with CO, NO, and O_2, which typically form highly stable complexes with ferrous globins (17). $SynNOS_{glb}$ exhibited typical binding characteristics for Fe^{II}-CO and Fe^{II}-NO; however, O_2 binding was not observed due to rapid oxidation of the ferrous heme to the ferric state (**Figure 4.2D**; **Table 4.2**).

Table 4.2. Soret maxima of selected globins.

Protein	Soret	ref
Fe^{III}		
$SynNOS_{glb}$	411	This work
Hemoglobin	411	(17)
C. elegans GLB-6	411	(16)
Fe^{II}		
$SynNOS_{glb}$	425	This work
Hemoglobin	430	(17)
C. elegans GLB-6	425	(16)
Fe^{II}-CO		
$SynNOS_{glb}$	420	This work
Hemoglobin	419	(17)
C. elegans GLB-6	Not observed	(16)
Fe^{II}-NO		
$SynNOS_{glb}$	417	This work
Hemoglobin	418	(17)
C. elegans GLB-6	Not observed	(16)
Fe^{II}-O_2		
$SynNOS_{glb}$	Not observed	This work
Hemoglobin	415	(17)
C. elegans GLB-6	Not observed	(16)

$SynNOS_{glb}$ Oxidation Kinetics

Stopped-flow spectroscopy was used to quantify the autoxidation rate of $SynNOS_{glb}$. A spectral transition from 424 to 408 nm was observed upon reaction of the ferrous protein with 21% O_2 (corresponding to 268 µM O_2). An intermediate was observed at 414 nm, corresponding to either the ferrous-oxy or ferric-superoxide complex (**Figure 4.3A**). The autoxidation rate was determined with a three-state, double-exponential fit (*i.e.* ferrous → ferrous-oxy → ferric) using a global analysis fit of the spectral window, 350-700 nm. The observed k_1 is 4.02 ± 0.91 s^{-1} (~80%) and k_2 is 1.35 ± 0.09 s^{-1} (~20%), leading an overall k_{obs} of approximately 3.49 ± 0.20 s^{-1}. Notably, the autoxidation rate of $SynNOS_{glb}$ is orders of magnitude faster than the majority of other characterized globins, including human hemoglobin, sperm whale myoglobin, soybean leghemoglobin, and human cytoglobin (16) (**Table 4.3**).

Table 4.3. Autoxidation rates of selected globins.

Protein	Autoxidation rate (s^{-1})	ref
$SynNOS_{glb}$	3.5	This work
C. elegans GLB-6	1.2	(16)
Mouse neuroglobin	5.3×10^{-3}	(18)
Human neuroglobin	1.5×10^{-3}	(18)
Soybean leghemoglobin	5.6×10^{-5}	(19)
Sperm whale myoglobin	1.5×10^{-5}	(20)
Human hemoglobin (α chain)	8.9×10^{-6}	(21)
Human hemoglobin (β chain)	1.0×10^{-6}	(21)
Human cytoglobin	Stable[a]	(22, 23)

[a] Negligible autoxidation observed (> 1000 s).

$SynNOS_{glb}$ Midpoint Potential

The redox potential of $SynNOS_{glb}$ was measured by potentiometric redox titration. The reduction midpoint potential ($E°$) is between -250 and -150 mV [versus the standard hydrogen electrode (SHE)] (**Figure 4.3B**). This value is higher than the midpoint potential of $SynNOS_{ox}$, determined to be -376 mV (Sarah Chobot, personal correspondence), and also substrate-bound NOS in other bacterial NOS enzymes (24). The midpoint potentials of NADPH, $FADH_2$, and $FMNH_2$ in mammalian nNOS were measured to be -320 mV, -280 mV, and -274 mV, respectively. Thus, the midpoint potential of $SynNOS_{glb}$ favors electron transfer from the flavins in NOS_{red} (4).

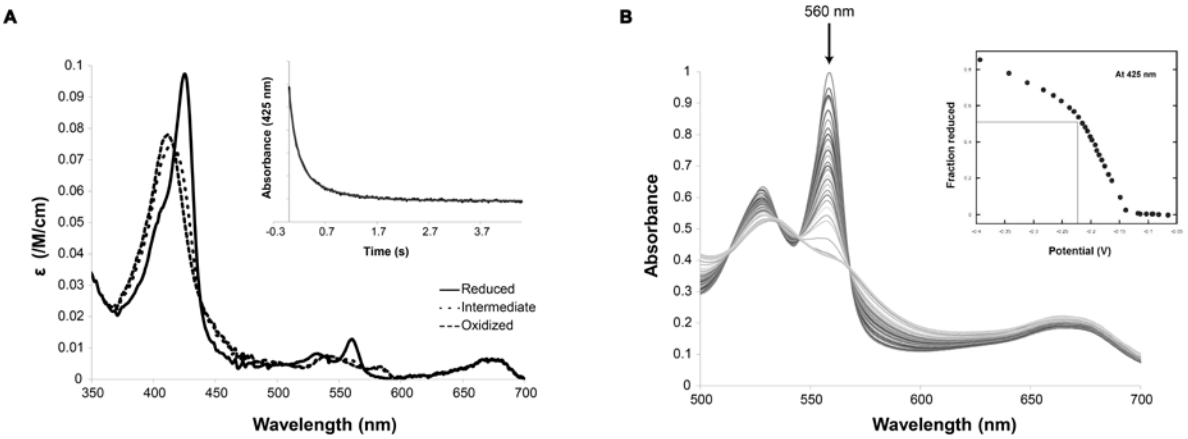

Figure 4.3. Spectroscopic and spectroelectrochemical characterization of $SynNOS_{glb}$. **(A)** Autoxidation rates of $SynNOS_{glb}$ measured by stopped-flow spectroscopy. Soret maxima for the different states: Fe^{II}: 425 nm; intermediate: 416 nm; Fe^{III}: 411 nm. The curve fitting of the change in A_{425} vs. time using a double-exponential model is shown in the inset. **(B)** Spectroelectrochemical potentiometric redox titrations of $SynNOS_{glb}$. The intensity of the α band maximum A_{560} of Fe^{II} $SynNOS_{glb}$ minus A_{560} of Fe^{III} $SynNOS_{glb}$ was normalized and plotted vs. the ambient potential (inset).

$SynNOS_{ox}$ NO Production

Mammalian NOS oxidase domains, scNOS, SiliNOS$_{ox}$, and other bacterial NOS enzymes were previously shown to convert NHA to NO in single-turnover experiments (13, 14, 25). SynNOS$_{ox}$ was also tested for NO formation in single-turnover conditions. SynNOS$_{ox}$ was reduced with an excess of dithionite and incubated with NHA and cofactors (H_4B, H_4F, or none). Aerobic buffer was added to initiate the reactions in sealed Reacti-Vials, and the headspace was tested for NO. NO was detected in the samples containing H_4B (**Figure 4.4**).

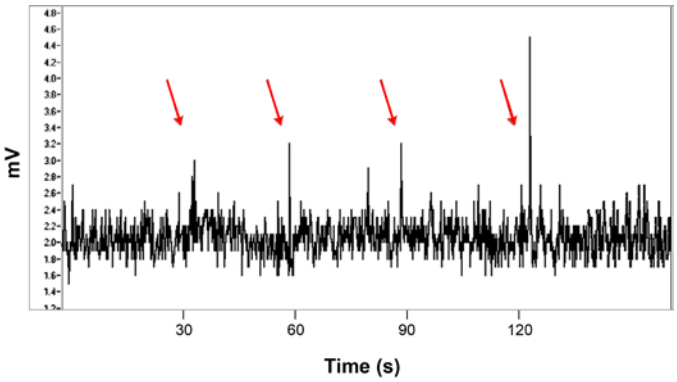

Figure 4.4. NOA single-turnover experiments with SynNOS$_{ox}$. Reactions containing reduced SynNOS$_{ox}$, H_4B, and NHA were initiated with aerobic buffer. NO detection was performed using 200 µL of headspace gas at 30 second intervals after addition of aerobic buffer (red arrows mark injections into NOA). SynNOS$_{ox}$ forms detectable levels of NO in the presence of H_4B and NHA.

Discussion

Newly-identified bacterial NOS proteins such as scNOS, SiliNOS, and SynNOS provide the first examples of bacterial NOS enzymes with reductase domains fused within a single polypeptide. In scNOS and SiliNOS, the reductase domain is fused to the N-terminal side of the oxidase domain. In SynNOS, the reductase domain is also fused to the oxidase domain at the C-terminus, in the same relative position as mNOS enzymes. Additionally, SynNOS contains a globin domain at the N-terminus, proximal to SynNOS$_{ox}$ that is unique among NOS proteins. BLAST searches using the sequence of SynNOS$_{glb}$ reveal sequence homology (~30% identity) with bacterial flavohemoglobin proteins, including *E. coli* nitric oxide dioxygenase.

Bacterial flavohemoglobins have been shown to be involved in NO detoxification by converting NO to nitrate (26, 27). While [Fe^{II}]-SynNOS$_{glb}$ formed stable complexes with CO and NO, O_2 binding was not observed due to rapid oxidation of the protein from the ferrous to ferric state. Stopped-flow spectroscopy revealed a transient [Fe^{II}-O_2] complex, and the oxidation rate of SynNOS$_{glb}$ was determined to be several orders of magnitude faster than that of hemoglobin or myoglobin (1.35 ± 0.09 s^{-1} for SynNOS$_{glb}$ versus $<10^{-5}$ s^{-1} for myoglobin and hemoglobin). Thus, SynNOS$_{glb}$ is more likely to function as a redox sensor or electron transfer domain rather than a gas transport or storage protein like most other globins.

The midpoint potential of $SynNOS_{glb}$ was measured to be approximately -225 mV, which is higher than that of $SynNOS_{ox}$ (-376 mV) (Sarah Chobot, personal correspondence), and similar to that of L-Arg-bound $mNOS_{ox}$ (4). In nNOS, the midpoint potential of NADPH is -320 mV, and $FADH_2$ and $FMNH_2$ are approximately -280 mV. Although the midpoint potentials of the flavins in SynNOS were not determined, they are likely to be similar to mNOS. In this case, electron transfer would be more favorable from NADPH and the flavins to the $SynNOS_{glb}$ heme, rather than to the $SynNOS_{ox}$ heme. Preliminary experiments indicate that there is redox communication between $SynNOS_{glb}$ and $SynNOS_{ox}$, and that $SynNOS_{glb}$ may be scavenging NO produced by $SynNOS_{ox}$ and producing nitrate (Sarah Chobot, personal correspondence).

It is unexpected that the same enzyme may possess the capabilities to both synthesize and scavenge NO. SynNOS may have evolved as a novel way to produce nitrate; another possibility is that the dual activity of the oxidase and globin domains in SynNOS is designed to regulate NO levels. Other pathways in biology support a mechanism that includes domains within a single protein that have competing functions. GGDEF domains possess diguanylate cyclase activity and synthesizes the bacterial second messenger cyclic-di-GMP, while EAL domains have phosphodiesterase activity and hydrolyzes cyclic-di-GMP (28, 29). Proteins have been discovered to have both GGDEF and EAL domains, and the opposing activities within these bifunctional enzymes regulate intracellular concentrations of cyclic-di-GMP. Similarly, $SynNOS_{glb}$ and $SynNOS_{ox}$ could fine-tune intracellular levels of NO, with NOS_{ox} responsible for synthesis, and NOS_{glb} converting excess NO to nitrate.

Homologs of SynNOS have been identified from *Spirosoma linguale* DSM 74, *Nostoc* sp. PCC 7107, and *Crinalium epipsammum*, conserving both NOS-like and flavohemoglobin-like domains. Experiments with $SynNOS_{glb}$ reveal that the globin domain could be involved in electron transfer or NO scavenging, suggesting that the globin domain regulates the NO levels produced by the heme/oxidase domain. This chapter represents the first characterization of a new subdivision of bacterial NOS enzymes.

References

1. Kerwin, J. F., Lancaster, J. R., and Feldman, P. R. (1995) Nitric Oxide: A New Paradigm for Second Messengers. *J. Med. Chem.* **38**, 4343–4362
2. Moncada, S., Palmer, R., and Higgs, E. (1991) Nitric oxide: physiology, pathophysiology, and pharmacology. *Pharmacol. Rev.* **43**, 109–142
3. Dinerman, J. L., Lowenstein, C. J., and Snyder, S. H. (1993) Molecular Mechanisms of Nitric Oxide Regulation - Potential Relevance to Cardiovascular Disease. *Circ. Res.* **73**, 217–222
4. Alderton, W. K., Cooper, C. E., and Knowles, R. G. (2001) Nitric oxide synthases: structure, function and inhibition. *Biochem. J.* **357**, 593–615
5. Griffith, O. W., and Stuehr, D. J. (1995) Nitric Oxide Synthases: Properties and Catalytic

Mechanism. *Annu. Rev. Physiol.* **57**, 707–736

6. Adak, S., Bilwes, A. M., Panda, K., Hosfield, D., Aulak, K. S., McDonald, J. F., Tainer, J. A., Getzoff, E. D., Crane, B. R., and Stuehr, D. J. (2002) Cloning, expression, and characterization of a nitric oxide synthase protein from Deinococcus radiodurans. *Proc. Natl. Acad. Sci. U. S. A.* **99**, 107–112
7. Pant, K., Bilwes, A. M., Adak, S., Stuehr, D. J., and Crane, B. R. (2002) Structure of a nitric oxide synthase heme protein from Bacillus subtilis. *Biochemistry*. **41**, 11071–11079
8. Shatalin, K., Gusarov, I., Avetissova, E., Shatalina, Y., McQuade, L. E., Lippard, S. J., and Nudler, E. (2008) Bacillus anthracis-derived nitric oxide is essential for pathogen virulence and survival in macrophages. *Proc. Natl. Acad. Sci. U. S. A.* **105**, 1009–1013
9. Kuroda, M., Ohta, T., Uchiyama, I., Baba, T., Yuzawa, H., Kobayashi, I., Cui, L., Oguchi, A., Aoki, K., Nagai, Y., Lian, J., Ito, T., Kanamori, M., Matsumaru, H., Maruyama, A., Murakami, H., Hosoyama, A., Mizutani-Ui, Y., Takahashi, N. K., Sawano, T., Inoue, R., Kaito, C., Sekimizu, K., Hirakawa, H., Kuhara, S., Goto, S., Yabuzaki, J., Kanehisa, M., Yamashita, A., Oshima, K., Furuya, K., Yoshino, C., Shiba, T., Hattori, M., Ogasawara, N., Hayashi, H., and Hiramatsu, K. (2001) Whole genome sequencing of meticillin-resistant Staphylococcus aureus. *Lancet*. **357**, 1225–1240
10. Crane, B. R., Sudhamsu, J., and Patel, B. A. (2010) Bacterial nitric oxide synthases. *Annu. Rev. Biochem.* **79**, 445–470
11. Crane, B. R. (2008) The enzymology of nitric oxide in bacterial pathogenesis and resistance. *Biochem. Soc. Trans.* **36**, 1149–54
12. Sudhamsu, J., and Crane, B. R. (2009) Bacterial nitric oxide synthases: what are they good for? *Trends Microbiol.* **17**, 212–218
13. Agapie, T., Suseno, S., Woodward, J. J., Stoll, S., Britt, R. D., and Marletta, M. A. (2009) NO formation by a catalytically self-sufficient bacterial nitric oxide synthase from Sorangium cellulosum. *Proc. Natl. Acad. Sci. U. S. A.* **106**, 16221–16226
14. Rao, M., Smith, B. C., and Marletta, M. A. (2015) Nitric Oxide Mediates Biofilm Formation and Symbiosis in Silicibacter sp. Strain TrichCH4B. *MBio*. **6**, 1–10
15. Winter, M. B., Woodward, J. J., and Marletta, M. A. (2013) An Escherichia coli Expression-Based Approach for Porphyrin Substitution in Heme Proteins. in *Methods in Molecular Biology*, pp. 95–106, **987**, 95–106
16. Yoon, J., Herzik, M. A., Winter, M. B., Tran, R., Olea, C., and Marletta, M. A. (2010) Structure and properties of a bis-histidyl ligated globin from Caenorhabditis elegans. *Biochemistry*. **49**, 5662–70
17. Di Iorio, E. E. (1981) Preparation of Derivatives of Ferrous and Ferric Hemglobin. *Methods Enzymol.* **76**, 57–72
18. Dewilde, S., Kiger, L., Burmester, T., Hankeln, T., Baudin-Creuza, V., Aerts, T., Marden, M. C., Caubergs, R., and Moens, L. (2001) Biochemical Characterization and Ligand Binding Properties of Neuroglobin, a Novel Member of the Globin Family. *J. Biol. Chem.* **276**, 38949–38955
19. Hargrove, M. S., Barry, J. K., Brucker, E. a, Berry, M. B., Phillips, G. N., Olson, J. S., Arredondo-Peter, R., Dean, J. M., Klucas, R. V, and Sarath, G. (1997) Characterization of recombinant soybean leghemoglobin a and apolar distal histidine mutants. *J. Mol. Biol.*

266, 1032–1042

20. Brantley, R. E., Smerdon, S. J., Wilkinson, A. J., Singleto, E. W., and Olson, J. S. (1993) The mechanism of autooxidation of myoglobin. *J. Biol. Chem.* **268**, 6995–7010
21. Mansouri, A., and Winterhalter, K. H. (1974) Nonequivalence of Chains in Hemoglobin Oxidation. *Biochemistry*. **12**, 4946–4949
22. Sawai, H., Kawada, N., Yoshizato, K., Nakajima, H., Aono, S., and Shiro, Y. (2003) Characterization of the heme environmental structure of cytoglobin, a fourth globin in humans. *Biochemistry*. **42**, 5133–5142
23. Fago, A., Hundahl, C., Dewilde, S., Gilany, K., Moens, L., and Weber, R. E. (2004) Allosteric regulation and temperature dependence of oxygen binding in human neuroglobin and cytoglobin: Molecular mechanisms and physiological significance. *J. Biol. Chem.* **279**, 44417–44426
24. Wang, Z.-Q., Lawson, R. J., Buddha, M. R., Wei, C.-C., Crane, B. R., Munro, A. W., and Stuehr, D. J. (2007) Bacterial flavodoxins support nitric oxide production by Bacillus subtilis nitric-oxide synthase. *J. Biol. Chem.* **282**, 2196–2202
25. Hurshman, A. R., and Marletta, M. A. (2002) Reactions catalyzed by the heme domain of inducible nitric oxide synthase: evidence for the involvement of tetrahydrobiopterin in electron transfer. *Biochemistry*. **41**, 3439–3456
26. Gardner, P. R., Gardner, a M., Martin, L. a, and Salzman, a L. (1998) Nitric oxide dioxygenase: an enzymic function for flavohemoglobin. *Proc. Natl. Acad. Sci. U. S. A.* **95**, 10378–83
27. Forrester, M. T., and Foster, M. W. (2012) Protection from nitrosative stress: A central role for microbial flavohemoglobin. *Free Radic. Biol. Med.* **52**, 1620–1633
28. Galperin, M. Y., Nikolskaya, a N., and Koonin, E. V (2001) Novel domains of the prokaryotic two-component signal transduction systems.[erratum appears in FEMS Microbiol Lett 2001 Oct 16;204(1):213-4]. *FEMS Microbiol. Lett.* **203**, 11–21
29. Galperin, M. Y. (2004) Bacterial signal transduction network in a genomic perspective. *Environ. Microbiol.* **6**, 552–567

CHAPTER 5:

FUTURE DIRECTIONS

Bacterial NO signaling has been shown to influence a diverse range of bacterial behaviors, including stress response, motility and biofilm formation, host colonization, and quorum sensing. The studies in this thesis explored bacterial NO signaling in its various facets. **Chapter 2** describes the elucidation of a full NO signaling pathway in *Silicibacter* sp. TrichCH4B. **Chapter 3** examines the interaction and inhibition of HKs by NO-bound H-NOX. **Chapter 4** introduces a novel class of bacterial NOS enzymes containing a globin domain of unknown function. However, there are many directions for future exploration and characterization of NO signaling in bacteria.

Bacteria with NOS and H-NOX

In **Chapter 2**, the NO signaling pathway in *Silicibacter* sp. TrichCH4B was characterized as the first bacteria to harbor both an NOS and H-NOX. NOS activation by the bacteria's algal symbiont results in biofilm formation, revealing a key role for NOS-derived NO in symbiosis. The inducer of SiliNOS activity was discovered to be a secreted protein from *T. erythraeum*; however, the mechanism of NOS activation has yet to be elucidated (1). Size-exclusion or charge-based fractionation of the concentrated *Trichodesmium* spent media (TSM) and proteomics approaches could be used to identify the algal activator of SiliNOS. Preliminary studies have shown that secreted protein levels in TSM are low, and large cultures of *T. erythraeum* may be required to collect adequate amounts of protein for fractionation. Each fraction would be added to *Silicibacter* sp. TrichCH4B cultures, and NO production would be measured. Fractions that induced higher NOS activity would be subjected to tryptic digestion and mass spectrometry analysis, leading to identification of the signaling protein from *T. erythraeum* that leads to SiliNOS activation.

T. erythraeum is a major marine diazotroph, harboring variety of bacteria in addition to *Silicibacter* on its algal filaments (2–4). BLAST searches for bacterial H-NOX domains revealed that there is another *Trichodesmium*-associated bacteria, *Roseidium* sp. TrichSKD4, which encodes an H-NOX found adjacent to a DGC. *Roseidium* does not appear to contain an NOS; however, NO derived from *Sili* NOS could freely diffuse if *Roseidium* is in the vicinity. This would resemble the mammalian NOS/sGC signaling, in which NO is synthesized in a generator cell and diffuses to a neighboring receptor cell, which contains sGC. NO generated from *Silicibacter* could affect the interactions between *T. erythraeum* and *Roseidium*, adding yet another role for NO in this marine ecosystem.

In addition to *Silicibacter* sp. TrichCH4B, there is currently one other sequenced bacteria shown to contain both an NOS and H-NOX, *Spirosoma linguale* (5). *Sl* H-NOX is in the same operon adjacent to an HK, which is positioned adjacent to a LytTR response regulator. LytTR domains are bacterial DNA-binding domains, most commonly found as the effector module in RRs, and have been associated with virulence and toxin production in a number of bacteria (6–10).

Sl H-NOX has been shown to inhibit *Sl* HK in the NO-bound form (unpublished data), but the effect of *Sl* HK on *Sl* LytTR is still unclear. Deletion of the NOS, H-NOX, HK, and LytTR genes in *S. linguale* could provide insight into the role of NOS and NO in the organism, and the targets of *Sl* LytTR could be identified by DNA-binding assays. As the second organism known to harbor both NOS and H-NOX, *S. linguale* would increase our understanding of bacterial NO signaling and the various roles that NO plays in bacterial processes, in particular transcription regulation via LytTR domains.

H-NOX and HK Interaction and Inhibition

Chapter 3 discussed the molecular details of the interactions between *So* H-NOX and *So* HK, revealing the binding interface on *So* H-NOX and key residues that contribute to complex formation. *In vitro* activity assays indicated that proper complex formation is essential for H-NOX regulation of HK activity. Further experiments would attempt to determine whether disruption of the H-NOX:HK complex would result in a biofilm formation defect *in vivo*. An *hnoX* deletion strain has been generated in *S. oneidensis* (11), and strains can be complemented with *hnoX* containing the point mutations identified in **Chapter 3** that resulted in weaker complex formation. Based on the result of the *in vitro* kinase assays, *S. oneidensis* mutants that have binding-deficient H-NOX should have decreased biofilm formation compared with wild-type in response to NO. These *in vivo* experiments would validate the biochemical results obtained in this study.

Determination of the H-NOX:HK complex structure would provide an important complement to the results from this study. Initial efforts towards crystallization of the complex structure have been described in the dissertation of Mark A. Herzik, Ph.D. (12). In addition, cryo-electron microscopy (cryo-EM) may be used as a tool to observe the overall conformation of the H-NOX:HK complex. Due to size limitations of cryo-EM, *So* HK would require an MBP tag to generate a dimer of ~180 kDa. Addition of *So* H-NOX would result in a final molecular weight of ~225 kDa, which would be suitable for cryo-EM studies (13). Finally, structural studies may be pursued with a different H-NOX:HK system. The *S. oneidensis* H-NOX signaling network is analogous to the one found in *V. cholerae*. *Vc* HK also contains an N-terminal domain of unknown function similar to the one in *So* HK, and *Vc* H-NOX contains the conserved residues important for binding, suggesting that the *Vc* H-NOX:HK complex would be similar to *So* H-NOX/HK. Thus, *Vc* H-NOX:HK could be an alternative system for crystallography as well as alternative structural studies.

Novel Bacterial Nitric Oxide Synthases

The discovery of a novel class of globin-containing bacterial NOS enzymes in *Synechococcus* sp. PCC 7335 was described in **Chapter 4**, with many follow-up experiments to pursue. $SynNOS_{ox}$ is mostly in the inactive P420 form at pH 7.5, and only has ~50% of the active P450 form at pH 8.7. In iNOS, the P450 → P420 transition is controlled by the conformational state of the enzyme, and iNOS with substrate and cofactors is "locked" in a dimer state and cannot

readily convert to P420 (14). However, addition of substrate and cofactors to $SynNOS_{ox}$ does not appear to increase the relative amount of P450. While the dimerization state of $SynNOS_{ox}$ is unclear, it does appear to be missing residues that are crucial for dimerization in iNOS. Thus, changes that occur at the putative dimer interface may propagate throughout the $SynNOS_{ox}$ domain, particularly at the heme active site, resulting in P420 formation. Further characterization of the heme pocket, including structural elucidation, may provide insight into the properties of the $SynNOS_{ox}$ heme active site.

The role of the unique globin domain in SynNOS also remains to be determined. The fast autoxidation rate suggests a role for electron transfer rather than gas storage and transport. The ability of $SynNOS_{red}$ to reduce $SynNOS_{glb}$ should be determined in order to map the electron transfer chain within SynNOS. Preliminary experiments that showed NO scavenging and nitrate production by $SynNOS_{glb}$ should be repeated. If further progress is made towards stabilization of $SynNOS_{ox}$, the three separate domains should be added *in situ* to mimic the full-length enzyme, and both NO and nitrate production should be measured to determine the activity of the oxidase and globin domains.

Analogous to SynNOS, the NOS from *S. linguale* also contains an N-terminal globin, and NOS enzymes with similar domain architecture are found in two other cyanobacteria *Nostoc* sp. PCC 7107 and *Crinalium epipsammum*. The NOS from these organisms could be more stable than SynNOS, making them more suitable for the experiments listed above. As more NOS proteins are discovered with the increasing number of bacterial genomes sequenced, novel roles for bacterial NOS-derived NO could be revealed using the same methodologies.

References

1. Rao, M., Smith, B. C., and Marletta, M. A. (2015) Nitric Oxide Mediates Biofilm Formation and Symbiosis in Silicibacter sp. Strain TrichCH4B. *MBio*. **6**, 1–10
2. Janson, S., Bergman, B., Carpenter, E. J., Giovannoni, S. J., and Vergin, K. (1999) Genetic analysis of natural populations of the marine diazotrophic cyanobacterium Trichodesmium. *FEMS Microbiol. Ecol.* **30**, 57–65
3. Hmelo, L., Van Mooy, B., and Mincer, T. (2012) Characterization of bacterial epibionts on the cyanobacterium Trichodesmium. *Aquat. Microb. Ecol.* **67**, 1–14
4. Thompson, A. W., and Zehr, J. P. (2013) Cellular interactions: lessons from the nitrogen-fixing cyanobacteria. *J. Phycol.* **49**, 1024–1035
5. Lail, K., Sikorski, J., Saunders, E., Lapidus, A., Glavina Del Rio, T., Copeland, A., Tice, H., Cheng, J.-F., Lucas, S., Nolan, M., Bruce, D., Goodwin, L., Pitluck, S., Ivanova, N., Mavromatis, K., Ovchinnikova, G., Pati, A., Chen, A., Palaniappan, K., Land, M., Hauser, L., Chang, Y.-J., Jeffries, C. D., Chain, P., Brettin, T., Detter, J. C., Schütze, A., Rohde, M., Tindall, B. J., Göker, M., Bristow, J., Eisen, J. a, Markowitz, V., Hugenholtz, P., Kyrpides, N. C., Klenk, H.-P., and Chen, F. (2010) Complete genome sequence of Spirosoma linguale type strain (1). *Stand. Genomic Sci.* **2**, 176–185
6. Lizewski, S. E., Lundberg, D. S., Michael, J., and Schurr, M. J. (2002) The

Transcriptional Regulator AlgR Is Essential for Pseudomonas aeruginosa Pathogenesis The Transcriptional Regulator AlgR Is Essential for Pseudomonas aeruginosa Pathogenesis. *Infect Immun*. **70**, 6083–6093
7. Shimizu, T., Shima, K., Yoshino, K., Yonezawa, K., Shimizu, T., and Hayashi, H. (2002) Proteome and Transcriptome Analysis of the Virulence Genes Regulated by the VirR / VirS System in Clostridium perfringens. **184**, 2587–2594
8. Nikolskaya, A. N., and Galperin, M. Y. (2002) A novel type of conserved DNA-binding domain in the transcriptional regulators of the AlgR/AgrA/LytR family. *Nucleic Acids Res.* **30**, 2453–9
9. Diep, D. B., Myhre, R., Johnsborg, O., Aakra, A., and Nes, I. F. (2003) Inducible bacteriocin production in Lactobacillus is regulated by differential expression of the pln operons and by two antagonizing response regulators, the activity of which is enhanced upon phosphorylation. *Mol. Microbiol.* **47**, 483–494
10. Dawid, S., Roche, A. M., and Weiser, J. N. (2007) The blp bacteriocins of Streptococcus pneumoniae mediate intraspecies competition both in vitro and in vivo. *Infect. Immun.* **75**, 443–451
11. Plate, L., and Marletta, M. A. (2012) Nitric Oxide Modulates Bacterial Biofilm Formation through a Multicomponent Cyclic-di-GMP Signaling Network. *Mol. Cell*. **46**, 449–460
12. Herzik, M. A. (2014) *Structural Insights into Gas Binding and Signal Transduction in the H-NOX Family of Heme Proteins*. Ph.D. thesis, 10.1017/CBO9781107415324.004
13. Gavira, J. A. (2015) Current trends in protein crystallization. *Arch. Biochem. Biophys.* **602**, 3–11
14. Sabat, J., Stuehr, D. J., Yeh, S.-R., and Rousseau, D. L. (2009) Characterization of the proximal ligand in the P420 form of inducible nitric oxide synthase. *J. Am. Chem. Soc.* **131**, 12186–92

APPENDIX A

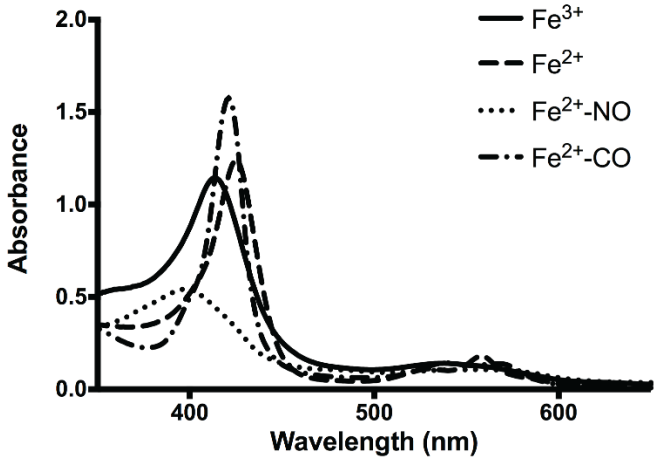

Figure A.1. UV/Vis spectra of SiliH-NOX in different oxidation and ligation states. Fe^{3+} λ_{max} = 411 nm; Fe^{2+} λ_{max} = 426 nm; Fe^{2+}-NO λ_{max} = 399 nm; Fe^{2+}-CO λ_{max} = 420 nm.

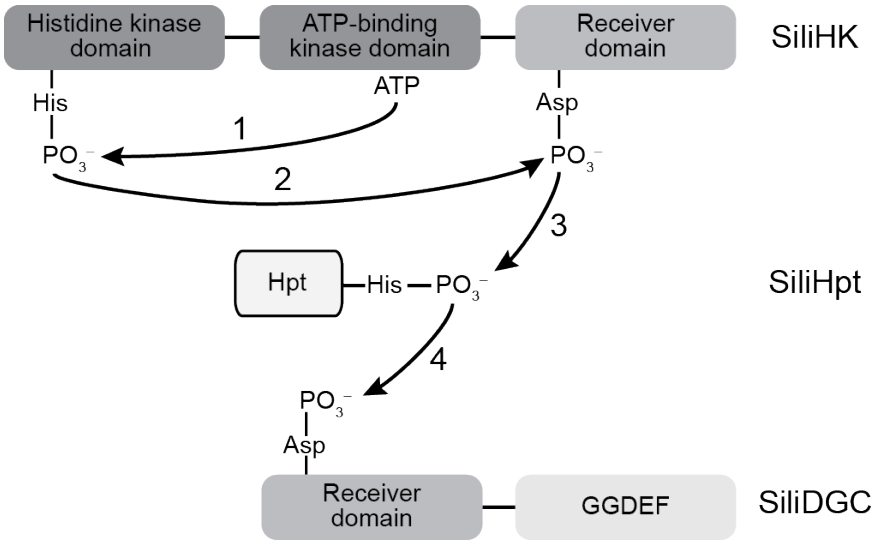

Figure A.2. *Silicibacter* sp. TrichCH4B two-component phosphorelay signaling system. SiliHK is a hybrid histidine kinase, which has a receiver domain containing an aspartate phosphoryl acceptor. A separate Hpt protein is required as an intermediary for phosphotransfer from the receiver domain of SiliHK to the receiver domain of the response regulator SiliDGC.

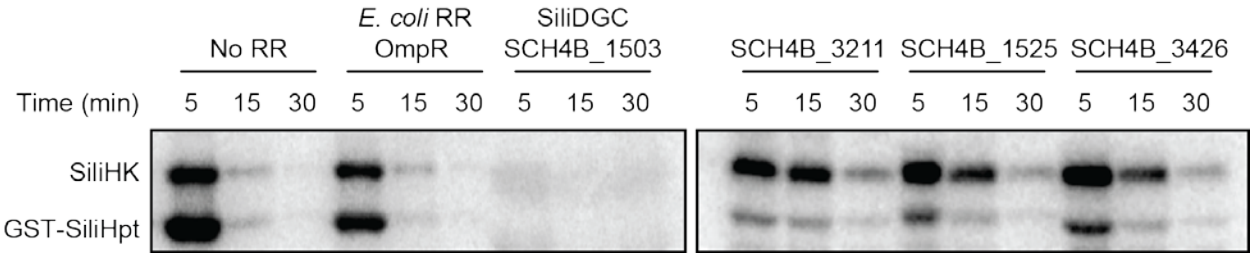

Figure A.3. Phosphotransfer from SiliHK/SiliHpt to orphan response regulators. SCH4B_3211, SCH4B_1525, and SCH4B_3426 are 3 representative orphan response regulators that did not cause rapid loss of SiliHK/SiliHpt phosphorylation. In contrast, SCH4B_1503 (SiliDGC), the cognate phosphotransfer partner of SiliHK/SiliHpt, caused complete loss of SiliHK/SiliHpt phosphorylation within 5 min. Control reactions with no response regulator added or with the *E. coli* response regulator OmpR also did not cause a rapid loss in SiliHK/SiliHpt phosphorylation.

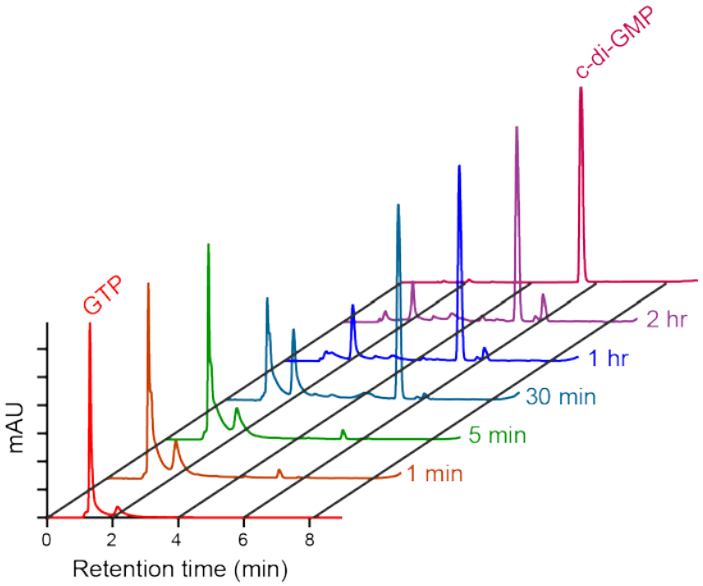

Figure A.4. SiliDGC activity assays. SiliDGC (10 μM) was mixed with 0.5 mM GTP, and aliquots were quenched at 1 min, 5 min, 30 min, 1 hr, and 2 hr time points, as described under Materials and Methods. Near complete conversion of GTP to c-di-GMP was observed through the 2 hour time-course.

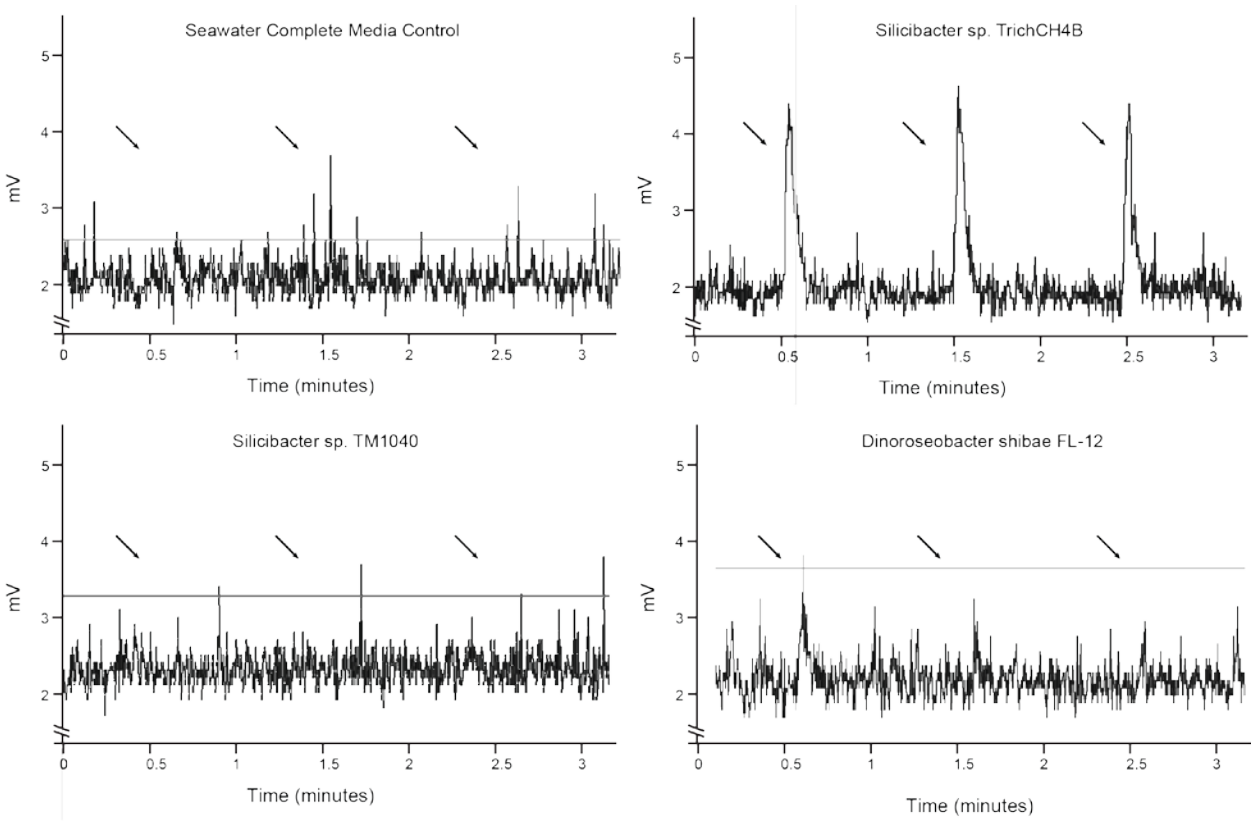

Figure A.5. *Silicibacter* sp. TrichCH4B NO formation comparison with other Roseobacter species. *Silicibacter* sp. TrichCH4B, *Silicibacter* sp. TM1040, and *Dinoroseobacter shibae* FL-12 were tested for NO formation using the NOA as described under Experimental Procedures. Only *Silicibacter* sp. TrichCH4B forms NO. Seawater Complete Media was also tested as a control.

APPENDIX B

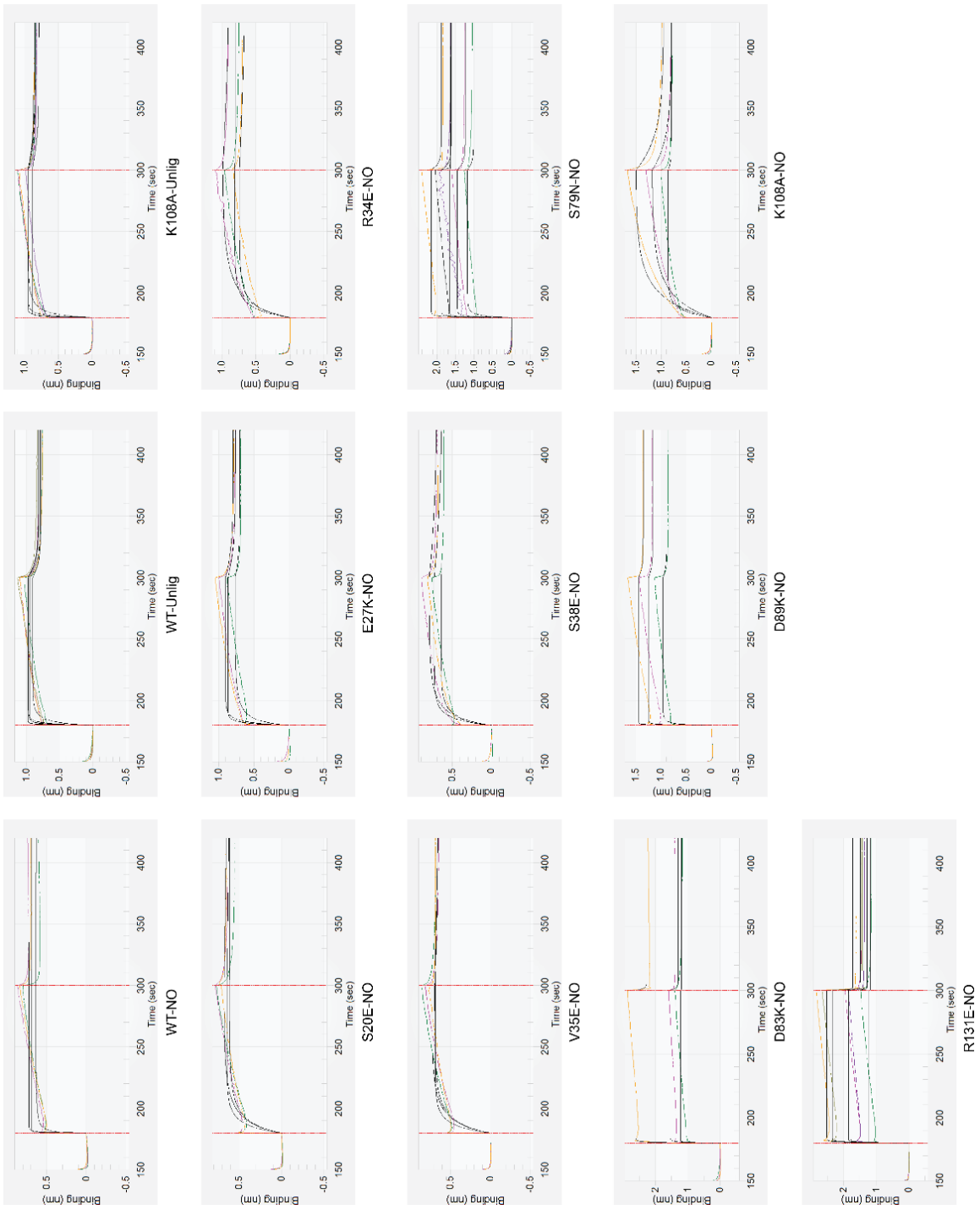

Figure B.1. BLItz experiment traces. GST-*So* HK was immobilized onto anti-GST biosensors as bait. Baseline, association, and dissociation phases of each experiment are shown with varying concentrations of *So* H-NOX.

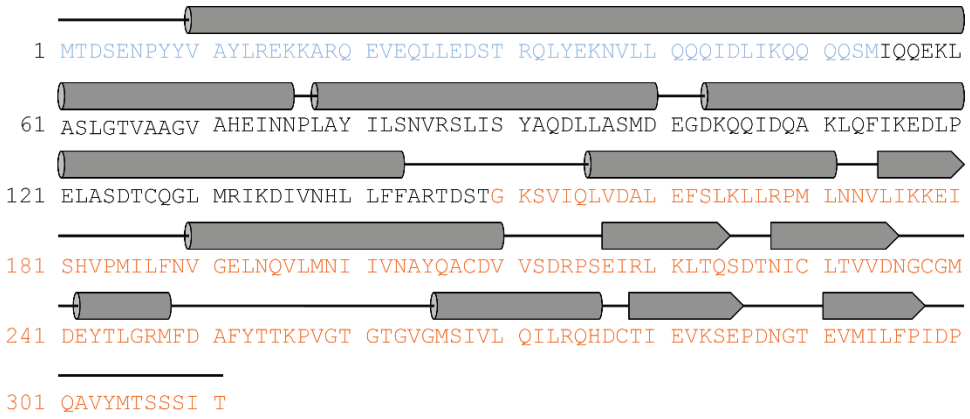

Figure B.2. Secondary structure prediction analysis for *So* HK. α-helices are shown as cylinders and β-strands are shown as arrows. The N-terminal domain (light blue), dimerization and histidine phosphorylation domain (black), and the catalytic domain (orange) are colored according to their domain boundaries.

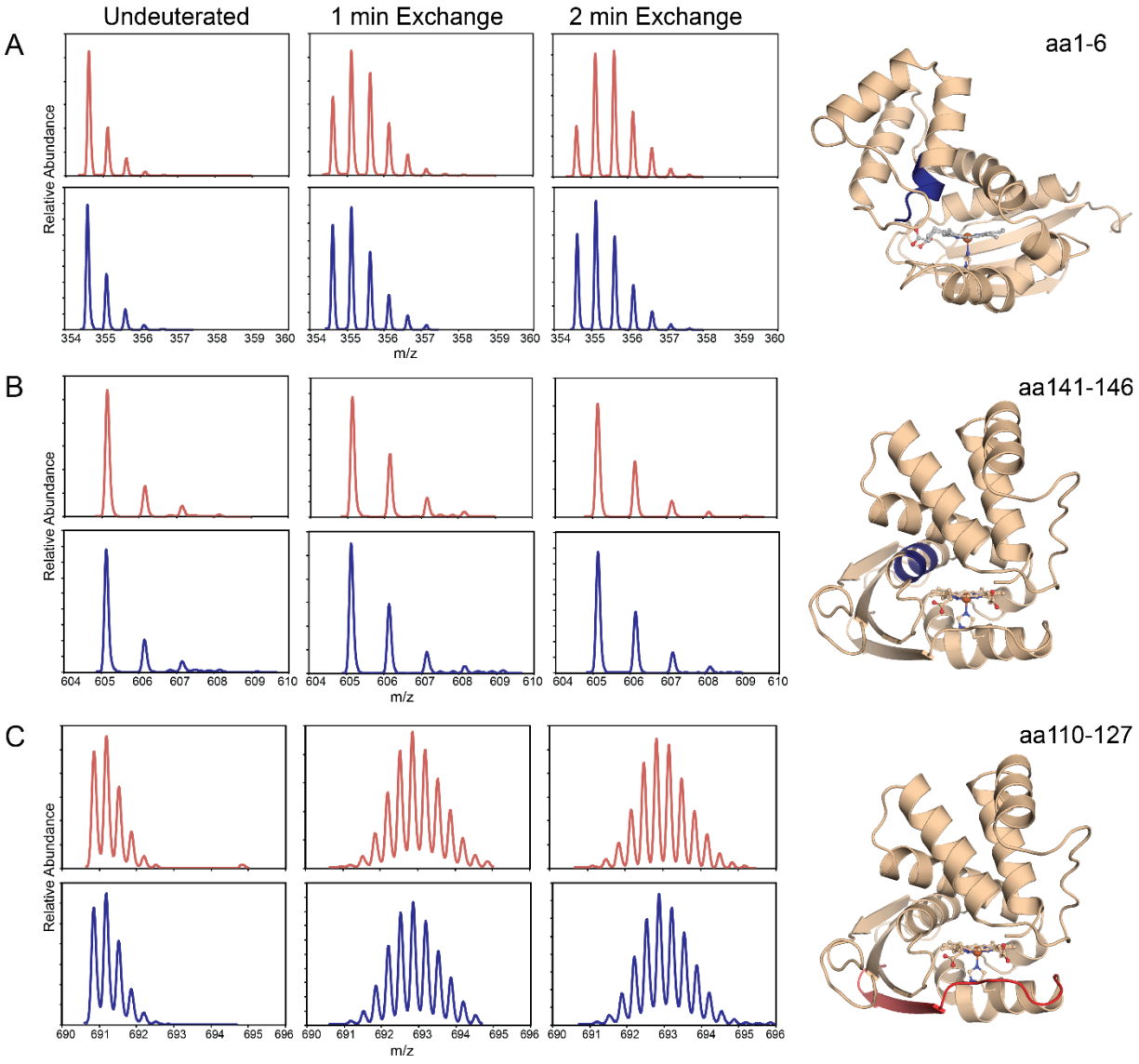

Figure B.3. Typical exchange time courses for deuteration of *So* H-NOX in the absence (red traces) or presence (blue traces) of *So* HK (five-fold excess). For each peptide chosen, the mass spectrum is reported following 0 min (undeuterated control), 1 min or 2 min incubation in D_2O. The corresponding amino acids from the exchange time course (colored either blue for slow exchange or red for fast exchange) are mapped to the structure of *So* H-NOX (shown in cartoon representation, wheat). (**A**) Amino acids 1-6, located at the N-terminal helix (shown in blue) exhibits ~30% slower exchange in the presence of the kinase. (**B**) Amino acids 141-146 within the helix αG exhibit very little exchange, indicative of a portion of the protein that is well-protected from D_2O. (**C**) The peptide corresponding to amino acids 110-127, comprising the αF-β1 loop and the β1 strand, exhibits ~50% deuteration from the first timepoint onward, indicating that the loop region exchanges very rapidly while the strand portion exchanges slowly.

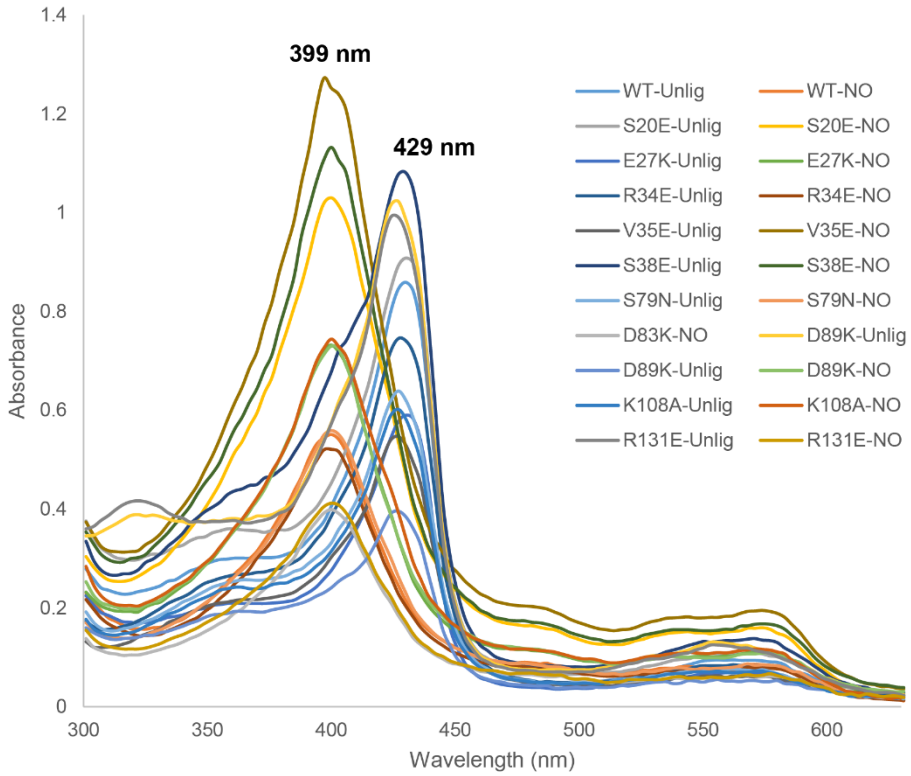

Figure B.4. UV-vis spectra of *So* H-NOX variants (wild-type or point mutants) in Fe^{II} and Fe^{II}-NO ligation states. Fe^{II} λ_{max} = 429 nm; Fe^{II}-NO λ_{max} = 399 nm.

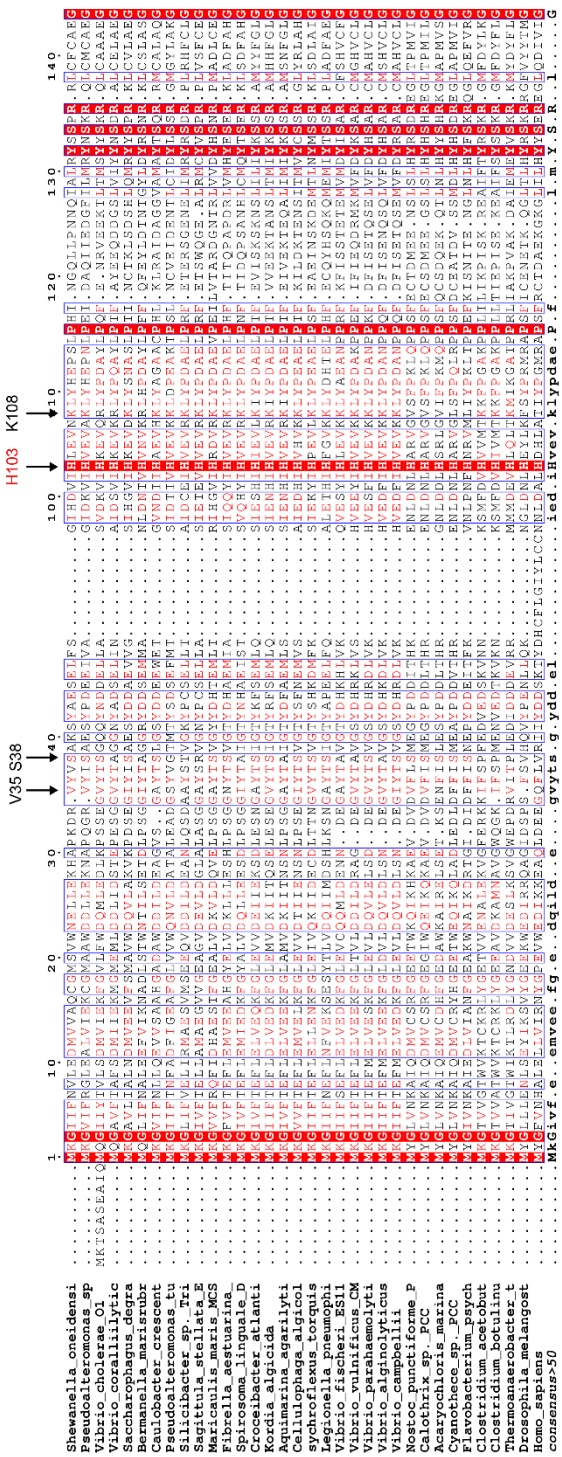

Figure B.5. Sequence alignment of 32 bacterial H-NOX proteins and H-NOX domains from *Drosophila melanogaster* and *Homo sapiens* soluble guanylate cyclase (sGC). Residue numberings are based on *S. oneidensis* H-NOX. H103 (red) is the absolutely conserved distal heme ligand. V35, S38, and K108 are generally conserved across all H-NOX proteins that have histidine kinase partners. Alignment prepared using MultAlign and ESPript.